NONLINEAR FATIGUE DAMAGE ACCUMULATION IN AIRCRAFT ENGINE ALLOYS UNDER MULTIAXIAL LOADING

A Dissertation
Submitted to the Graduate Faculty
of the
North Dakota State University
of Agricultural and Applied Science

By

Sandip Kumar Suman

In Partial Fulfillment of the Requirements
for the Degree of
DOCTOR OF PHILOSOPHY

Major Department:
Mechanical Engineering

October 2013

Fargo, North Dakota

North Dakota State University
Graduate School

Title

Nonlinear Fatigue Damage Accumulation in Aircraft Engine Alloys Under Multiaxial Loading

By

Sandip Kumar Suman

The Supervisory Committee certifies that this ***disquisition*** complies with North Dakota State University's regulations and meets the accepted standards for the degree of

DOCTOR OF PHILOSOPHY

SUPERVISORY COMMITTEE:

Dr. Alan Kallmeyer
Chair

Dr. Ghodrat Karami

Dr. Chad Ulven

Dr. Frank Yazdani

Approved:

11/7/2013	Dr. Alan R. Kallmeyer
Date	Department Chair

ABSTRACT

Fatigue is considered to be one of the most frequent phenomena in the failure of many machine parts. Most of the prior studies on fatigue have been limited to uniaxial loading cases with a primary focus on constant amplitude cycles. A detailed exploration of multiaxial fatigue under constant and variable amplitude loading scenarios for a wide variety of aircraft engine alloys has been performed in this study, and a new methodology for the accurate prediction of fatigue damage is developed. A critical-plane based constant amplitude fatigue damage model has been developed in this study which is simple in comparison to prior models developed by other researchers and reduces the computational effort. The constant amplitude fatigue damage model is further used in the development of a multiaxial variable amplitude damage estimation method, with an emphasis on estimating the damage created by both low cycle fatigue (LCF) and high cycle fatigue (HCF) cycles. A significant increase in overall fatigue damage was observed in the tests with the introduction of HCF cycles in the mission histories. The damage due to the HCF cycles has been found to be much greater than predicted by linear damage accumulation theories, although the degree of interaction between the LCF and HCF cycles was found to be very dependent on the multiaxial load paths. In addition, the HCF cycles did not contribute significantly to the accumulation of damage until a certain amount of "pre-damage" had been caused by the LCF cycles. Separate HCF damage computing approaches have been adopted in this study to accurately compute the damage produced by tensile and shear dominant HCF cycles, and a significant improvement in the accuracy of fatigue life prediction has been achieved using the new methodology.

ACKNOWLEDGEMENT

Funding for this research has been provided by General Electric (Aviation) and the Air-force Office of Scientific Research (AFOSR). I would like to sincerely acknowledge my supervisor Dr. Alan Kallmeyer for his continuous encouragement, efforts and right approaches in this research. Dr. Kallmeyer has been an academic as well as a professional guardian for me since the beginning of my doctoral education. I would also like to extend my sincere thanks to Dr. Ghodrat Karami, Dr. Chad Ulven and Dr Frank Yazdaani for being in my graduate committee and showing right directions for this research.

Sincere gratitude is extended to Dr. Peter Kurath (Adjunct professor at the University of Illinois), Dr. Robert Van Stone (GE Aviation), Mr. Tim Tibbals (Arnold Engineering Development Center) , and Dr. Daniel Adams (University of Utah) for their help in providing us with the experimental facilities and several additional fatigue datasets to validate this research

Dr. Alan Kallmeyer, Dr. Ghodrat Karami, Dr. Chad Ulven and other faculty members in the Mechanical Engineering Department at NDSU are also deeply appreciated for teaching me several courses. These courses have helped me in building the required fundamentals for this research. The Mechanical Engineering Department office staff members (Donna, Tiffany and Tanya) have provided all the administrative requirements for this research and my doctoral education.

Finally, I would like to thank my wife Smita for her continuous encouragement and support, my son Adit, my brothers (Manish and Bineet), my parents (Sushil and Yasodhara) for their continuous support throughout my entire education and this research, and Dr. Alan Kallmeyer in helping me with the editing of this thesis.

TABLE OF CONTENTS

LIST OF TABLES

Tables Pages

LIST OF FIGURES

Figures Pages

CHAPTER 1. INTRODUCTION

Fatigue is a common phenomenon among machine components subjected to dynamic loading. The sources of these dynamic or fatigue loadings may be due to the reaction forces coming from other linking mechanisms in the machine during operation, the direct fluctuating load, or it may be simply due to vibrations in the machine. Many engineering structures experience fatigue loading even due to atmospheric air movements. It is a phenomenon experienced by almost all machine components during their life time. As it is a time dependent phenomenon, the modeling of physical loading situations with suitable mathematical equations for predicting the damage caused by fatigue is no doubt a challenging task. The modeling of fatigue damage in machine components requires consideration of parameters like geometry, metallurgy and loading conditions to be congregated into one mathematical equation.

The study of fatigue initiated during the late 19^{th}century; however significant amount of attention wasn't directed to this subject until the mid 20th century due to some well publicized failures, such as Comet aircraft. The initial investigation of the Comet accidents did not relate the failures to the phenomenon of fatigue, and responsibility was thrown on the faulty piloting of the aircraft and other design failures. After careful investigation, however, the final cause of failure was determined to be due to the initiation and growth of fatigue cracks due to cyclic loading conditions in the airframe. [1-3]

Fatigue loading can be distinguished from monotonic or static loading in terms of the behavior of the material under the action of fluctuating stresses or strains. The standard definition of fatigue as provided by ASTM [1] is as follows: *The process of progressive localized permanent structural change occurring in a material subjected to conditions that produce*

fluctuating stresses and strains at some point or points and that may culminate in cracks or complete fracture after a sufficient number of fluctuations. This ASTM definition implies that fatigue is a progressive phenomenon that occurs over a certain time interval with permanent localized deformation. The word localized refers to the location in the structure or component having higher values of stresses and strains, and once the damage due to this fluctuating load occurs, it becomes an irreversible phenomenon. In many cases these fatigue failures do not give any warning before significant damage has occurred. The initiation of cracks due to fatigue loading occurs at a microscopic level, and by the time a visible crack appears, sufficient irreversible damage would have occurred. Hence, the modeling of fatigue failure is a difficult task and the damage caused by cyclic loading should be considered from the very early stages of machine or structure design.

Fatigue loading is often classified into two broad categories defined by the stress state and load level. The stress state classification separates fatigue loading into two categories of uniaxial and multiaxial fatigue. Uniaxial fatigue is the case of loading where the cyclic stresses are uniaxial in nature, such as that produced by axial or bending loads, whereas multiaxial fatigue consists of fluctuating loading that results in cyclic stresses acting in multiple directions, such as may be experienced by combined axial and torsion loads.

Fatigue loading can also be classified by the level of loading. If the amplitudes of loading cycles are significantly high, resulting in failure of components in less than approximately 10^6 cycles, it is termed low cycle fatigue (LCF). However, if the fatigue lives are longer than 10^6 cycles due to the low level of cyclic amplitude, it is referred to as high cycle fatigue (HCF). The

deformations created in machine components are predominantly elastic during high cycle fatigue; however, low cycle fatigue may result in elastic or plastic (permanent) deformations.

While uniaxial fatigue models are well developed and accepted, the modeling of multiaxial fatigue damage is still an active area of research. Multiaxial fatigue modeling approaches can broadly be classified into three major categories of equivalent-stress/strain based theories, energy-based theories, and critical plane theories. Equivalent stress/strain theories typically make use of the von-Mises or Tresca failure criterion and an equivalent stress or strain representation of the multiaxial stress or strain state in the component. These criteria ignore many of the complications caused by the multiaxial stress or strain state and cannot distinguish between proportional and non-proportional loading conditions. Energy-based approaches attempt to relate the strain energy within the loading cycle to a critical value. Since energy is a scalar value, these criteria do not provide a physical representation of the process by which fatigue cracks initiate and propagate along certain planes, or orientations, in the material. A more sophisticated approach of multiaxial fatigue modeling was proposed by Findley [2] among others. It is based on the orientation of the crack initiation site inside the material and referred to as the critical plane methodology. This concept has achieved widespread appreciation from many fatigue researchers and several improvements have been proposed. Findley [2] started his work with a shear stress-based critical plane fatigue parameter. Brown & Miller [3] further changed Findley's [2] stress-based approach into a strain-based approach, with the argument that strain is better for modeling low cycle fatigue failures. Fatemi & Socie [4] further improved this strain-based concept by incorporating an extra normal stress term to account for the cyclic hardening in the material that occurs on the critical plane. These concepts were further propelled by Erickson

et al. [5] in terms of a stress-based damage parameter with consideration of multiple normal-stress subcycles that may occur within the dominant shear stress cycle on the critical plane.

The objective of this research is to further investigate the critical-plane concept for purposes of multiaxial fatigue life prediction of metallic alloys. As part of this study, two issues are addressed. The first concerns the effect that normal-stress subcycles have on the fatigue damage computation process when utilizing a shear based critical plane parameter, such as that proposed by Erickson et al. [5]. Specifically, in their parameter, the fatigue damage from each normal-stress subcycle was summed with the damage caused by the dominant shear cycle, which could result in an overestimate of fatigue damage if multiple subcycles exist. A novel set of multiaxial fatigue tests have been conducted to experimentally assess the effect of multiple subcycles and provide a validation measure for multiaxial fatigue life prediction models. Using these results, an improved version of the critical-plane parameter is proposed.

The second issue concerns the nature of fatigue damage accumulation under variable amplitude loading conditions. Currently, the Palmgren-Miner [6,7] linear damage rule is the most widely used method for summing fatigue damage from different cycles in a variable load history. While this technique has been found to be reasonably accurate for simple uniaxial loadings, it has been shown to significantly underestimate fatigue damage accumulation when applied to multiaxial loading conditions in which the load path and load level may change substantially from cycle to cycle. A new lifing methodology is proposed to better account for load-path and load-level (LCF/HCF) interactions under multiaxial, variable-amplitude loading conditions. The development of this approach is based on the results of a comprehensive experimental study of cumulative fatigue damage under multiaxial loading in Ti-6Al-4V, a

common titanium alloy used in the aerospace industry. In addition, multiaxial fatigue data from a variety of other titanium and steel alloys, generated by General Electric Aviation, are used to provide validation of both the critical plane and cumulative damage methodologies.

Both material nonlinearity and the nonlinearities associated with the damage accumulation process have been included in this study. Cyclic elastic plastic stress-strain curves have been used to model the material nonlinearities for the very low cycle fatigue load cases and a non-linear approach for cumulative fatigue damage analysis is developed, in contrast with the linear damage accumulation rule proposed by Palmgren-Miner [6,7].

CHAPTER 2. LITERATURE REVIEW

2.1. History of Fatigue

The phenomenon of metal fatigue was first noticed by Rankine in 1840 when he observed the initiation and growth of fatigue cracks in railway axles. His discoveries were not widely accepted and most of the scientists of that time assumed that the failure was caused by recrystallisation of metals due to the stress and the effect of repeated loading on the growth of cracks in railway axles was negligible. Later, Joseph Glynn observed similar kinds of slow growth of brittle cracks in railway axles, and he supported the concept of damage due to repeated loading. In later studies, the theory of recrystallisation was proved meaningless when William Fairbairn showed the weakening effect in large beams due to repeated flexural stresses [7-9].

The microscopic aspects of fatigue crack nucleation and growth were observed by Ewing and Humfrey [8] in 1903 when they published their classical paper on the fracture of metals under repeated alteration of stresses. They noticed in their lab that slip lines were visible in some of the crystals after a few reversals of stress were applied. The slip lines became more distinct after more reversals, and eventually changed into comparatively wide bands with rather hazily defined edges. After a continuous increase in the number of reversals, sharp cracks were visible in the crystals and an additional increase in reversals led to the final fracture of the crystal [8]. This discovery was astonishing at that time and was probably one of the first to microscopically explain fatigue phenomena. Most researchers of that time were not convinced by the phenomenon of fatigue. They believed that the failure of any metal specimen was due to extreme stresses, and the alternation of stresses did not have any significant impact on the fracture. This discovery showed a different picture of failure, where the stress level was well below the

ultimate strength and fracture still occurred due to stress alteration. These authors [8] also explained that the stress reversals applied after the initiation of a crack aided in the propagation of that crack.

The studies on fatigue done during the late 19^{th} century and early 20^{th} century were mainly focused on uniaxial loading cases, and multiaxial cases were rare in the minds of researchers due to the unavailability of experimental facilities and supporting mathematical explanations.

2.2. Uniaxial Fatigue Models

The simplest loading case under which a specimen can be analyzed is uniaxial cyclic loading. The fatigue behavior of metals under uniaxial loading can be modeled either by classical stress-life or strain-life approaches. For a given material, the long-life fatigue strength may vary depending upon the surface finish or size of the specimen, type of loading (tensile or compressive), temperature, environment, mean stress, residual stress and stress concentration [9]. For steel alloys, uniaxial fatigue analysis is often performed by examining the fully reversed fatigue limit (S_f) with respect to its ultimate strength (S_u). Stress-based fatigue analysis under uniaxial loading is commonly performed using the widely accepted Goodman, Morrow or Gerber models. All three of these stress based uniaxial fatigue models are used in fatigue design for infinite life in conjunction with suitable yield criteria. Both the modified Goodman model and Morrow model are in agreement with the observed beneficial effect of compressive mean stresses whereas the Gerber model predicts that the compressive mean stress has a detrimental effect. For this reason, the Gerber model is the least used among these three. Strain-life analysis,

often referred to as low cycle fatigue analysis, is commonly performed using the Smith, Watson and Topper [10] model.

2.2.1. Stress Based Uniaxial Fatigue Models

The common mean stress models used with the stress-life approach can be expressed as follows [9].

Modified Goodman model

$$\frac{S_a}{S_f} + \frac{S_m}{S_u} = 1 \tag{2.1}$$

Gerber model

$$\frac{S_a}{S_f} + \left(\frac{S_m}{S_u}\right)^2 = 1 \tag{2.2}$$

Morrow model

$$\frac{S_a}{S_f} + \frac{S_m}{\sigma_u} = 1 \tag{2.3}$$

Where S_a, S_m, and σ_u are the stress amplitude, mean stress, and true fracture strength, respectively.

2.2.2. Strain Based Uniaxial Fatigue Models

The Smith Watson & Topper [10] model commonly used with the strain-life approach, is expressed as

$$\sigma_{max} E \frac{\Delta\varepsilon}{2} = (\sigma'_f)^2 (2N_f)^{2b} + \sigma'_f \varepsilon'_f \, E (2N_f)^{b+c} \tag{2.4}$$

Where $N_f, \sigma'_f,$ and ε'_f are the fatigue life, fatigue strength coefficient and fatigue ductility coefficient respectively. The constants b and c are referred to as the fatigue strength and fatigue ductility exponents.

2.2.3. Fracture Mechanics

The mechanics of the fatigue failure process can be divided into the two categories of crack initiation followed by the propagation of the crack until catastrophic failure. The nucleation and growth of a micro crack can be considered as the crack initiation process, whereas the propagation of the crack to failure can be put into the category of crack propagation. Most of the crack initiation theories refer to the development of a fatigue crack up to a length of approximately 1mm [9]. Once the fatigue crack has grown to this length (1 mm), it is often visible with the unaided eye. Depending upon the amount of plasticity at the crack tip, propagation of these cracks can be analyzed using either linear-elastic fracture mechanics (LEFM) or elastic-plastic fracture mechanics. The focus of this study is on the crack initiation phase.

2.3. Multiaxial Fatigue

Many machine components in real-life situations are subjected to combined cyclic loading (e.g., bending, torsion and axial loadings) which can broadly be classified as multiaxial fatigue loading. However, the majority of research performed on metal fatigue over the last few decades has been limited to uniaxial cases. Fewer studies have been carried out focusing on experimental or theoretical analysis for multiaxial cases. Combinations of axial, torsion and bending fatigue loads create biaxial and tri-axial stress states in machine components. The classical approach to analyzing such types of loading cases utilizes the von Mises or Tresca

failure theories and computes the equivalent stress to compare it with the failure criteria. These approaches can be considered as extensions of static yield theories to analyze multiaxial fatigue cases and do not deal with the several other complexities caused by multiaxial cyclic stress states. A high safety factor is required to account for the uncertainties caused by fatigue reversals while using these theories [11]. The concepts behind using either the von Mises or Tresca failure theories are also different among researchers. The work done by Fatemi & Stephens [12] recommends use of the von Mises theory over the Tresca criterion for better multiaxial fatigue life predictions. However, equivalent stress-based models provide very crude estimations of the stress state for multiaxial cyclic loading. They often cannot properly account for non-proportional loading and multiaxial mean stress effects. Multiaxial fatigue loads cannot be adequately analyzed by static multiaxial theories due to the cyclic nature of loads where the amplitude and mean value of the loads vary with time. The evaluation of this type of fluctuating load with classical continuum mechanics based yield criteria does not account for the complexity involved with the initiation and propagation of fatigue cracks. Several researchers have proposed modifications of these theories; however, most of the results do not produce good agreement when compared with experimental values of fatigue life.

Findley [13] is considered as one of the earliest researchers to work in the area of multiaxial fatigue. Findley [14] devised several modifications to fatigue test equipment during his experimental research and constructed a testing machine in 1942 to carry out tests on metal specimens under fully reversed combined bending and torsion fatigue loading. Furthermore, he carried out several multiaxial fatigue tests with combined mean stresses present. His mean stress multiaxial fatigue tests indicated that the fatigue strength of materials is reduced significantly due to the presence of mean stresses [13]. He also observed the fact that the propagation of

fatigue cracks happens more rapidly under high mean stresses [15]. Findley [15] did not find very good agreement between experimental data and empirical results considering only the effect of the range of stress. Furthermore, he observed the mode of fracture for this type of combined loading. Notably, Findley revealed that fatigue cracks in any combination of bending and torsion often initiated on or near the plane of maximum alternating shear stress. This was an important finding by Findley in the area of multiaxial fatigue and lead to the development of the critical plane fatigue modeling concept. Most of the models derived by Findley were stress based and no strain terms were present.

Another research group lead by Brown and Miller [16] at the University of Cambridge advanced the study of multiaxial fatigue by introducing strain terms into the critical plane concept. Similar work has also been performed by the research group led by Darrel Socie [17] at the University of Illinois. The concept of including strain in fatigue modeling was also supported by Fatemi and Kurath [11]. All of these researchers agree that the low-cycle fatigue behavior can better be analyzed using strain-based multiaxial fatigue models due to the plasticity at the higher load levels.

You and Lee [18] carried out an important review of multiaxial fatigue theories developed after 1980. They classified these theories into five major categories of (1) modification of the Coffin-Manson equation, (2) application of stress or strain invariants, (3) space averages of stress and strain, (4) critical plane approaches, and (5) energy based fatigue approaches. You and Lee [18] suggested the use of the von Mises or Tresca equations for dealing with multiaxial fatigue; however, their recommendation involved the use of additional factors to reflect the variation of fatigue properties due to multiaxial loading and environment. They also

discussed the effects on crack initiation from factors such as characteristics of the material, strain ratio and shape of the specimen. The idea of an energy-based model proposed by Ellyn et al. [19] was not supported by You and Lee as it did not incorporate the effect of the loading path and the interaction between out-of-phase strain or stress components. However, the method proposed by Liu using the virtual strain energy derived by constructing the Mohr's circle for out-of-phase multiaxial fatigue loading was highly appreciated by You and Lee [18].

2.4. Crack Initiation and Propagation

The main purpose of the study of fatigue is to understand the initiation and propagation of cracks due to uniaxial or multiaxial cyclic loads. Both uniaxial and multiaxial fatigue loads initiate cracks which gradually propagate and lead to final failure. For common metals and alloys, the fatigue failure process consists of four main stages of cyclic deformation [20]. The first stage of deformation is due to the repeated application of stress or strain, which is followed by the second stage of crack initiation and micro-crack nucleation phenomena. The third phase is of coalescence of micro-cracks into macro-cracks, and in the final stage macro-cracks propagate until catastrophic failure occurs [20].

Many theories attempt to predict the total fatigue life consisting of both crack initiation and propagation; however, it is often ambiguous to determine how many cycles were consumed by crack initiation and how many cycles were consumed by crack propagation phenomena. Ewing and Humfrey [8] observed in their tests that only a few more cycles were needed to cause fracture after the formation of a long continuous crack. However, it is not clear from their report how many cycles the specimen consumed before the development of a long continuous crack from its initiation. The microscopic evaluation of fatigue crack initiation and growth done by

Connor et al. [21] found that micro cracks initially form subsurface in riveted aluminum alloy panels and then grow to the surface. The model proposed by David McDowell [22] in 1997 incorporates micro structural interactions in the fatigue crack growth process. He proposed the concept that when a small fatigue crack approaches the micro structural barriers, misoriented grain boundaries with lower resolved shear stresses may arrest the crack due to lack of slip transfer to the adjacent grains.

2.5. Effect of Load-Path on Multiaxial Fatigue

Multiaxial fatigue experiments are typically carried out using combinations of torsional and axial loads that may be applied proportionally or non-proportionally. When axial and shear loads on the specimen start from zero and follow the same increment over time, it is called proportional loading, whereas if the increment in these stresses over time is not proportional, it is called non-proportional loading. The load path can also be classified as in-phase or out-of-phase. An in-phase cyclic loading means the normal and shear stress cycles have peaks in the same direction at the same time, whereas during out-of-phase loading, the peaks of stresses or strains may occur at different times with different orientations. Several researchers [12, 23] have reported that the fatigue life of specimens loaded under out-of-phase conditions is less than the life of specimens loaded under in-phase conditions. Non-proportional or out-of-phase loads cause the principal stress or strain axes to rotate and often result in extra cyclic hardening in the material [12].

In a study of proportional and non-proportional loading on 304 stainless steel, Socie [17] found that the non-proportional tests were more damaging (by a factor of 10) than proportional tests when compared on the basis of maximum principal strain range. His work also supports the

results presented by Fatemi and Stephens [12], who found an increase in cyclic hardening under out-of-phase loading. The critical plane, or plane for crack initiation, in Socie's [17] work is reported as the plane of maximum principal strain range for in-phase loading. A rotation of the crack initiation plane was reported in his work for out-of-phase load paths. The cracking direction found by Socie in his work [17] provides physical significance in support of a principal strain based theory.

The work done by Wu and Yang [24] on 304 stainless steel investigating the influence of load path on the strain-controlled multiaxial fatigue behavior of tubular specimens also supports the fact that the fatigue life, and direction of crack initiation and propagation, are highly dependent on the type of load path used. Their experiments showed that the fatigue lives of pure torsional tests were longer than those of pure axial tests under the same equivalent stresses. These findings are somewhat contradictory with the shear based theory of Findley [13]. The shear based fatigue theories proposed by Findley emphasize the importance of the maximum shear stress range as a key factor in the initiation of a fatigue crack whereas the results of Wu and Yang [24] show the importance of strain based tests and the analysis of strain for determining crack initiation and propagation phenomena. These findings on the other hand, support the strain based damage concepts proposed by Socie [17] and Brown and Miller [3]. Both of these research groups agree on the importance of normal strain on the maximum shear plane in the reduction of fatigue life. Tests consisting of combined axial and torsional loading were among the tests having the highest reduction in fatigue life [24], which reinforces the complexity caused by multiaxial loading in predicting fatigue lives.

2.6. Multiaxial Fatigue Modeling

Multiaxial fatigue models for crack nucleation can be classified into three major groups of equivalent stress based, energy based and critical plane based theories. The equivalent stress based fatigue models calculate the scalar equivalent stress from the multiaxial stress state, typically using the von-Mises or Tresca equations, and compares it to the uniaxial fatigue strength of the material. The energy based fatigue models [25, 26] take different approaches toward this problem and assume that fatigue crack nucleation is a function of the cyclic strain energy in the vicinity of the crack. However, the energy approach has its own limitations. The critical plane based fatigue models are derived on the observation that cracks initiate on certain planes (orientation) in the material, such as planes of maximum shear stress range, and are hence referred to as critical planes.

2.6.1. Equivalent Stress Based Models

The most common practice in analyzing multiaxial fatigue loading is to compute the equivalent stress amplitude from the cyclic stress components compare it with a failure criterion derived from suitable yield criteria. Two basic theories are widely used for this type of analysis. One is the Distortion Energy Theory of von-Mises and another is the Maximum Shear Stress Theory of Tresca [9]. Both of these static yield theories are being used to reduce the multiaxial fatigue stresses into equivalent uniaxial cyclic values. The original von-Mises and Tresca equations have been modified by several researchers, however, the most frequently used von-Mises and Tresca equations are shown below.

von-Mises Criterion

$$J_2 = \frac{1}{6}[(\sigma_1 - \sigma_2)^2 + (\sigma_2 - \sigma_3)^2 + (\sigma_3 - \sigma_1)^2] = \frac{\sigma_f^2}{3} \quad (2.5)$$

Tresca Criterion

$$\sigma_1 - \sigma_2 = 2\tau_f, \sigma_2 - \sigma_3 = 2\tau_f, \sigma_3 - \sigma_1 = 2\tau_f \quad (2.6)$$

Where J_2 is the second invariant of the stress tensor; σ_1, σ_2 and σ_3 are the principal stresses; and τ_f and σ_f are the fatigue failure stresses in shear and tension respectively [27]. Despite several controversies associated with these equations for their over and under prediction of fatigue life, these equations are widely used for proportional fully-reversed fatigue loading cases. However, these equations do not usually predict fatigue lives accurately when the loading cases are non-proportional; i.e., when the slope of the loading path in stress space does not remain constant. Several modifications to the von-Mises and Tresca equations have been proposed by researchers to incorporate the material properties, loading conditions and temperature effects.

Another important equivalent stress model was proposed by Gough et al. [28]. This model is basically a combined form of the von-Mises and Tresca criteria. Therefore, the model can be used for both ductile as well as brittle materials. This model, shown in Eq. 2.7 can be changed into the Maximum Principal Stress criterion when the ratio of the fatigue limits in torsion and tension becomes 1 and into the Maximum Shear Stress criterion when this ratio is 0.5.

$$\left(\frac{\tau_a}{\tau_f}\right)^2 + \left(\frac{\sigma_a}{\sigma_f}\right)^2 \left(\frac{\sigma_f}{\tau_f} - 1\right) + \left(\frac{\sigma_a}{\sigma_f}\right)\left(2 - \frac{\sigma_a}{\sigma_f}\right) = 1 \tag{2.7}$$

The equivalent stress criterion for multiaxial fatigue proposed by Lee [29] modified Gough's equation to incorporate the phase difference between bending and torsional loading. He also validated the following equation with his experimental data.

$$\sigma_{eq} = \sigma_a \left[1 + \left(\frac{bK}{2t}\right)^{\alpha}\right]^{\frac{1}{\alpha}} \tag{2.8}$$

where, $\alpha = 2(1 + \beta sin\varphi)$

The parameter K in this equation is twice the ratio of torsional and tension stress amplitudes. The constants b and t are the bending and torsional fatigue strengths for a given fatigue life, respectively; β is a material constant; and ϕ is the phase difference between bending and torsion loads. This equation was later modified by Lee [29] himself to incorporate mean stress effects.

Mowbray [30] modified the von-Mises equation and proposed functions in terms of the hydrostatic stress ratio to explain the variation of the fatigue properties σ_f and τ_f. Both of these terms are dependent upon the multiaxial loading and hydrostatic stresses. The final form of his

equation is similar to the Coffin and Mansion equation for prediction of fatigue life and is shown below. In this equation, A is a material constant, ν is Poisson's ratio, and λ_σ is the stress ratio.

$$\frac{\Delta\varepsilon_1}{2} = \frac{\sigma_f^{'}}{E} f(\lambda_\sigma, \nu)(2N_f)^b + \left(\frac{3}{3-A}\right)\varepsilon_f^{'} g(\lambda_\sigma, A)(2N_f)^c \tag{2.9}$$

where,

$$f(\lambda_\sigma, \nu) = \frac{(1-\nu\lambda_\sigma)}{\sqrt{\left(1-\lambda_\sigma+\lambda_\sigma^2\right)}}$$

$$g(\lambda_\sigma, \nu) = (2-\lambda_\sigma)\left[\frac{3\sqrt{\left(1-\lambda_\sigma+\lambda_\sigma^2\right)} - A(1+\lambda_\sigma)}{6\left(1-\lambda_\sigma+\lambda_\sigma^2\right)}\right]$$

2.6.2. Energy Based Approaches

One of the most widely known energy based fatigue theories was developed by Garud [25]. Garud calculated the plastic work per cycle of loading and suggested that this plastic work is the representation of shear stress and plastic strains. He divided each stress or strain cycle into several increments. The plastic work done in each increment was then computed and summed (Eq. 2.10) to determine the plastic work for one whole stress or strain cycle. The stress-strain curve used in the analysis done by Garud [25] was determined from uniaxial fatigue tests of smooth specimens. He further computed the total plastic work (Wc) and fatigue life (N) to crack

initiation. F in Eq. 2.11 is a monotonically decreasing function of Wc which is to be determined experimentally from common strain controlled axial tests on smooth specimens [25].

$$W_c = \int_{cycle} \Delta W_p = \sum_{cycle} \Delta W_p \tag{2.10}$$

$$N = F(W_c) \tag{2.11}$$

Another strain-energy based multiaxial fatigue criterion was proposed by Ellyn et al. [26] in 1988. This criterion is based on the assumption that the damage caused by fatigue loads is a function of the mechanical energy input into the material. Their criterion takes the hydrostatic stress, or mean stress, into consideration; however, they did not present any validation of this effect with the experimental data. They suggested that the total damaging strain energy density can be computed from the linear summation of elastic and plastic strain energy components of the fatigue cycle. This criterion is shown below in Eq. 2.12-2.14

$$\Delta W_t = \Delta W_e + \Delta W_p = (a\rho + b){N_f}^{\alpha} + C \tag{2.12}$$

$$\Delta W_e = \frac{1+\vartheta}{3E}(\bar{\sigma}^{max})^2 + \frac{1-2\vartheta}{6E}({\bar{\sigma}_{kk}}^{max})^2 \tag{2.13}$$

$$\Delta W_p = \frac{2(1-n')(2K')^{-1/n'}}{1+n'}(\Delta\bar{\sigma})^{(1+n')/n'} \tag{2.14}$$

In these equations $\bar{\sigma}$ is von-Misses equivalent stress, and n' and K' are the cyclic hardening exponent and cyclic strength coefficient, respectively. The total strain energy density was further related to the fatigue life (N_f) with a power-law type of equation. The constants k,ρ, α, and C were defined as material dependent parameters that must be determined from experiments. Ellyn et al. [26] claimed that the model can be used for both LCF as well as HCF multiaxial loading. Eqs. 2.13 & 2.14 do not contain any strain ratio terms nor the terms accounting for out-of-phase multiaxial loadings. Hence, recommendation of this equation for complex, non proportional load paths may not be appropriate.

In an experiment done by Findley [31] to discriminate between the stress based and energy based theories of fatigue, he loaded a disk along its diameter and the disc was then rotated relative to the loading under constant load. He determined that the strain energy at the center of the disk remained constant in spite of the fluctuating stress. From his experiment, Findley deduced that energy theories for fatigue cannot be taken as valid theories. As energy is not a linear function of stress, it must be calculated from the total stress and not from the components [31]. Hence, when plotting the energy cycle versus the stress cycle, energy cycles are not sinusoidal like stress cycles. Findley [31] further argued that energy can never be zero or negative whereas stress can be, and hence energy itself cannot be taken as the sole measure of damage when the stress is fluctuating. This argument presented by Findley [31] in 1957 demonstrated the better ability of stress based fatigue theories for estimation of fatigue damage over energy based theories.

To overcome the limitation of the pure energy based theories, Glinka [32] proposed an energy-based fatigue theory computed on the critical plane. Glinka computed the sum of the

elastic and plastic strain energy densities on the critical plane as shown in Eq. 2.15. His equation also included a mean stress term in it. Another critical plane based energy criterion (Eq. 2.16) presented by Farahani [33] takes the sum of the normal and shear energy ranges on the critical plane. The modified version of Glinka's [32] criterion (Eq. 2.17) was proposed by Pan Weng-Fang et al. [34]. They put emphasis upon the fact that the influence of shear strain energy on fatigue life should be different from the influence of normal strain energy. The constants k_1 and k_2 in Eq. 2.17 are weighting constants for stress and strain amplitudes, respectively.

$$W = \frac{\Delta\gamma_{12}}{2}.\frac{\Delta\sigma_{12}}{2}\left(\frac{1}{1-\frac{{\sigma_{12}}^{max}}{\tau'_f}}+\frac{1}{1-\frac{{\sigma_{22}}^{max}}{\sigma'_f}}\right) \tag{2.15}$$

$$W = \frac{1}{\sigma'_f\varepsilon'_f}.(\Delta\sigma_n\Delta\varepsilon_n)+\frac{\left(1+\frac{\sigma_n^m}{\sigma'_f}\right)}{\tau'_f\gamma'_f}(\Delta\tau_{max}\Delta\gamma_{max}) \tag{2.16}$$

$$W = \frac{\Delta\gamma_{12}}{2}.\frac{\Delta\sigma_{12}}{2}+k_1k_2\frac{\Delta\varepsilon_{22}}{2}\frac{\Delta\sigma_{22}}{2} \tag{2.17}$$

In an experimental study done by Wang and Yao [35] to compare the critical plane based energy criteria [32, 33, 34], they found the Farahani criterion to be the most satisfactory. However, significant scatter was observed [35] among all these energy based criteria. The scatter in the fatigue life predictions and argument proposed by Findley in 1957 [31], provides evidence that the consideration of energy on the critical plane does not produce a satisfactory prediction of fatigue behavior.

2.6.3. Critical Plane Modeling (Importance and Benefits)

Critical plane based theories represent another approach for the modeling of uniaxial and multiaxial fatigue crack development. The complete development of a significant fatigue crack can be considered as having two phases: nucleation and propagation. Both of these phases separately occur on particular planes which are called critical planes. The definition of a critical plane varies from researcher to researcher; however, one of the earliest critical plane models presented by Findley [13] refers to a critical plane as the plane of maximum shear stress range. He observed that the initial crack in any combination of multiaxial loadings lay in planes on or near the plane of maximum cyclic shear stress. Findley [13] writes in his paper that the repeated stressing causes repeated or reversed slip in certain grains, resulting in a disruption of the ordered atomic array along planes of slip and finally in the formation of a crack. As the crack becomes larger, the shear displacement between the faces of the crack increases with a consequent mechanical interference between the irregularities left in the wake of the crack. The resulting abrasion causes fine particles of the material to be torn and exude from the crack as dust [13]. The main benefit of critical plane theories is that they predict an orientation and location of dominant fatigue crack nucleation because they utilize a combination of normal and shear stresses or strains on the particular plane. Brown and Miller [16] also supported the concept that the crack initiates on the maximum cyclic shear plane. Their paper explains that shear strain and strain normal to the plane of maximum shear strain are the governing parameters for fatigue crack initiation and early growth.

The value of shear stress or strain on the critical plane can be computed by any plane rotation concepts of continuum mechanics. For proportional loading, this rotation is straight forward for each cycle, whereas for non-proportional loading, the orientation of the principal

stress and strain axes rotates relative to a fixed coordinate system on the specimen [12]. Because the rotation of the principal axes causes additional cyclic hardening of the material [12], low-cycle non-proportional loading is more damaging than low-cycle proportional loading. As a result of this phenomenon, Fatemi and Kurath [11] do not recommend the damage parameter of Brown and Miller [16] to be used for non-proportional load paths. Fatemi and Socie [4] proposed a damage parameter that incorporates the normal stress on the maximum cyclic shear strain plane to take into account this extra cyclic hardening due to non-proportional loading.

The critical plane based models vary in nature depending upon their ability to deal with actual loading cases. These models can also be categorized depending upon whether the model is good for high cycle fatigue or low cycle fatigue. The models are also categorized depending upon the stress-based or strain-based terms in them. Both the high-cycle and low-cycle fatigue models are good for each particular type of loading. However, practical cases generally consist of a mixture of these two types of loadings; hence, the interaction between high-cycle fatigue and low-cycle fatigue damage becomes important to consider.

2.6.3.1. Stress Based Critical Plane Fatigue Damage Parameters

One of the earliest stress-based critical plane models was proposed by Findley in 1957 [13]. His model relied on the physical observation of the orientation of the initial fatigue crack in steel and aluminum alloys. He also considered the influence of the normal stress acting on the maximum shear stress plane. He suggested that the sum of the shear stress and normal stress amplitude and maximum normal stress on the critical plane dictated the rate of fatigue crack initiation, and suggested a parameter of the following form:

$$\tau_a + k\sigma_{max} = f(N_f) \tag{2.18}$$

Where k is a material dependent parameter.

Another stress-based critical plane fatigue model was proposed by McDiarmid [36]. His criterion (equation 2.19) is similar to the Findley [13] model, but with each of the shear stress and normal stress terms divided by their respective fatigue strengths (τ_f, σ_f). He suggested that the fatigue life is a function of the shear stress amplitude and the maximum normal stress on the plane of maximum shear stress amplitude:

$$\frac{\tau_a}{\tau_f} + \frac{{\sigma_n}^{max}}{2\sigma_f} = f(N_f) \tag{2.19}$$

The stress-based criterion proposed by Matake [37] equated the linear combination of normal and shear stress amplitudes on the critical plane with a product term of torsional fatigue strength and life ratio. The terms $\tau_f,\ N_\tau,\ N_f$ & m_τ in equation 2.20 are the torsional fatigue strength, number of cycles to failure, number of cycles corresponding to the torsional fatigue limit and the exponent of the S-N curve for torsional loading respectively. Carpinteri and Spagnoli [38] proposed a nonlinear relationship (Eq. 2.21) between the maximum normal stress and the shear stress amplitude on the critical plane. The parameters l_c, m_c, n_c are the direction cosines of the critical plane and T_e and S_e are the torsional and uniaxial endurance limits.

$$\tau_a + k\sigma_a = \tau_f \left(\frac{N_\tau}{N_f}\right)^{\frac{1}{m_\tau}} \tag{2.20}$$

$$\left(\frac{\tau_a(l_c, m_c, n_c)}{T_e}\right)^2 + \left(\frac{{\sigma_n}^{max}(l_c, m_c, n_c)}{S_e}\right)^2 \leq 1 \tag{2.21}$$

In a comparative study performed by Ninic and Stark [39], using McDiarmid's [36] and Carpinteri and Spagnoli's [38] criteria, the later model (Eq. 2.21) was found to be effective at predicting multiaxial fatigue life with significant accuracy. McDiarmid's [36] criterion also found to be good for predicting the fatigue life of ductile metals. The only weakness of Carpinteri and Spagnoli's [38] criterion was its inability to deal with mean stresses.

Another recent work performed by Erickson et al. [5] considered the effects of shear mean stress, maximum normal stress, and the possibility of multiple normal stress subcycles on the plane of maximum shear stress range:

$$DP = \tau_{max}\left(1-\frac{\tau_{min}}{\tau_{max}}\right)^{w_1}.\left[1+\frac{k^{+}\sigma_{max}+k^{-}\sigma_{min}}{\sigma_y}\right]^{w_2}+k_2\sum\sigma_{max}\left(1-\frac{\sigma_{min}}{\sigma_{max}}\right)^{w_3} \quad (2.22)$$

The first stress based term in the above Eq. 2.22 was introduced to model the torsional mean stress effect. The second multiplicative term in this parameter was intended to model the effect of normal (tensile) stress on the maximum shear stress plane. The maximum shear stress and maximum normal stress may not occur at the same time during non-proportional loading conditions, and considering only the maximum normal stress over the cycle into the computation cannot account for the entire effect created by the normal stress cycles in the opening of a crack [5]. Hence, an additional term was introduced to include the value of the normal stress acting at the shear stress reversal points by Erickson et al. [5]. The third term was introduced into the model to account for the effect of multiple normal stress "sub-cycles" occurring within the dominant shear stress cycle on the critical plane. A summation sign in the third term was applied to take into account all the normal stress sub-cycles within the particular shear cycle on the

critical plane. This criterion has shown a good correlation between experimental and predicted fatigue life for a wide range of proportional as well as non-proportional multiaxial fatigue data. The only weak part of this model is the complexity of implementation and large number of material dependent parameters.

Most of the stress-based fatigue damage models work well with high cycle fatigue data where the amplitude of fatigue loading is almost elastic and the stresses experienced by a specimen produce little or no plastic deformation. However, when the material is exposed to stresses in the range of the yield strength or higher (as in the case of low cycle fatigue), due to plastic yielding, a small increase in stress may cause a very large increase in strain within the material. The microscopic explanation to this phenomenon has been reported by Fisher et al. [40]. Austenite transformation to martensite during plastic yielding results in intense local plasticity which consequently leads to strong hardening and a significant increase in uniform strain [40]. From an experimental point of view, the measurement of strain at this high stress level is more precise than measuring corresponding stress.

2.6.3.2. Strain Based Critical Plane Fatigue Damage Parameters

A well known strain based critical plane fatigue damage parameter was obtained by modifying a uniaxial model proposed by Smith, Watson and Topper [10]. The mathematical form of the model is shown in Eq. 2.23. The parameters $\sigma_f^{'}, \varepsilon_f^{'}, b, c$ are the fatigue strength and ductility coefficients and exponents obtained from uniaxial fatigue tests. $\Delta\varepsilon/2$ is the maximum principal strain amplitude and σ_{max} is the maximum normal stress on the critical plane. This equation has been found to be good for predicting the low cycle fatigue behavior of certain materials.

$$\sigma_{max}\left(\frac{\Delta\varepsilon}{2}\right) = \frac{\sigma_f^{'2}}{E}(2N_f)^{2b} + \sigma_f^{'}\varepsilon_f^{'}(2N_f)^{b+c} \quad (2.23)$$

Another strain based critical plane damage parameter was proposed by Brown and Miller [3]. Their model (Eq. 2.24) is simple and efficient for multiaxial in-phase loadings. Brown & Miller [3] suggested the sum of the maximum shear strain and the strain normal to the maximum shear strain as the governing parameter for fatigue crack development. In this equation, S is a material parameter and can be determined experimentally. This theory has been shown to not correlate multiaxial out-of-phase fatigue data due to the rotation of principal stress and strain axes.

$$\gamma_{max} + S\varepsilon_n = constant \quad (2.24)$$

A model (equation 2.25) proposed by Fatemi and Socie [4] used the normal stress value on the critical plane multiplied with the shear strain amplitude. The definition of critical plane used by Fatemi & Socie was the plane of maximum damage parameter value. Zhao and Jiang [41] proposed another strain based model, and the mathematical form is shown below in Eq.2.26. $\Delta\varepsilon$ is the strain range and N_f is the number of cycles to failure. The symbols ε_o, ξ and C are constants obtained by fitting experimental data.

$$\frac{\Delta\gamma_{max}}{2}\left(1 + K\frac{\sigma_n^{max}}{\sigma_y}\right) = constant \quad (2.25)$$

$$\left(\frac{\Delta\varepsilon}{2} - \varepsilon_0\right)^{\xi} N_f = C \quad (2.26)$$

2.7. Mean Stress Effects in Multiaxial Fatigue

Mean stress (or mean strain) can have a substantial effect on the fatigue behavior under multiaxial loading. However, the nature of the mean stress plays an important role in the damage process. It has been observed in most cases that tensile mean stresses are detrimental and compressive mean stresses are beneficial in nature. The effects of mean stresses in uniaxial fatigue loading cases have accounted for by the classical fatigue models of Goodman, Gerber and Morrow among others. A review of the literature suggests that the effect of mean stress on the fatigue behavior of a specimen depends upon the material; however, for uniaxial loading, the Gerber parabola well represents most of the experimental data sets when the ratio of mean stress to ultimate tensile strength is plotted against the ratio of alternating stress and fully reversed fatigue strength. For multiaxial loading, mean stress effects are included in the fatigue models proposed by Findley [13], Sine et al. [42], Crossland and coworkers [43], Fatemi and Socie [4], Erickson et al. [5]. The mean stress fatigue model (Eq. 2.27) of Sine et al. [42] takes an average of the mean principal stresses whereas Crossland & coworkers [43] proposed a mean stress model (Eq. 2.28) with the maximum value of hydrostatic stress instead of the average normal stress.

The mean stress models of Sine et al. [42] and Crossland & coworkers [43] are specially derived to account for mean stress effects. The models of Findley [2], Fatemi & Socie [4], and Erickson et al. [5] use the maximum stress as a combination of amplitude and mean over the fatigue cycle. Findley performed mean stress studies under combined bending and torsion

loadings [2] in HCF regime. Socie et al. [17] also studied mean stress effects on Inconel 718 under combined tension and torsion loading. He [17] applied two loading cases with one having zero to tension and another having zero to compression loading. The experiments revealed the fact that a specimen with a crack that had already nucleated did not exhibit any further growth under compressive mean stress. Fatemi and Kurath [11] performed an experimental study on Inconnel 718 and 1045 steel with a variety of load paths and concluded that mean stresses can have a significant influence on the fatigue life if they do not relax. One of the important findings of their experiments was that mean strains did not affect the fatigue life in situations where the mean stresses quickly relaxed.

Sine et al. model [42]

$$\tau_a + \alpha_s p_m = \beta_s \tag{2. 27}$$

Where,

$$p_m = \frac{\sigma_1^m + \sigma_2^m + \sigma_3^m}{3}$$

Crossland and coworkers [43]

$$p_{max} = \frac{\sigma_1^{max} + \sigma_2^{max} + \sigma_3^{max}}{3} \tag{2.28}$$

2.8. Effect of Temperature on Fatigue

Metals used in aircraft engine components or the exhaust systems of an automotive engine are subjected to multiaxial fatigue conditions at high temperatures. These high temperatures with multiaxial fatigue loads complicate the damage process. In the research done by Uematsu et al. [45] on smooth specimens of type 444 stainless steel under fully-reversed axial

loading, he observed a significant decrease in the fatigue strength of the material with increasing temperatures. The crack initiation phenomenon in stainless steel occurred much earlier at a high temperature in comparison to that at normal room temperature [45]. However, the effect of high temperatures on the initiation of fatigue cracks is still not completely investigated.

Much of the literature available on high temperature fatigue focuses on the growth of cracks. This area of study has received significant attention among researchers working on the automotive exhaust systems or aircraft engine components due to increased sensitivity towards engine emissions and efficiencies. Maintaining a high temperature during fatigue experimentation is another challenging issue. Xu et al. [46] used high temperature water to conduct a series of low cycle fatigue experiments on stainless steel. During cyclic loading, the irreversible nature of dislocation glide leads to the development of surface roughness and strain localization in persistent slip bands, which eventually leads to the formation of extrusions and intrusions. As a result, micro cracks may form in the persistent slip bands or at the edges of slip band extrusions [46]. The conclusion can be deduced from this literature that the amount of damage increases in multiaxial fatigue loading cases in elevated temperature environments.

2.9. Cumulative Damage Approach

A loading spectrum may consist of uniform (constant) amplitude cycles or variable amplitude cycles. Constant amplitude fatigue loading implies that the alternating cycles have a consistent amplitude and range of stress or strain. Variable amplitude loading is a more complicated but realistic scenario of fatigue loading where the amplitude of the load cycles varies in each cycle. Most machine components experience variations in loading amplitude during their service lifetimes, where cyclic amplitudes may vary from small to large cycles. Each

cycle contributes to the overall fatigue damage in the specimen, in a manner proportional to the magnitude of load. To predict the fatigue life of a component subjected to variable amplitude loading; it is required that fatigue damage caused by each cycle be accurately computed and summed over all the cycles in the load spectrum.

A suitable model for fatigue crack nucleation must address all the complexities in these variable load cycles and should account for the damage caused by each of the different types of loading in the total fatigue damage computation. The process of calculating the fatigue damage per cycle, and summing the damage until a critical value for failure is reached, is referred to as fatigue damage accumulation or cumulative damage. A reliable cumulative damage model should address the damage caused by both, large, highly damaging (LCF) cycles, and smaller, low damage (HCF) cycles, as well as account for the possibility of nonlinear interaction effects between them. The precise computation of damage for both of these types of cycles can be a difficult task since both of the LCF and HCF load levels can have different mechanisms of fatigue damage in materials.

2.9.1. Linear Damage Rule

The simplest method for computing cumulative fatigue damage was conceptually described by Palmgren [6] in 1924 and subsequently presented in mathematical form by Miner [7] 20 years later. The concept of a linear summation of fatigue damage is currently known as the Palmgren-Miner linear damage rule (Eq.2.29). This rule calculates the fatigue damage as the ratio of the number of applied cycles at a given load level to the number of cycles to failure at that level. These cycle ratios are then summed for all the load levels in the history. The rule predicts failure when this summation reaches a value of unity. The physical concept behind this

rule is the constant absorption of work per cycle and a characteristic amount of work associated with failure of the material [48]. As shown in equation 2.29, damage is computed for i^{th} loading level, and summed over a total number of j load levels.

$$D_i = \sum_{i=1}^{j} \frac{n_i}{N_i} \tag{2.29}$$

Experimentally, it has been found that, this rule provides a very rough estimation of the fatigue damage under variable amplitude loading. Although this rule does not account for many complex issues like load sequence effects, load level dependency and load interaction effects, it is the oldest and most widely accepted cumulative damage theory. This rule often over-predicts or under-predicts the actual damage depending upon the type and sequence of the load levels. For example, when load sequence is arranged in such a way that high load level cycles are followed by low load level cycles; this ratio generally does not reach a one at failure when compared to experimental data. Similarly, when the load sequence is arranged from low levels to high levels, this summation is often greater than one at the time of failure.

Several other linear damage rules [49, 50, 51] were proposed during the mid-20th century. Lim et al. [49] proposed a linear cumulative damage theory based on metallurgical concepts. Coffin and co-workers [50] presented a linear damage rule in terms of plastic strain range, and Topper and Biggs [51] related a linear damage rule to experimental values. However, all of these versions of linear cumulative damage rules possess the same deficiencies, and do not provide good agreement with experimental data.

2.9.2. Double Linear Damage Rule

The double linear damage rule (DLDR) is an extension of the linear damage rule (LDR). This model decomposes the whole fatigue damage process into two stages, with each stage modeled by a separate linear damage rule. The two stage cumulative damage concept was first proposed by Grover [52]. The concept is mathematically similar to Miner's rule, but when applied to two different stages; it improves the capability of the linear damage rule to account for the deficiencies of Miner's rule [7]. The concept was later presented by Manson [53] in a more practical form in 1966. Manson's recommendation was initially similar to the concept proposed by Grover [52].

Initially, Manson [53] performed experiments on only one material and proposed that the crack initiation period be $N_i = N_f - 15N_f^{0.6}$ for $N_f > 750$ cycles and 0 for $N_f < 750$ cycles. The relation for the propagation period was given as $15N_f^{0.6}$ and N_f for greater than and less than 750 cycles, respectively. This rule was proposed based on a limited number of experimental data, and no further explanation on the generalization of the rule for other materials was suggested by Manson [53]. Subsequently, a revised version of the DLDR was proposed by Manson [53], with the model being tested on several materials. He also explained that the terms "crack initiation" and "propagation" do not have any physical basis, and it is very ambiguous at which life values the physical crack initiates and starts propagating [54]. Manson [54] named these two stages of crack development as stage I and stage II, as illustrated in Fig. 2.1. The intersection point between these two LDR lines was named as knee point [54]. The experimental observation by Manson and Halford [54] did not observe any physical crack at this knee point. The shifting of

knee point was another problem in Manson and Halford [54] DLDR when dealing with combination of different load levels.

The difficulty in determining this knee point precisely is the main deficiency of the double linear damage rule. Manson and Halford [54] later on did not invalidate the potential use of this concept, but were not satisfied with the experimental validation of their mathematical model of the DLDR.

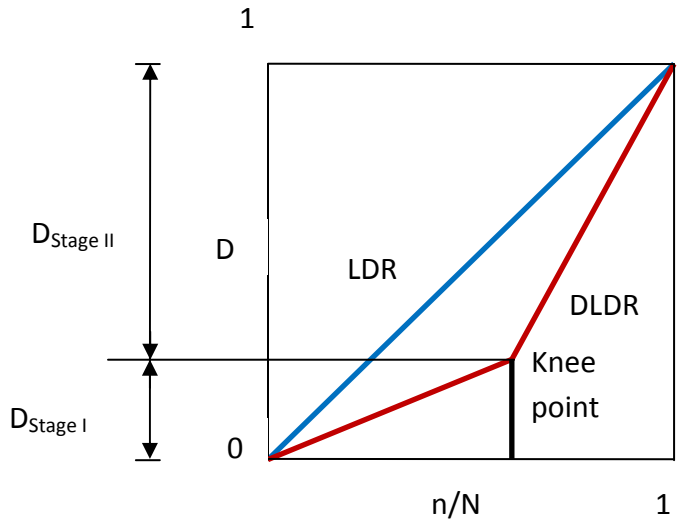

Figure 2.1: Illustration of LDR and DLDR

2.9.3. Nonlinear Cumulative Damage

Several nonlinear cumulative damage rules have been proposed in the technical literature. Generally, these rules change the linear and double linear damage lines into smooth curves when damage is plotted versus the cycle ratio (cycles applied over cycles to failure). The damage curve or nonlinear damage accumulation concept was first proposed by Richart and Newmark [55]. They articulated that the modeling of the fatigue damage process cannot be represented by a

single or double linear line; it progresses in a nonlinear manner. The concept was later presented in a quantitative form by Marco and Starkey [56] as the first nonlinear damage rule.

If $r_i = \frac{n_i}{N_{f_i}}$

$$D = \sum r_i^{x_i} \tag{2.30}$$

Marco and Starkey [56] presented a power-law type of nonlinear damage equation (Eq. 2.30), where they used an exponent on the cycle ratio for each load level. This exponent was introduced to take sequence effects into account. This theory can thus be taken as an improvement on the linear damage rule, as it can account for the sequence of loading and predict the damage more precisely than the Miner's rule [7]. The value of the exponent x_i is a variable number depending upon the type of sequence (high-low or low high), and must be assigned for each load sequence. Hence, this rule a little difficult to implement as each load sequence needs an extra parameter to be evaluated. The rule reduces to Miner's [7] rule when this value is equal to 1.

The nonlinear damage rule proposed by Manson and Halford [54] suggests that damage accumulates nonlinearly along a curve associated with a particular life (or load) level and each level has a separate nonlinear damage curve. The damage curve concept [54] comes from the fact that damage accumulation does not follow a linear or double linear line when represented in a damage (D) versus cycle ratio (r = n/N) diagram. The damage accumulation process moves from

one damage curve in the (D-r diagram) to another damage curve (D-r diagram) on as each new load level is applied. The graphical representation of the damage curve can be observed in Fig. 2.2. Each of the blue lines represents the amount of incurred for a given number of applied cycles (n_i) at a particular load level associated with a life of N_i . Hence, if several load levels are applied, the damage curves can be used to approximate the nonlinear progression of damage contributed by each load level. The mathematical model of Manson and Halford [54] came after several revisions.

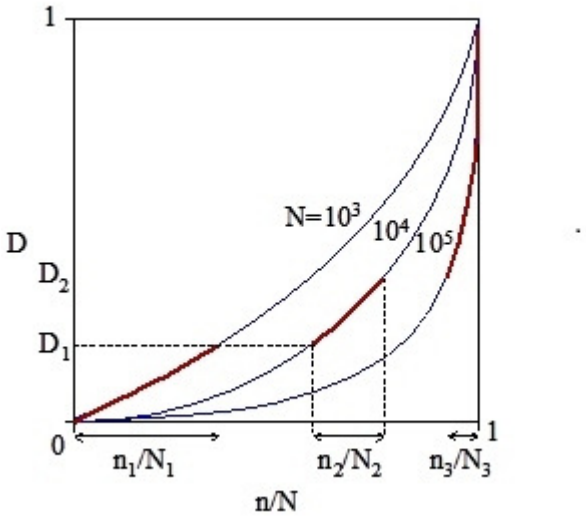

Figure 2.2: Damage Curve Approach

$$D = \left(\frac{n}{N_f}\right)^{\left(\frac{N_f}{N_{ref}}\right)^{\alpha}} \tag{2.31}$$

$$D = \frac{1}{0.18}\left[a_0 + (0.18 - a_0)\left(\frac{n}{N_f}\right)^{\left(\frac{2}{3}\right)N_f{}^{0.4}}\right] \tag{2.32}$$

The most general form of the equation for the damage curve is shown in equation 2.31. The symbols n and N_f are the number of applied cycles and cycles to failure at a particular load level, respectively, N_{ref} is the life level at which damage accumulates linearly, and α is a material parameter that must be determined experimentally. The value of N_{ref} is often taken as 1, since the accumulation of damage within a single cycle cannot easily be determined. For two-level fatigue tests, Manson and Halford [54] recommended a value for α of 0.4, and proposed a specific form of the damage curve equation shown in equation 2.32. Here, a_0 represents the initial length of the fatigue crack, which may be assumed to be zero.

The cumulative damage rules proposed by Miner [7], Grover [52], Marco & Starkey [56] and Manson and Halford [54] were based on uniaxial test data, and no comments about multiaxial fatigue data were made in these papers. The biaxial and tri-axial stress states experienced by the combination of axial and torsion loading with varying phase angle can create a very complicated situation.

$$D_1 = \frac{n_1}{N_1} \tag{2.33}$$

$$D_2 = \left(\frac{n_2}{N_2}\right)^{\left(\frac{1}{\beta J}\right)\left(\frac{N_1}{N_2}\right)^{0.4}} \tag{2.34}$$

$$J = \frac{1.57}{T\varepsilon_{1max}} \int_0^T |sin\xi(t)| \,.\, \varepsilon_1(t) dt \tag{2.35}$$

The multiaxial cumulative damage rule recently proposed by Xu et al. [58] was validated using sequential biaxial fatigue data. Xu et al. [58] conducted a series of axial/torsion fatigue tests with both in-phase and out-of-phase loading in different combinations and correlated the data with their proposed model (Eq. 2.33, 2.34 & 2.35). This model resembles Manson & Halford's [54] uniaxial cumulative damage model (Eq. 2.31) with a different exponent, which is modified to fit the multiaxial fatigue data [58]. The symbols n_1 and n_2 are the applied number of cycles at two loading levels and N_1 and N_2 are the cycles required to fail at those particular loading levels. They introduced a non-proportionality factor J in the exponent of Manson and Halford's [54] two-level cumulative damage equation (Eq. 2.32). This non-proportionality factor, J, which was originally introduced by Itoh et al. [59] , is based on the absolute value and the angle of maximum principal strain at a particular time step [59]. It can also be taken as the area under the principal strain curve for non-proportional loading [58]. J becomes 0 for proportional loading and 1 for completely 90^0 out-of-phase loading. For the non-proportional loading cases of Xu et al. [58], J was found to be 0.35 and 0.31. The integral equation for J has been shown in equation (Eq. 2.35). The constant β is the material hardening coefficient. β becomes 0 for the cases where no additional hardening has occurred.

2.10. Multiaxial Cumulative Damage Under Variable Amplitude Loading

Multiaxial variable amplitude cycling involves loads which cause the stress state to vary in magnitude, direction and time. Most of the cumulative damage theories [7,52,54,55,56] discussed so far only considered uniaxial loading conditions and the experiments performed by researchers to validate the models consisted of uniaxial block loading tests in which two or more level of constant amplitude fatigue cycles were applied in different combinations. Multiaxial

variable amplitude fatigue tests were performed by Xu et al. [58] in which for two and three levels of multiaxial cyclic loading were applied in different sequences. Some of the theories [54,56,58] have been shown to be capable in simulating the sequence effect and load interaction effects for both uniaxial and multiaxial loading cases. However, actual service loadings are much more complicated than ordered multilevel multiaxial loadings. For example, the stress or strain histories in aircraft engine components may vary in a random manner and it becomes difficult to simulate these loading scenarios through multi load-level experiments. Furthermore, specimens are tested under variable amplitude cyclic loading; the mathematical computation of damage faces two major difficulties. The first involves the identification of the significant damaging cycles, and the second involves the definition of the tensile or shear stress and strain values for each of the identified cycles.

Several cycle identification techniques such as the rainflow method, range-pair method, race-track counting method, level-crossing method or peak counting method can be found in the literature [9]. All of these techniques have different methods for identifying the significant damaging cycles from the entire variable amplitude load spectrum, and there are situations where many of these methods may identify unreasonable cycles. The range-pair counting method can under-predict the damage since it eliminates the smaller cycles from consideration and takes only the range of major peak values. Similarly, the racetrack method also eliminates all the small ranges. The level crossing and peak counting methods do not retain the order of cycles and thus eliminate all the sequence effects present in the original spectrum [9]. The rainflow counting method, on the other hand, has been the well accepted [60-62], and is considered one of the more reasonable cycle counting methods since it takes all the significant peaks into consideration, and it better represents the actual stress-strain behavior of the material.

Once the cycles have been defined, the next task is to identify the corresponding stress and strain values for each of significant damaging cycles. Most accepted cycle identification techniques, like the rainflow cycle counting method, form a new set of cycles with peaks and valleys that do not necessarily retain the original sequence of loading. During multiaxial loading, the situation is further complicated since the individual stress and strain components may all cycle independently of one another. This creates an additional problem in locating all the stress and strain values required by the damage parameter for a particular cycle within the logic of the cycle identification technique. The method proposed by Bannantine and Socie [60] counts one of the normal strain or shear strain cycles using the rainflow method on each plane. The selection of normal strain or shear strain for cycle counting is dependent upon the type of cracking mode (I or II) for the particular material. The other stress and strain terms are separately located for each identified cycle on each plane. The final value of cumulative damage is computed using Miner's rule on each plane, and the plane having a maximum value of Miner's damage summation is considered as the critical plane or failure plane. Wang and Brown [61] proposed another theory based on the computation of the equivalent strain at each time point. This equivalent strain is computed using the von-Mises definition at major turning points [61]. The value of normal and shear strain are computed relative to this equivalent strain. Langlais et al. [62] cycle counted shear strain with the rainflow method and considered it as the main channel for the cycle counting algorithm. All the other parameters like shear and normal stress and strain are determined on the basis of the main channel data. Each time point in the main channel is taken as the basis to search for the maximum values of stress and strain from the auxiliary channels. The values of normal and shear stress and strain from the main and auxiliary channels are then used to compute the amount of cumulative damage and fatigue life of the specimen.

The methods proposed by Bannatine and Socie [60], Wang and Brown [61] and Langlais et al. [62] have one thing in common. They all rainflow count only one stress or strain component, and all the other components are evaluated on the basis of the primary rainflowed term. The approach of Bannatine and Socie [60] fails to address the complexity of the computation of maximum normal and shear stress/strain components at a particular time point because these terms do not always coincide. This theory also includes the deficiencies of the Miner's rule and hence, sequence and load interaction effects are neglected. The theory proposed by Wang and Brown [61] changes the critical plane for each reversal, hence it is more logical. However, this concept can result in over-prediction of damage. The concept of extending the uniaxial rainflow method to multiaxial loading presented by Langlais et al. [62] takes the maximum value of the normal stress between the identified time points of the main channel. This theory may under-predict the damage if more than one similar peak of the auxiliary components are available in between the time points of the main channel.

2.11. Influence of Cyclic Loads Below the Endurance Limit

Fatigue cycles below the endurance limit have very low stress or strain amplitudes and are generally considered non-damaging by most of the cumulative damage methodologies. However, several experimental and analytical results have been presented by researchers [63,64,65] which advocate the consideration of damage caused by these small loading cycles or HCF damage. The widely accepted Miner's rule assumes no damage is caused by cycles with load levels below the endurance limit. As Miner's [7] rule is dependent upon the S-N curve only, researchers [66,67] have used several extrapolation techniques for the S-N curve to compute the HCF(small cycle) damage. The concept of the S-N curve extrapolation was originally proposed

by Haibach [66]. If the slope of the S-N curve above the endurance limit is taken as k (as determined from S-N tests at stress levels above the endurance limit), it can be modified in three different ways. The S-N curve can be extrapolated with the same slope k to the lower stress levels to predict the damage value using the Miner elementary rule proposed by Mayer et al. [67]. Haibach [66] proposed the modified Miner rule [7] where the S-N curve below the endurance limit is extrapolated by a second linear line with a slope of $k' = 2k - 1$. Using the original Miner rule, the slope value for loads below the endurance limit is zero because the line becomes horizontal in this region. The graphic illustration of the three Miner rules are explained by Mayer et al. [67] and shown in Fig 2.3.

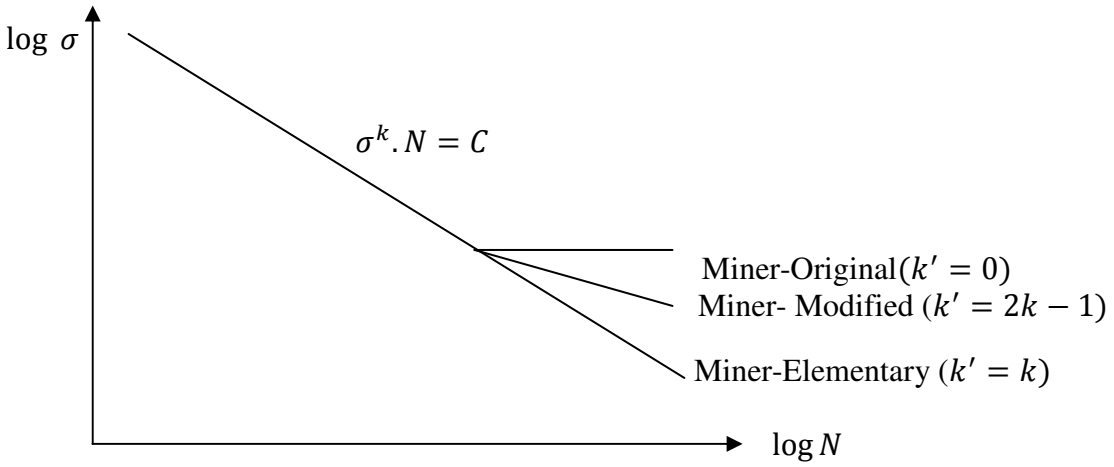

Figure 2.3: Modified Miner rules [67]

The experimental results of Mayer et al. [67] reveal that the fatigue life may be reduced is reduced by a factor of 2 to 4 compared to the value predicted by the original Miner rule when

smaller cycles are introduced. Mayer et al. [67] validated the results by performing two and three level block loading tests with cycles above and below the endurance limit in different combinations. Reductions in fatigue lives and increased rates of fatigue crack propagation due to small load cycles have also been reported by other researchers [63,64,65]. In a microscopic study conducted by Hines and Lutjering [68] on two microstructures of Ti-6Al-4V (a commonly used material for aircraft engine components), a significant number of small fatigue cracks were observed due to low load cycles. The damage parameter (Eq. 2.36) for smaller cycles proposed by Ngiau and Kujawski [63] also used the basic concept of Miner's rule. Their comparisons of the predicted and experimental values of damage also contained different combinations and sequences of LCF and HCF loading. Their study revealed that intermittent small cycles with amplitudes as low as 50% of the endurance limit, within regular LCF service loading conditions, created significant damage [63].

$$D_{small} = 1 - \frac{N_{applied}}{N_{failure}} \tag{2.36}$$

Most of the research studies [63-68] that have been performed for computing fatigue damage due to small cycles use Miner's rule as the basis for damage computation. Hence, all of these models carry the deficiencies (load interaction and load sequence effects) of Miner's rule with them. The damage created by HCF cycles when coupled with LCF cycles, creates non-linear damage accumulation, and the linear summation of cycle ratios ignores all the load interaction and load sequencing effects.

2.12. LCF and HCF Interactions

Low cycle fatigue research received had gotten a significant amount of attention during the 1960's and 1970's. A significant improvement in the fatigue resistance of aircraft engine components from LCF cycles was observed [69] due to these efforts. However, failures due to HCF cycles and failures caused by the interaction of both LCF and HCF cycles are still being studied. Many of the common testing methodologies like accelerated mission testing are designed to test primarily LCF failures. Recent studies [70,57,71,72] have shown that it is not only the LCF cycles that are responsible for fatigue damage accumulation in metals. The damage from HCF cycles and the interaction effects of the LCF and HCF cycles are critical in the fatigue damage accumulation process.

Recent research done by Goodin et al. [71,72] on Ti-6Al-4V tested under several simulated mission histories (consisting of different combinations of axial and torsional loading) has demonstrated a strong interaction between LCF and HCF cycles in contributing to the fatigue damage accumulation. The experiments done by these researchers [70-72] consisted of several two-level and three-level cyclic block loading tests which consisted of, highly damaging (LCF) cycle ad 5-50 small (HCF) cycles. The load path for the LCF cycle was often non proportional in these tests. Life reductions of a factor of 3 to 25 were reported due to the introduction of 5-50 HCF cycles in the mission histories, when compared with the corresponding LCF fatigue life [71]. However, their experimental results revealed the fact that the interaction of LCF and HCF cycles is significantly influenced by the type of load path applied. Goodin et al. [57] considered used several critical plane based damage parameters and found that the critical plane model proposed by Findley predicted better and more reasonable results than others. The damage values were computed on each plane for both LCF and HCF cycles by these researchers and the

interaction effects were observed by comparing the orientations of the critical planes for both the LCF and HCF cycles. The load paths which resulted in the most significant reductions in fatigue life during experimentation had coinciding critical plane orientations between the LCF and HCF cycles. The experimental results obtained from these tests also support the fact that the primary cause of fatigue crack initiation in metals is cyclic shear stresses/strains [72].

CHAPTER 3. RESEARCH METHODOLOGY

3.1. Overview

The study of metal fatigue can be divided into two broad categories of constant amplitude and variable amplitude loading. The study of constant amplitude metal fatigue is normally used to obtain the stress-life or strain-life curves for a particular material and it provides a broad understanding of the fatigue damage accumulation process in materials under various cyclic loading conditions. However, most real-world fatigue conditions are variable amplitude in nature, and may consist of several combinations of LCF and HCF cycles. Hence, a systematic study of metal fatigue needs careful analysis of the fatigue behavior under both constant and variable amplitude loading conditions.

Constant amplitude or baseline fatigue tests give the material response under any combination of proportional or non-proportional cyclic loading cases. Hence, a careful analysis of baseline fatigue test data is required to develop a reliable methodology to predict the life under this type of loading. Variable amplitude metal fatigue cases involve more complicated combinations of constant amplitude loading cycles. Hence, the study and analysis of constant amplitude fatigue data provides the foundation for more complicated metal fatigue analyses.

The study of variable amplitude fatigue may involve the consideration of various combinations of different constant amplitude load levels (LCF & HCF) completely random loading histories. Both LCF and HCF cyclic loads contribute to the overall fatigue damage accumulation process [57, 71, 72]; however, the analysis of fatigue damage due to LCF/HCF interactions is still not fully understood. The traditional S-N curve extrapolation approaches proposed by other researchers [66 & 67] give very crude estimations of the effects of HCF cycles

on the overall fatigue damage accumulation process. As HCF cycles have very small amplitudes of load, they are often considered to contribute o damage in common fatigue analysis models. This assumption is valid when the material is loaded separately with LCF or HCF cycles. However, most actual cases of fatigue loading involve the application of both LCF and HCF cycles mixed in a very complex manner. The results of previous fatigue tests with various combinations of LCF and HCF cycles have shown the strong influence of HCF loading on fatigue damage accumulation in high strength alloys. Recommendations for the consideration of HCF cycles and their interactions with LCF cycles during damage analysis have also been advocated by other research groups [54, 57, 71 & 72]. All of these studies demonstrate the influence of the LCF load path, load level, and the LCF/HCF interaction effect on the overall reduction of the component fatigue life. The effect appears to be more prominent when the nature of the cyclic loading is multiaxial and non-proportional.

Another important aspect of variable amplitude fatigue analysis is the level of LCF pre-damage required to initiate HCF damage. Experimental results have shown that the level of LCF/HCF interactions varies with the type of loading in the history. The analysis of previous test data [89] prompts further research to investigate the amount of pre-damage created by the LCF cycles that is required before the HCF cycles will contribute to a significant increase in damage accumulation. In other words, there a "threshold" level of LCCF damage that must be exceeded before HCF damage starts to accumulate (even if the HCF cycles are below the endurance limit).

This concept of an LCF threshold damage level can be related to some of the previous studies [70, 74, 75] done in this area. Nicholas and Maxwell [70] investigated LCF/HCF interactions with completely reversed LCF cycles and HCF cycles having a stress ratio of 0.5.

Laning et al. [74] carried out similar studies. Mall et al. [75] studied the effect of LCF pre-damage and LCF/HCF interactions with different LCF stress ratios. All of these groups agree on the fact that if a crack has already been formed during the LCF testing, overloading or under-loading may subsequently influence the remaining HCF fatigue strength of the metal. However, none of these groups have come up with a mathematical model to correlate these interactions with the overall fatigue life of the specimen. It should also be noted that type of fatigue loadings used in these studies [70, 74 & 75] was uniaxial. Multiaxial loads can add to the complexity and types of interactions between LCF and HCF cycles.

Another important consideration is the nonlinearity present in the fatigue damage accumulation process. Most of the studies [70, 74, 75 &76] done on the LCF threshold damage concept ignore the possibility of nonlinearity and suggest using Miner's rule for the estimation of cumulative damage. Miner's rule is a linear rule and ignores all the complexities of nonlinear damage accumulation. It also ignores load interaction and load sequence effects.

The damage created by HCF cycles following the pre-damage of multiaxial LCF cycles can be influenced by several factors, such as the magnitude and type of multiaxiality involved with the LCF cycles, the nature (tensile or compressive) of the LCF and HCF loading cycles, the number of LCF cycles applied before HCF damage begins to accumulate, the critical plane orientation of the LCF and HCF cycles, and the sequencing of LCF/ HCF loads. All of these factors need to be explored in order to explain how the HCF cycles reduce the fatigue life of the material in comparison to the LCF life.

3.2. Objective of This Research

The main objective of this research is to develop an improved lifing methodology for aircraft engine materials under complex mission loading conditions. The methodology must be able to address a wide variety of multiaxial loading conditions that simulate realistic mission spectra. The methodology should also address the physical basis and mechanisms for fatigue crack initiation in aircraft engine materials subjected to complex combinations of cyclic loads. As this research is focused on the initiation or nucleation of small fatigue cracks, the propagation phase of large cracks has not been investigated. In many situations, it has been found that the majority of the fatigue life of a component is consumed in the initiation and growth of small cracks, and the propagation of large cracks to failure consumes a relatively small number of cycles. Another objective of this modeling effort is to provide design engineers with a fast and efficient tool to predict the fatigue life of engine components with adaptability to current engine lifing algorithms. Previous approaches of lifing have been very complex and often required a large number of parameters to be determined from testing to predict the failure life. This approach is intended to simplify the previously developed complex lifing algorithms to a useable simplified and precise model.

3.3. Scope of Work

This research work has been divided into three major phases. In the first phase, an improved multiaxial damage parameter for constant amplitude fatigue loading is developed, and a new crack initiation model is proposed. This model is based upon an improvement of a previously developed critical plane damage model (Eq. 2.22), which has been modified to simplify its use and improve its ability to handle both LCF and HCF fatigue data. Several

previously developed critical plane models (Eqs. 2.18, 2.22 & 2.25) have been evaluated using several sets of uniaxial and multiaxial fatigue test data from a wide variety of titanium and nickel based super alloys. After analysis of all the models and fatigue data, a simplified and efficient crack initiation model has been developed.

The second phase of this research project consists of in-depth experimental study of LCF/HCF interactions and nonlinear fatigue damage accumulation in Ti-6Al-4V. For this phase, simulated “mission" tests were designed to represent various multiaxial cyclic loading scenarios using actual service conditions in aircraft engine materials. Two and three level block loading tests with various combinations of uniaxial, torsion, proportional, and non-proportional load paths were designed to experimentally assess the effects of LCF pre-damage and LCF/HCF interactions on the rate of the fatigue damage accumulation in the titanium alloy. The mission tests were specifically designed to study the relationships between the LCF and HCF load paths and load levels on nonlinear damage accumulation, in order to document and characterize how these important aspects influence the fatigue life of advance alloys. The results of this test program are presented and analyzed to study the effect of LCF ad HCF critical plane orientations on damage accumulation.

In the third phase of this study, a nonlinear cumulative damage methodology has been developed to model the observed experimental results from the mission tests. The intent of this effort is to develop a model that can be easily implemented by design engineers and which is adaptable to current fatigue life algorithms. Formulate using the principles of the Damage Curve Approach [53,54], the new nonlinear damage model is capable of accounting for differing damage mechanisms between LCF ad HCF cycles, and thus is able to account for the effects of

pre-damage and load path interactions in the damage accumulation process. The resulting life predictions from this model are compared to the experimental data, and contrasted with the corresponding predictions obtaining using the linear damage assumption of Miner's rule.

Finally, the proposed multiaxial damage parameter is integrated into the newly developed nonlinear cumulative damage model, resulting in an efficient fatigue life prediction methodology that is capable of predicting the fatigue life of high-strength alloys subjected to complex, multiaxial loading spectra.

3.4. Experimental Program

3.4.1. Baseline Fatigue Tests

Baseline fatigue tests were conducted on solid ad tubular specimens of two high strength metal alloys: DA718, a nickel based steel alloy, and Ti-6Al4V, a common titanium alloy used in aircraft engines. These tests, which consisted of constant amplitude cycles under uniaxial, torsion, proportional, and non-proportional load paths, were conducted for the purpose of formulating and calibrating the new multiaxial critical- plane damage parameter. For each material, a new set of material parameters was determined by optimization of the damage parameter values. The LCF load levels and load paths used in the variable amplitude fatigue test program were also determined on the basis of the constant amplitude data.

3.4.2. Multiaxial Two Level and Three Levels Block Loading Tests

Two and three level block loading tests, using different combinations of LCF and HCF load paths, were used to form the mission histories. All multiaxial mission tests in this program were performed using solid & tubular specimens of Ti-6Al-4V. The LCF cycles, with levels and

load paths defined from the baseline tests were coupled with HCF cycles with varying load levels and load paths. The HCF cycles used in the block loading tests are similar to the load paths used in the constant amplitude tests, but the levels and combinations of cycles were varied. The intent of these mission tests was to understand the effects of varying load path and interactions between LCF and HCF cycles on the damage accumulation process, as well as to calibrate the nonlinear damage accumulation model developed in this research study.

3.4.3. Additional Material Data Sets

In addition to the experimental data generated as part of this study, several other material data sets were used in the evaluation of the multiaxial critical plane parameter. These data sets, supplied by GE Aviation, were comprised of uniaxial, torsion and multiaxial fatigue data for several high strength steel alloys commonly used in aircraft engines. Additional multiaxial fatigue data sets obtained from the technical literature were also used to evaluate the damage parameter in order to gain a better understanding of its applicability to different materials. The results from this study are compared with correlations obtained using other multiaxial damage parameters.

3.4.4. Testing Limitations

Due to complex nature of multiaxial fatigue testing ad limitations of equipment available at North Dakota State University, all multiaxial fatigue tests were performed at the university of Illinois and the University of Utah. These tests were performed in accordance with test conditions and load levels specified by NDSU.

CHAPTER 4. MATERIALS AND EXPERIMENTAL DETAILS

Several material data sets with a wide variety of load paths and load levels were used in the various phases of this research. The materials used in this study included titanium (Ti-6Al-4V) and nickel-based super alloys (Rene 104, Rene 88DT, IN718, DA718). Some of these materials data sets consisted of different processing conditions and test temperatures. The data set for IN718 was taken borrowed from the work of Daniel Morrow [77] to validate the damage models and analysis developed in this study. The development of the damage parameter was conducted primarily using the Ti-6Al-4V and DA718 data. However, the other data sets were also used to validate the damage parameter under a wide variety of temperature and processing conditions.

For the variable amplitude fatigue loading experiments, tests were carried out under several combinations of LCF and HCF cycles. The load paths and levels of the LCF and HCF cycles were varied in order to validate the development of the proposed multi-axial damage parameter concept. The baseline load levels for the variable amplitude cyclic tests were defined from the results of the constant amplitude fatigue data generated for the various data sets. Several "mission tests" were conducted using two and three level fatigue loading histories, some of which included MCF (mid cycle fatigue) cycles along with the LCF and HCF cycles. The majority of the studies involving interactions between LCF and HCF cycles were conducted using Ti-6Al-4V data.

4.1. Material Details

4.1.1. Ti-6Al-4V

Ti-6Al-4V is a titanium alloy with 60% primary alpha phase (hexagonally closed packed) and 40% of the lamellar transferred beta phase (body centered cubic) materials. The chemical composition of Ti-6Al-4V is listed in Table 4.1.

Table 4.1: Chemical Composition of Ti-6Al-4V [78]

Element	**Amount (wt. %)**
Titanium	Balance
Aluminum	6.3
Vanadium	4.2
Iron	0.2
Oxygen	0.18
Nitrogen	0.012

This material has been considered as a good and efficient material for high strength applications at moderate temperatures (300 to 1000^0F). It is also good for applications requiring low weight and high corrosion resistance. These characteristics of Ti-6Al-4V have promoted its use by industries involved in the production of aircraft engines, aircraft structures, high performance automotive parts and marine parts. Due to the presence of alpha and beta phases, this material is easily heat treatable to achieve increased strength. The material properties of Ti-6Al-4V are show in Table 4.2.

Table 4.2: Material Properties of Ti-6Al-4V [78]

Property	**Value (ksi)**
Modulus of Elasticity (E)	16870
Shear Modulus (G)	6253
Cyclic Yield Strength (σ_y')	110
Monotonic Yield strength (σ_y')	109
Ultimate Strength (σ_{ut})	142

Two sets of Ti-6Al-4V data were used in this research. The first data set (Data Set 1) was generated as part of United States Air Force (USAF) HCF science and technology program conducted during the 1990's [84] and the second data set (Data Set 2) was generated as part of the current Air Force Office of Scientific Research (AFSOR) program to study the effects of LCF-HCF interactions on multi-axial fatigue damage accumulation. All of the fatigue data for the latter study were generated within the laboratory facilities at the University of Illinois and the University of Utah. Due to the different material pedigrees and sample preparation techniques, these two data sets were analyzed separately.

4.1.2. DA 718

Direct aged (DA) 718 is a nickel based $\gamma - \gamma''$ super alloy with good thermal and fatigue properties. This alloy has a very fine grain size to improve the fatigue properties [81]. The chemical composition of DA718 is listed in Table 4.3. This alloy is frequently used to manufacture aircraft engine components due to its high temperature properties.

There were five different sets of DA718 data evaluated in this study each with a different pedigree or test temperature (labeled here a Data Sets 1 through 5). All of the uniaxial and multiaxial test data were either supplied by General Electric or generated as part of this study by the University of Illinois at Urbana Champaign. The DA718 data were used to validate the damage parameter developed in this study.

Table 4.3: Chemical Composition of DA-718 [81]

Element	**Amount (wt. %)**
Nickel	Balance
Iron	18.6
Chromium	17.6
Molybdenum	2.95
Niobium+Tantalum	5.22
Titanium	0.91
Aluminum	0.48
Carbon	0.04
Boron	0.003

4.1.3. Rene 104

Rene 104 was developed in the 1990's as a damage tolerant material to be used in gas turbine disk applications. It can tolerate high temperature fatigue loading conditions without a significant change in mechanical properties. Rene 104 is an advanced version of a $\gamma - \gamma'$ nickel

based super alloy with increased high temperature properties [79]. The chemical composition of this material is presented in Table 4.4.

Table 4.4: Chemical Composition of Rene 104 [79]

Element	**Amount (wt. %)**
Nickel	Balance
Cobalt	18.1
Chromium	9.55
Tantalum	2.5
Tungsten	3
Molybdenum	2.9
Zirconium	0.05
Niobium	2
Titanium	3.6
Aluminum	3.6
Rhenium	1.25
Carbon	0.03
Boron	0.03

4.1.4. Rene 88

Rene 88 is the previous generation of nickel based $\gamma - \gamma'$ super alloys in comparison to Rene 104. This material is also known for its high temperature fatigue properties, and is also capable of handling high cycle fatigue loading. This material is generally produced using a

powder methodology and slow oil quenching heat treatment process to achieve the desired fine grain size [79 & 80]. The chemical composition of this material is presented in Table 4.5.

Table 4.5: Chemical Composition of Rene 88 [80]

Element	**Amount (wt. %)**
Nickel	Balance
Cobalt	13
Chromium	16
Tungsten	4
Molybdenum	4
Zirconium	0.03
Niobium	0.7
Titanium	3.7
Aluminum	2.1
Carbon	0.03
Boron	0.015

4.1.5. Inconel 718

Inconel 718 is another nickel-based super alloy with Ni_3CrFe FCC matrix strengthened by FCC $Ni_3(Al,Ti)$ γ' and by orthorhombic Ni_3Nb $\gamma - \gamma''$ precipitates [77]. The fatigue data for this material were borrowed from the doctoral dissertation of Daniel Morrow (University of Illinois) [77]. The chemical composition of this material is presented in Table 4.6.

Table 4.6: Chemical Composition of IN718 [77]

Element	**Amount (wt. %)**
Nickel	52.12
Chromium	18.23
Iron	19.48
Niobium	5.03
Molybdenum	2.89
Titanium	1.01
Aluminum	0.54
Cobalt	0.28
Mangnese	0.09
Silicon	0.06
Copper	0.28
Carbon	0.034
Phosporus	0.007
Boron	0.0035
Sulphur	0.001

4.1.6. Material Propertied of Steel Alloys

Due to the proprietary nature of nickel-based steel alloys (DA718, Rene 104, Rene 88, IN 718), the full set of material properties are not included here. However, an abbreviated set of material properties is shown in Table 4.7

Table 4.7: Material Properties of Nickel-Based Steel alloys

Material	Test Temp.	Yield Strength MPa	Young's Modulus, GPa
Rene' 104	427^0C (800^0F)	900	200
Rene' 88	400^0C (750^0F)	960	200
DA 718	149^0C (300^0F)	1050	200
In 718	149^0C (300^0F)	1160	209

4.2. Constant Amplitude Fatigue Tests

Constant amplitude uniaxial and multiaxial fatigue tests were conducted on all the materials under a variety of load paths to provide the data needed for the development and validation of the multiaxial damage parameter. These tests included uniaxial, torsion, and proportional and non-proportional biaxial (axial-torsion) load paths, in order to generate a broad set of loading conditions by which the damage parameter could be evaluated. Both strain controlled and load-controlled testing conditions were used, depending on the magnitude of the applied loads. The general specimen geometry used for the multi-axial tests is shown in Fig. 4.1.

Both solid and tubular specimens were used for experimentation depending on the load magnitude and material characteristics. The diameter for the solid specimens was 12.5 mm whereas the inner and outer diameters of the tubular specimens were 6.35 mm and 9.5 mm,

respectively. Both the inner and outer surfaces of these specimens were ground and polished to eliminate surface defects.

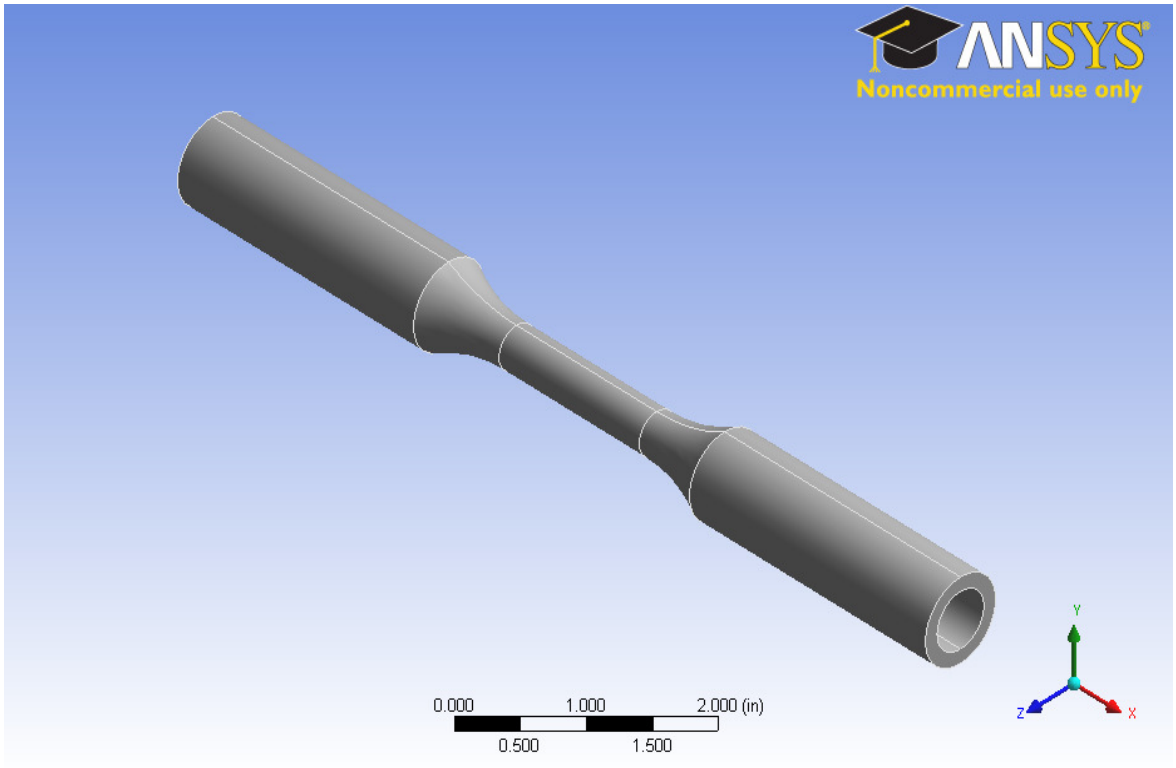

Figure 4.1: Specimen Geometry for Mutiaxial Tests

An extensive amount of baseline fatigue data was available for each material to assist in the development and validation of the damage parameter. As previously noted, the data included uniaxial, torsion, and biaxial load-paths. The biaxial load paths used in this study are illustrated schematically in Fig, 4.2, show in "axial-torsion" (Normal/Shear) space. The first to load paths (torsion and proportional) provide the necessary data for calculation of material constants required by the multiaxial damage parameter. The remaining load paths represent non-proportional loading conditions, providing discriminating tests that are useful for validation of the model. The box, triangle, and torsion-mean tension paths have been commonly used in the

past for multi-axial parameter validation. The remaining load paths (torsion-tension, check, S-path, and double check) were specifically designed for this study to examine the effects of normal-stress "sub cycles" occurring on the critical plane within a single dominant shear stress cycle. These tests produced conditions in which the sub cycles varied in phase and number relative to the major shear cycle, as discussed in next chapter.

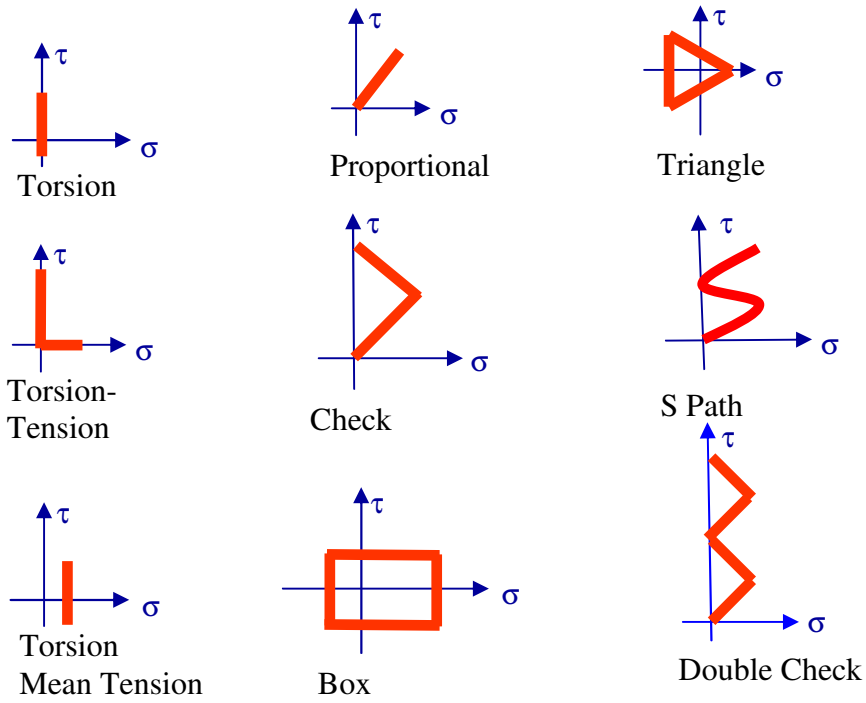

Figure 4.2: Load Paths Used in the Development and Validation of the Multiaxial Damage Parameter

Table 4.8 presents a summary of the number of fatigue tests conducted on each material for each loading conditions. In addition to these tests, several "mission" tests were conducted on Ti-6Al-4V to study LCF-HCF interactions and damage accumulation. These tests are described in detail in section 4.4.

Table 4.8: Constant Amplitude Fatigue Tests Summary

Material	Uniaxial	Torsion	Proportional	Non- Proportional
DA718(300F) (Data Set-1)	21 (R = 0) 5 (R = 0.5) 5 (R = -1)	5 (R = 0) 3 (R = 0.5) 6 (R = -1)	5 (R = 0) 1 (R = -1)	4 (Torsion-Mean Axial) 1 (Triangle) 1 (S path) 1 (Check) 1 (Double Check) 1 (Torsion- Axial)
DA718(750F) (Data Set-2)	28 (R = 0) 5 (R = 0.5) 5 (R = -1)	1 (R = 0) 2 (R = -1) 4 (R = -0.5)	1 (R = 0) 2 (R = 0.5)	2 (Torsion-Mean Axial) 1 (Triangle) 1 (Backward Triangle) 1 (S path) 1 (Check)
DA718(1000F) (Data Set-3)	25 (R = 0) 3 (R = 0.5) 8 (R = -1)	9 (R = -1)	0	0
DA718 Old (Data Set-4)	4 (R = 0) 3 (R = -0.4) 8 (R = -1)	5 (R = 0) 3 (R = -1)	5 (R = 0)	4 (Check) 1 (Circle)
DA718CF34 (Data Set-5)	7 (R = 0) 5 (R = 0.5)	3 (R = 0) 3 (R = -1)	10 (R = 0)	0
IN718	4 (R = 0) 4 (R = -1)	6 (R = 0) 8 (R = -1)	7 (R = 0) 6 (R = -1)	6 (Torsion-Mean axial) 2 (Elliptical) 6 (Circular) 13 (Bi-axial) 6 (Various Non-Proportional)
Rene 88	5 (R = 0) 4 (R = 0.6) 5 (R = -1)	4 (R = 0) 2 (R = -1)	7 (R = 0)	8 (Check) 2 (Backward Proportional) 1 (Torsion-Mean Axial) 2 (Axial-Mean Torsion)
Rene 104	22 (R = 0) 5 (R = 0.5) 6 (R = -0.5) 6 (R = 0.6) 7 (R = -1)	3 (R = 0) 3 (R = -1)	6 (Various R values)	10 (Check)
Ti-6Al- 4V (Data Set-1)	34 (R = 0.1) 19 (R = 0.5) 26 (R = -1)	5 (R = 0.1) 1 (R = 0.5) 5 (R = -1)	2 (R = 0.1) 1 (R = -1)	4 (Triangle) 4 (Box) 4 (Check) 3(Torsion-Mean Axial)
Ti-6Al-4V (Data Set-2)	7 (R = 0) 2 (R = -1)	9 (R = 0) 8 (R =-1)	4 (R = 0)	0

4.3. Elastic-Plastic Stress-Strain Analysis

The values of stress and strain used in the development of the damage parameter and the subsequent life prediction analyses were the cyclically stabilized "half-life" values on the outer surfaces of the specimens. Those specimens which experienced only elastic stress and strain during the tests were analyzed using theoretical elastic by stress-strain relationships. In contrast, Specimens which experienced plastic strains on the surface were analyzed by the finite element method to accurately determine the surface stress and strain values.

The cyclic elastic-plastic stress-strain curves for each material were generated from the uniaxial fatigue test data at different stress ratios. The cyclically stabilized hysteresis loops from these tests were recorded ad used to generate the cyclic stress-strain curve. The Ramberg-Osgood relationship was then fit to the data to produce an analytical model for subsequent analyses. The Ramberg-Osgood equation, shown in Eq. 4.1, separates the total strain into elastic and plastic components. Once the modulus of elasticity, E, has been determined from the elastic strains the material constants K' and n' can be calculated by fitting a power-law curve to the stress vs. plastic strain data.

$$\varepsilon = \frac{\sigma}{E} + \left(\frac{\sigma}{K'}\right)^{\frac{1}{n'}} \tag{4.1}$$

The cyclic elastic-plastic stress-strain curves generated in this manner were used in the finite element analysis to determine surface stresses and strains using ANSYS. The resulting

stress-strain curves at R = 0 and R = -1 for Ti-6Al-4V are shown in Fig. 4.3, along with the conventional monotonic curve. Similar results were obtained for the other materials considered in this study. The experimental load values from the fatigue tests were used as input for finite element analyses and the stress-strain values on the surface of the specimens were determined. These surface stress-strain values were then used in the proposed damage estimation methodology. The critical plane values of stress and strain were subsequently computed using a Mohr's circle or Euler angle analysis.

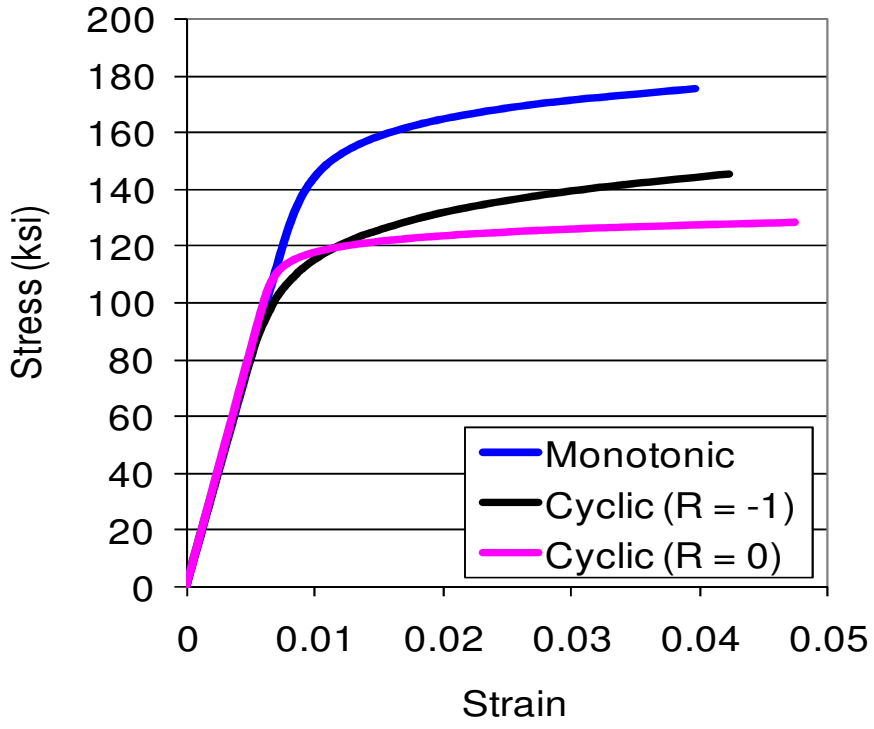

Figure 4.3 Monotonic and Cyclic Stress-Strain Curve for Ti-6Al-4V

As can be seen in Fig. 4.3, Ti-6Al-4V exhibited significant softening due to the application of cyclic loads. This was also observed in the other materials. It can also be seen that the degree of softening, relative to the monotonic curve, was dependent on the stress ratio. Notably, the R = 0 curve exhibited greater softening, likely as a result of the tensile mean stress which cased additional stress relaxation. As a result, the data from the R = 0 and R = -1 tests were analyzed using separate curves.

4.4. Mission Tests

Simulated "mission" tests, consisting of two or three load levels of fatigue cycles performed to investigate LCF-HCF interactions and aid in the development of the cumulative fatigue damage models. These tests were constructed from various combinations of axial, torsion, and biaxial load paths, combining 1 LCF cycle with 5-50 HCF cycles. All of the mission tests were conducted on Ti-6Al-4V, using the two material pedigrees associated with data sets 1 and 2. The load paths used for the mission histories on the two sets of Ti-6Al-4V data are shown in Figs. 4.4 and 4.5 respectively.

Load levels were chosen to produce LCF lives in the range of $10^4 – 10^5$ cycles and HCF lives in the range of $10^8 – 10^9$ cycles. For those mission histories containing three levels, MCF (Mid Cycle Fatigue) life levels were chosen in the life range of 10^5 - 10^6 cycles. All the mission tests for Ti-6Al-4V (Data Set 1) were carried out under strain controlled conditions. The load paths for these tests are shown in Fig 4.4. For Ti-6Al-4V (Data Set 2), both solid and tube specimens were tested under strain-controlled as well as load-controlled conditions. These load paths are show in Fig. 4.5. Summary of number of specimens tested at each load path is show in Table 4.9.

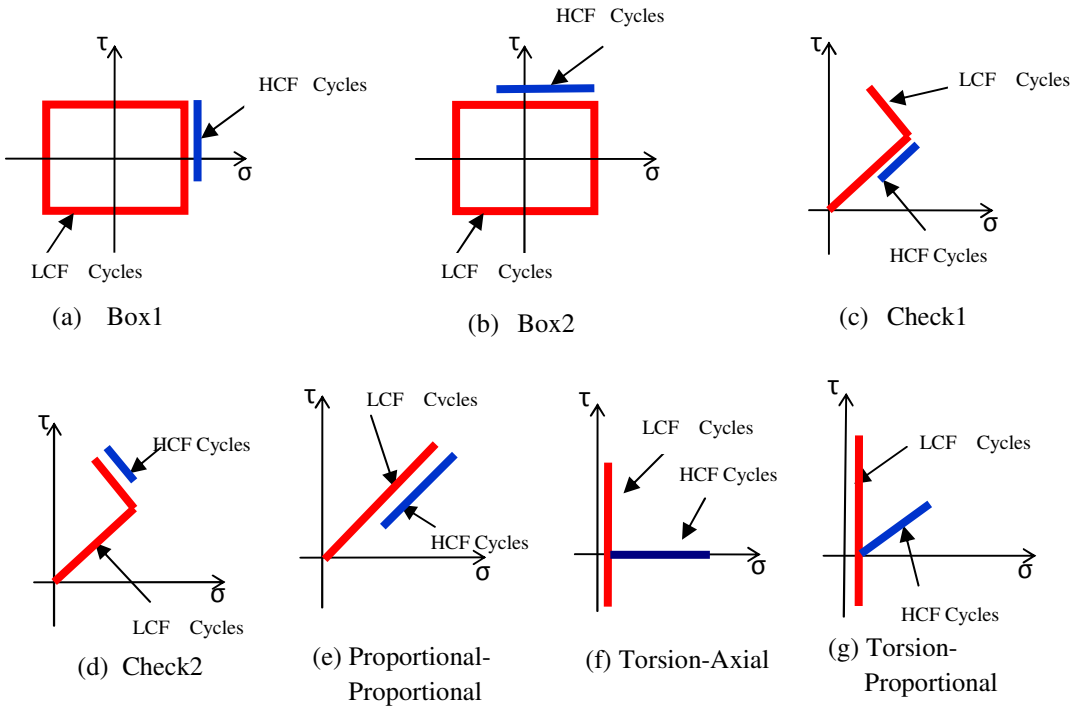

Figure 4.4: Mission Test Load Paths for Ti-6Al-4V (Data Set 1)

As described in previous chapters, of particular interest in this study was the relationships ad interactions between shear based damage and tensile-based damage in the various LCF and HCF cycles. The load paths used in the mission histories were designed to highlight these aspects. For example, the "torsion-axial" history couples shear based damage from the LCF torsion cycle on the same (critical) plane with tensile-based damage from the HCF axial cycle. The "axial-torsion" cycle reserves the shear/tensile damage phenomenon on the critical plane. The relative amounts of shear and tensile damage from the LCF and HCF cycles are varied in the other load paths. Through careful analysis of the various stress states on the critical planes in each history, the damage interactions can be thoroughly studied and documented as described in subsequent chapters

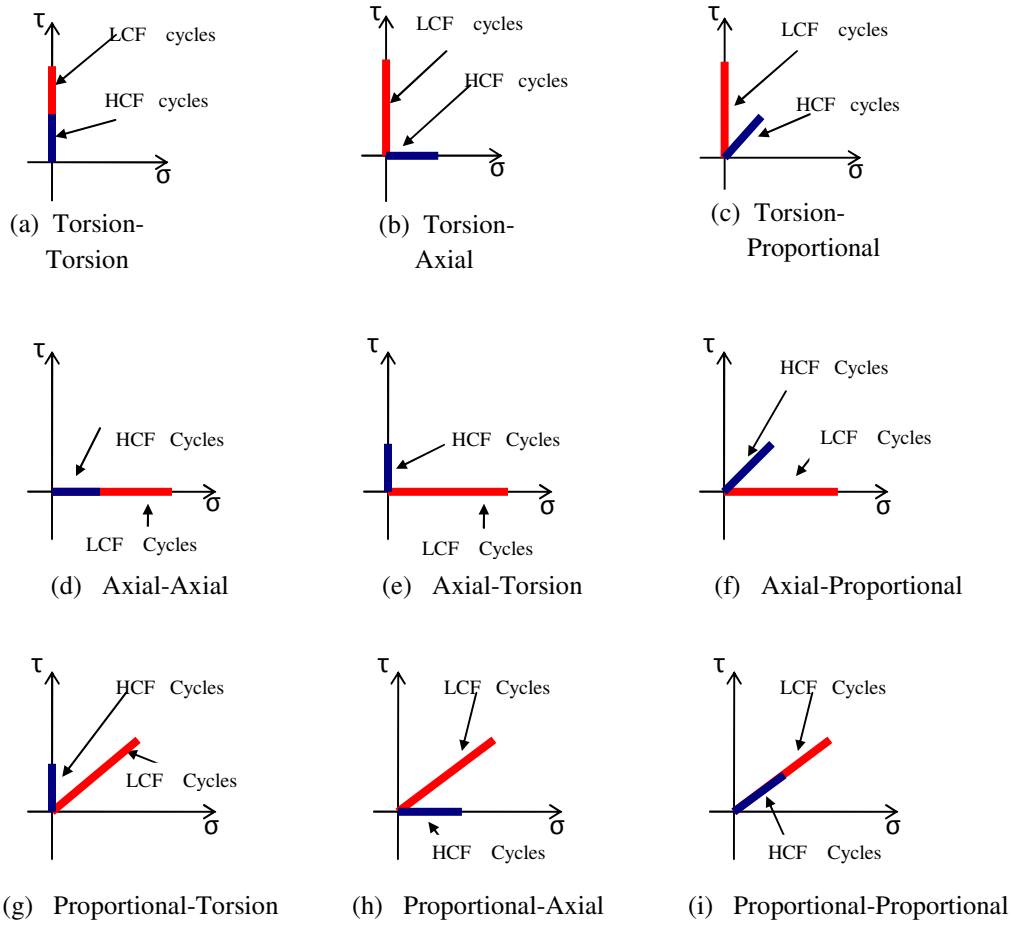

Figure 4.5: Mission Test Load Paths for Ti-6-Al-4V (Data Set 2)

4.5. Summary

As summarized in this chapter, a total of ten material data sets were considered in this study to analyze various phases of the research. The primary data sets used in the evaluation of the critical plane parameter and cumulative damage model were DA718 at three different test temperatures (Data Sets 1,2, and 3) and the two data sets of Ti-6Al-4V (Data Sets 1 and 2). Four additional data sets (DA 718 data sets 4 & 5, Rene 88, and Rene 104) were provided by General

Electric to validate the critical plane parameter developed in this study. One additional data set, IN 718, obtained from the published doctoral thesis of Morrow [77], was also used for this purpose.

Table 4.9: Summary of Mission Tests Conducted on Ti-6Al-4V (Data Set 1 & 2)

Mission Tests	Ti-6Al-4V (Data Set-1)	Ti-6Al-4V (Data Set-2)
Torsion-Torsion (1 LCF-50 HCF)		6
Torsion-Axial (1 LCF-50 HCF)	2	5
Torsion-Proportional (1 LCF-50 HCF)	1	3
Axial-Axial (1 LCF-50 HCF)		4
Axial-Torsion (1 LCF-50 HCF)		2
Axial-Proportional (1 LCF-50 HCF)		1
Box 1 (1 LCF-50 HCF)	4	
Box 2 (1 LCF-50 HCF)	3	
Check 1 (1 LCF-50 HCF)	2	
Check 2 (1 LCF-50 HCF)	2	
Proportional-Axial (1 LCF-50 HCF)		1
Proportional-Torsion (1 LCF-50 HCF)		1
Proportional-Proportional (1 LCF-50 HCF)		1
Torsion/Axial/Proportional (1 LCF-25 HCF-25 HCF)		1
Torsion/Proportional/Axial (1 LCF-5 MCF-25 HCF)		1
Proportional/Torsion/Axial (1 LCF-25 HCF-25 HCF)		1
Axial/Proportional/Torsion (1 LCF-5 MCF-25 HCF)		1

CHAPTER 5. DEVELOPMENT OF STRAIN-BASED DAMAGE PARAMETER

5.1. Critical Plane Analysis

The critical plane methodology for of fatigue crack initiation involves the analysis of the fatigue damage created by a particular cyclic stress-strain state where the crack is expected to initiate. The orientation of the plane on which the crack initiates is known as the critical plane. The orientation of the critical plane may be influenced by several factors, such as the microscopic behavior of the material, load level and the type of fatigue loading. The definition of the critical plane used in this research is based upon the observation that the initiation of the fatigue crack in many materials is due to the cyclic shear stress/strains. Hence, the plane with the maximum value of cyclic shear stress (strain) has been taken as the plane of crack initiation, or critical plane. In contrast, several other researchers have defined the critical plane as the plane where a particular damage parameter is maximized. Comparison of the two definitions of critical plane using several different parameters has been done in this research and in the vast majority of cases, the two definitions were found to yield very similar orientations indicating that these parameters are maximized on planes very near the plane of maximum cyclic shear stress (strain). It has been observed that the computational effort can be reduced significantly when the critical plane is defined on the basis of maximum cyclic shear stress in comparison to the maximum damage parameter value. In addition, all the material dependent parameters required by the model, need to be determined only on the maximum shear stress plane.

The critical plane for variable amplitude loading cannot be identified using a similar process as in the case of constant amplitude loading. The orientation of the critical plane may change from cycle to cycle in variable amplitude fatigue loading. Using the assumption of the

maximum shear stress plane as the critical plane, all the constant and variable amplitude test in this study were evaluated on this plane using a Mohr's circle analysis for two dimensional stress states and the Euler angle concept to identify the max shear plane under three dimensional loading conditions.

5.2. Damage Parameter Development for Life Estimation

The multiaxial critical plane damage parameter developed by Erickson et al. [5] (Eq. 5.1) was evaluated for its potential to handle a wide range of multiaxial fatigue data. The model developed by Erickson et al. [5] is a very complex formulation of crack initiation phenomena. One of the main difficulties with this multiaxial fatigue model (Eq. 5.1) is the large number (six) of material dependent parameters required to compute the damage parameter for a given stress states. Computationally, it becomes very expensive to determine all six parameters for each data set, and a large number of experimental tests are required to reliably evaluate these parameters.

$$DP = \tau_{max}\left(1 - \frac{\tau_{min}}{\tau_{max}}\right)^{w_1} . \left[1 + \frac{k^{+}\sigma_{max} + k^{-}\sigma_{min}}{\sigma_y}\right]^{w_2} + k_2 \sum \sigma_{max}\left(1 - \frac{\sigma_{min}}{\sigma_{max}}\right)^{w_3} \quad (5.1)$$

Another uncertainty with the Erickson model is the summation of "sub-cycles" in the last term of the parameter. According to this model, when multiple normal stress sub-cycles occur on the critical plane within a single shear-stress cycle, damage accumulates in a linear manner within the cycle. This characteristic has the potential to overestimate the value of the damage parameter for shear cycles containing multiple normal-stress sub-cycles. To further investigate

this uncertainty, Feierabend [82] performed a series of additional fatigue tests that focused on the importance of the sub-cycle term in the equation proposed by Erickson. Specifically, Feierabend conducted fatigue tests on DA-718 with the same cyclic shear stress level on the critical plane, but with a varying number of normal stress cycles. The load paths for these specially designed tests consisted of torsion, proportional, triangle, check, double-check, and S-path load paths, as illustrated in Fig. 4.2. When rotated onto the critical (maximum shear) plane, these load paths produced cycles with nearly identical shear stress levels, but with one to four normal stress sub-cycles per shear cycle. The test results [82] revealed that the number of normal stress sub-cycles on the critical plane had almost negligible influence on the fatigue life of the specimens. The critical plane stresses for these tests are shown in Fig. 5.1.

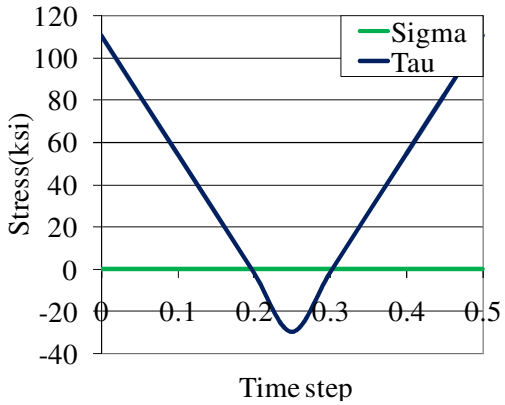

Torsion Path (N_f=209,750)

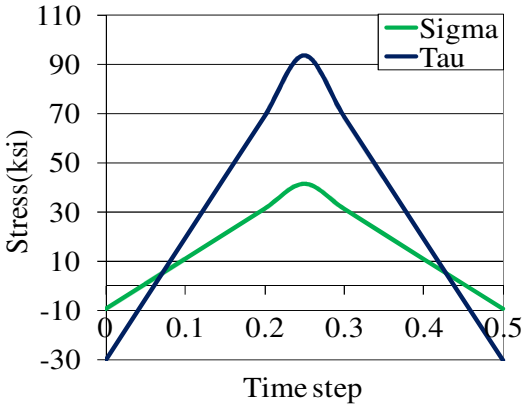

Proportional Path (N_f=36,078)

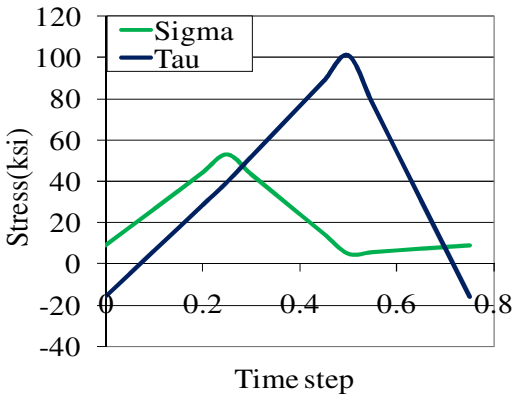

Triangle Path (N_f=176,559)

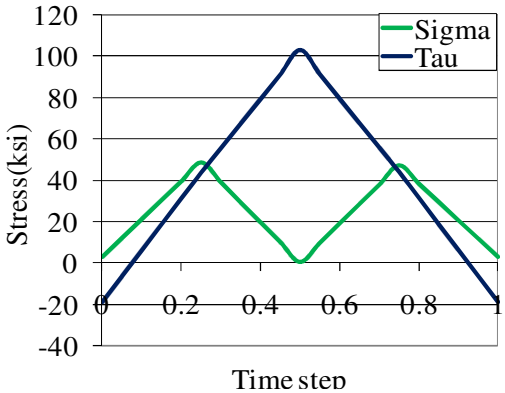

Check Path (N_f=168,803)

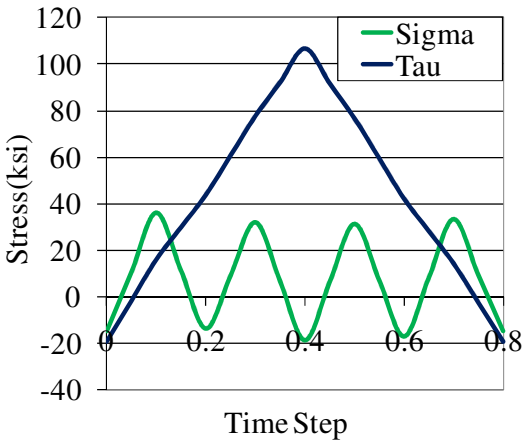

Double Check Path (N_f =141,421)

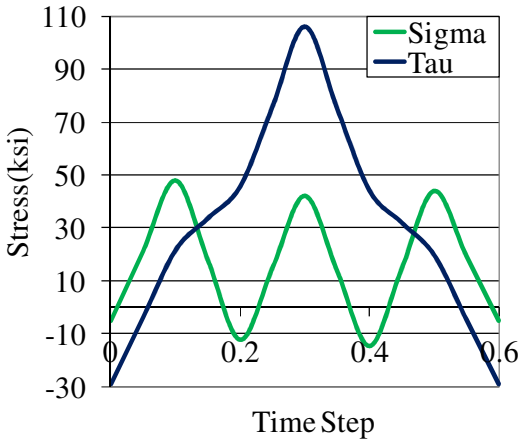

S Path (N_f =141,421)

Figure 5.1: Critical Plane Stresses For the Tests Conducted on DA 718 by Feierabend [82], and Associated Fatigue Lives

It can be observed from the plots shown in Fig. 5.1 that the cyclic shear stress levels for the proportional load path, with one normal stress sub-cycle, and the S-path, "with three normal stress sub-cycles" are almost identical. The model proposed by Erickson et al. [5] shown in Eq. 5.1, assumes that the number of normal stress sub-cycles has a direct influence on the fatigue damage, and hence life. Thus, according to this model, the S-path should have a lower value of fatigue life in comparison to the proportional load path. However, experimental results do not agree with this prediction, as almost identical values of fatigue life were recorded during these two tests. Similar results were observed for the "triangle", "check" and "double check" load paths which all consisted of a different number of sub-cycles. Hence, according to the experimental data, the effect of the number of normal stress sub-cycles on the fatigue damage analysis cannot be considered to be a significant factor. This leads towards the elimination of the summation term in the Erickson model, since the summation term tends to over-predict the damage. After evaluation and optimization of several other damage parameters, Feierabend [82] finally suggested a formulation based on the cyclic mean stress, the static normal stress at the shear reversal points, and the shear stress at the maximum normal stress time points (Eq. 5.2). Feierabend's [82] formulation is similar to Erickson's model with some changes in the third additional term. This model eliminates the summation term in Erickson's model, and replaces it with a term consisting of the shear stress value at the maximum normal stress time point.

$$DP = \tau_{max}\left(1-\frac{\tau_{min}}{\tau_{max}}\right)^{w_1}.\left[1+\frac{k'\sigma_{maxrev}+k'\sigma_{minrev}}{\sigma_y}\right]^{w_2}+\frac{k}{\sigma_y}\,\tau_{@\sigma_{max}}\times\sigma_{max}\left(1-\frac{\sigma_{min}}{\sigma_{max}}\right)^{w_3} \quad (5.2)$$

The model proposed by Fierabend [82] still has the complexity of a large number of material dependent parameters. Another drawback of this model is that it is purely a stress-based model, and thus it does not lend itself for use in predicting the fatigue life for LCF data. Hence, a strain-based term should be introduced along with stress terms to compute the damage for a wide range of fatigue data.

Additional tests were carried out to determine the values of the material dependent parameters in Eq. 5.2. Analysis of these test results and the optimization of the damage parameter with several other material data sets revealed that the effects of the normal stress value at the shear reversal points did not significantly affect the fatigue damage accumulation process. The analysis of this model (Eq. 5.2) with several other material data sets resulted in zero values for k', w_2 and w_3. The analysis also suggested that the normal stress value at the shear reversal time points, and the term with the normal stress ratio in Eq. 5.2 have no direct impact on the damage accumulation process, and the value of damage remains unchanged after removal of these terms from Eq. 5.2. The removal of these unwanted terms makes the model simple and efficient during utilization with large volumes of fatigue data. However, a term which can model the interaction of normal and shear stresses on the critical plane must be introduced.

It has been well documented that the cyclic shear stress initiates the fatigue crack, and the tensile normal stress further expands it. Hence, both the normal and the shear stress are important parameters to be considered. Evaluation of Erickson et al.'s [5] and Fierabend's [82] models using several hundred data points from different nickel-based and titanium-based super-alloy materials ultimately directed the research towards the analysis of the interaction between the normal and shear stresses on the critical plane.

After careful observation of the available fatigue data, it was noted that the product of the normal stress and shear stress values is inversely proportional to the fatigue life of the specimens (Fig. 5.2). The importance of this product term can also be explained by analyzing the tests (Fig.5.1) done by Fierabend [82]. All of the proportional and non-proportional tests shown in Fig. 5.1, have unique maximum values of this product (normal and shear stress), depending upon their load levels. If the maximum values of the product of normal stress and shear stress on the critical plane for the proportional and S path (Fig. 5.1) are computed, they result in identical values. Similar observations can be made for the triangle, check and double check load paths. Hence, this product term explains the similarity in the values of experimental failure lives for these load paths better than any other interaction terms present in Erickson's [5] and Fierabend's [82] models. This discovery simplifies these models (Eq. 5.1 & Eq. 5.2). Figure 5.2 illustrates the dependence of fatigue life on the product of normal and shear stresses on the critical plane in DA 718 specimens; similar results have been observed in other materials.

Through evaluation of several hundred fatigue data points, a new critical plane damage model has been developed in this study. This parameter contains stress and strain terms, as well as a term consisting of the maximum value of the product of normal and shear stresses on the critical plane. The proposed damage parameter, (shown in Eq. 5.3) eliminates many of the shortcomings of the earlier developed critical plane fatigue damage models shown in Eq. 5.1 & Eq. 5.2. Notably, the present model contains strain term and requires only two material dependent parameters, k and w.

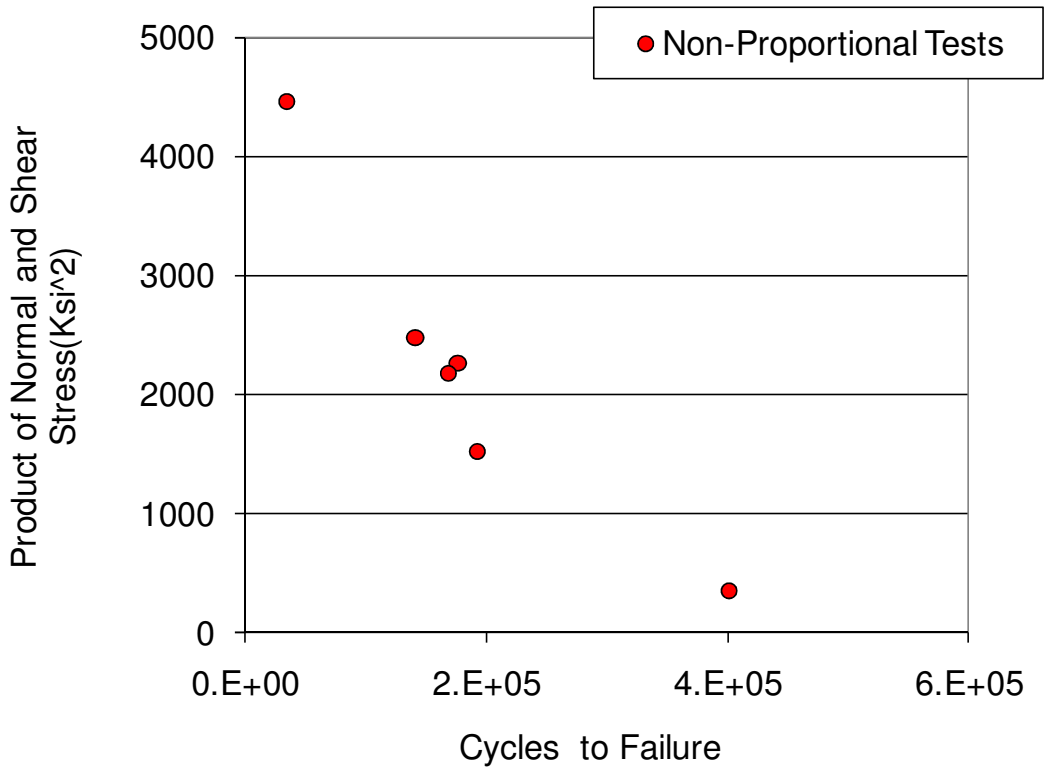

Figure 5.2: Effect of Product Term (Normal & Shear stress) on Fatigue Life (DA718 Data Set 1)

$$DP = (G \times \Delta\gamma)^{w} \times \tau_{max}^{(1-w)} \left(1 + k\frac{(\sigma \times \tau)_{max}}{\sigma_o^2}\right) \tag{5.3}$$

The inclusion of both stress and strain terms in Eq. 5.3 allows this parameter to better model fatigue data over a very broad life range. Typically, strain-based parameters have been used to model LCF data, and stress-based parameters have been used primarily for HCF data. By incorporating both stress and strain terms, this parameter will be able to account for cyclic hardening or softening that may occur at higher load levels.

The damage model developed in this work has an improved capability for handling both uniaxial as well as multiaxial fatigue data, and it has been validated using the ten different material data sets listed in Table 5.1, with varying processing conditions, temperatures and loads. The material dependent parameters (w & k) can be adjusted to account for different material processing techniques and test temperatures.

5.3. Critical Plane Damage Analysis with Newly Developed Damage Model

The experiments for this study were conducted under both load and strain controlled conditions, and all the test data were analyzed using a finite element analysis to compute the values of stresses and strains at the surface of the specimen. These stress and strain values were then used to evaluate the stress/strain state on the critical plane using Mohr's circle (2D) and Euler angles (3D) concepts. The results of this analysis for the ten material datasets described in chapter 4 are shown in Fig. 5.3 and 5.4.

The graphs shown in Fig. 5.3 are presented in the form of damage parameter vs. life plots. In this form, an effective damage parameter would collapse all the data points (uniaxial, torsion, and multiaxial) into a single curve represented by the solid line in these plots. The data sets shown in Fig. 5.4 are presented in the form of predicted life vs. experimental life plots, due to the proprietary nature of these data sets. In these plots, an effective model would collapse all the data onto the diagonal line representing a one-to-one correlation between experimental and predicted lives. Scatter bands representing a factor of two difference between experimental and predicted lives are also shown in these plots for comparison purposes.

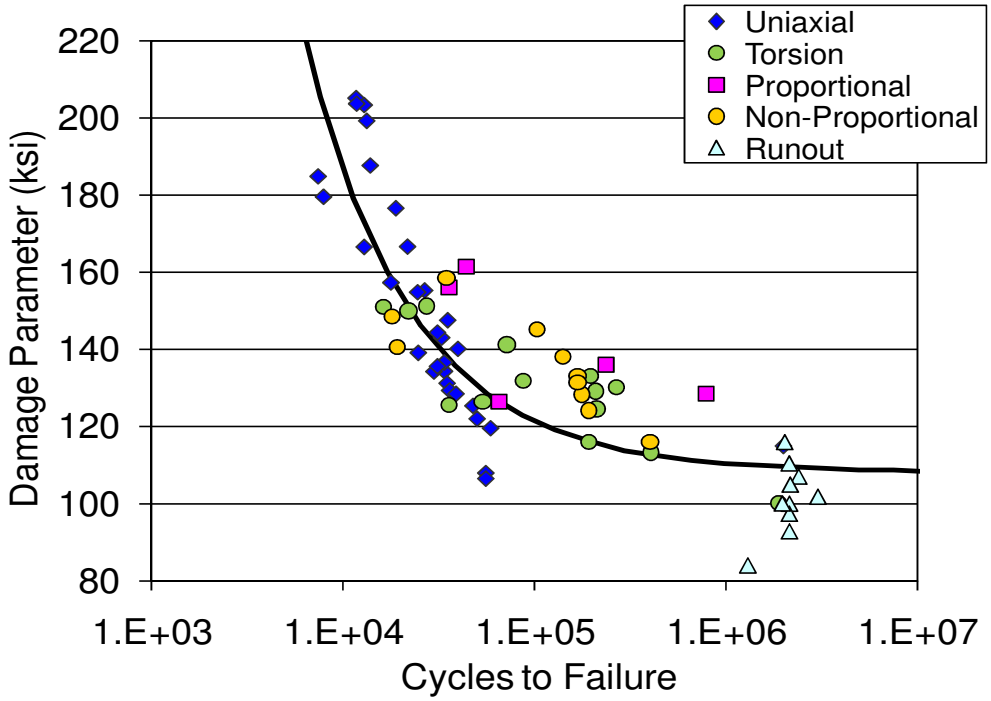

Figure 5.3(a): Damage Parameter vs. Life Using the Newly Developed Model (DA718 Data Set 1)

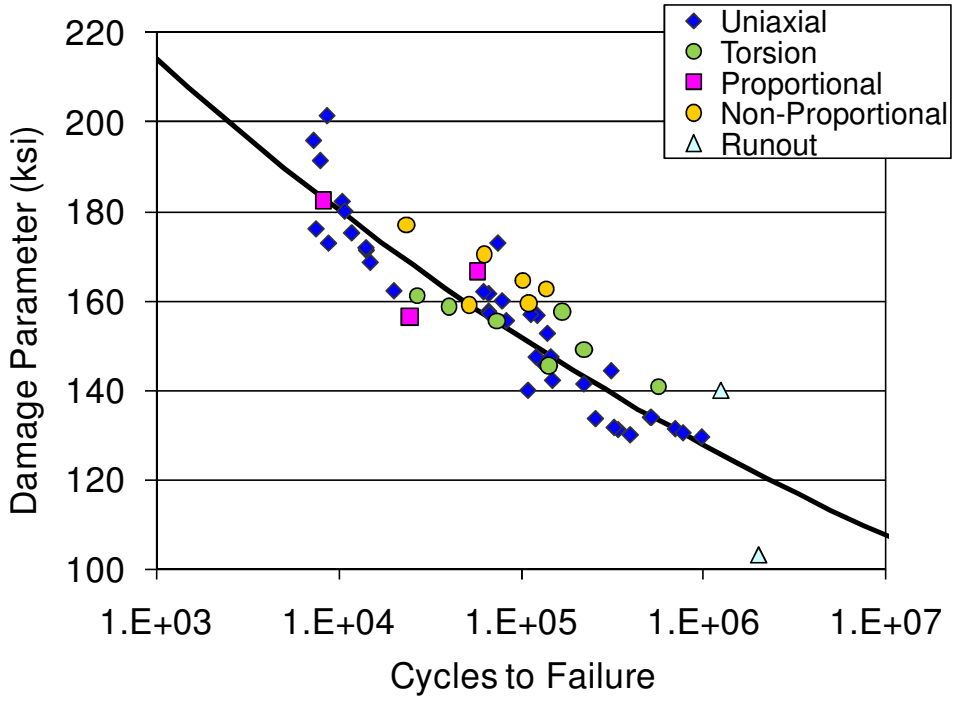

Figure 5.3(b): Damage Parameter vs. Life Using the Newly Developed Model (DA718 Data Set 2)

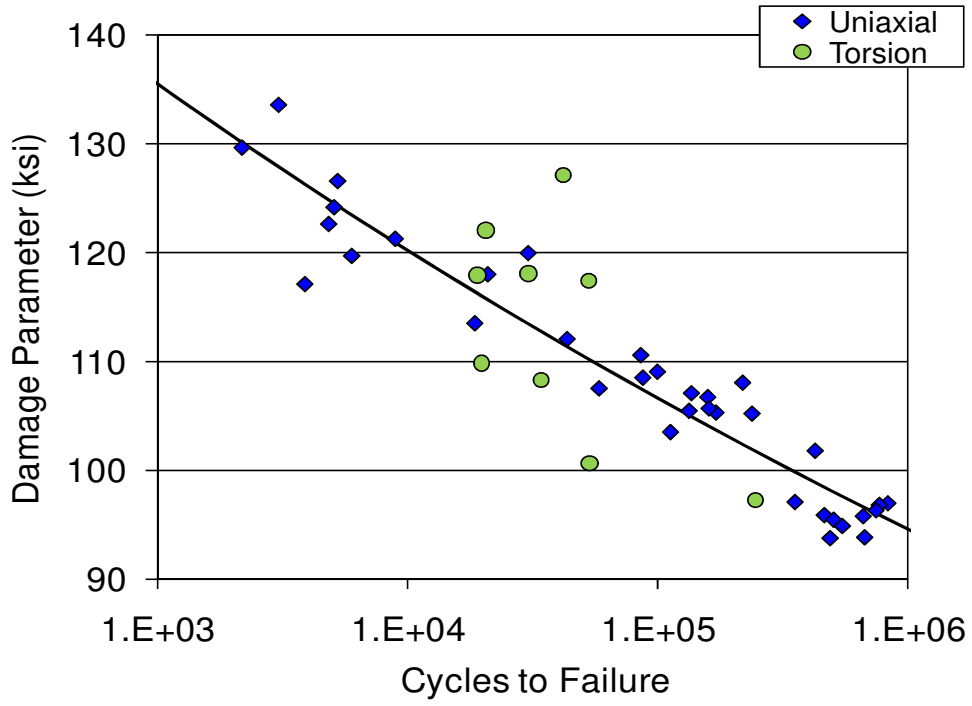

Figure 5.3(c): Damage Parameter vs. Life Using the Newly Developed Model (DA718 Data Set 3)

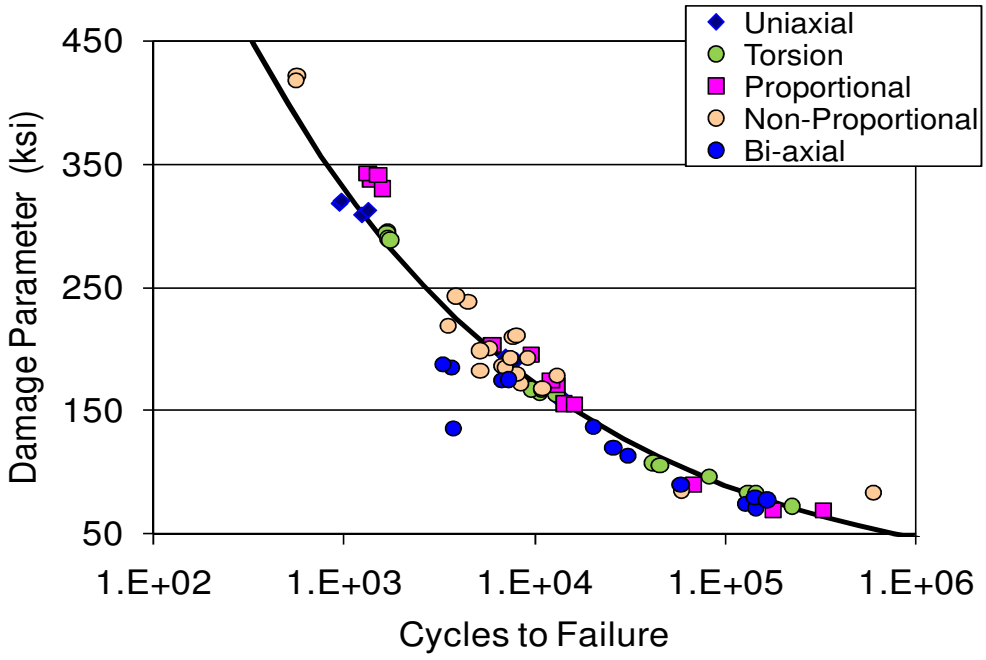

Figure 5.3(d): Damage Parameter vs. Life Using the Newly Developed Model (IN718)

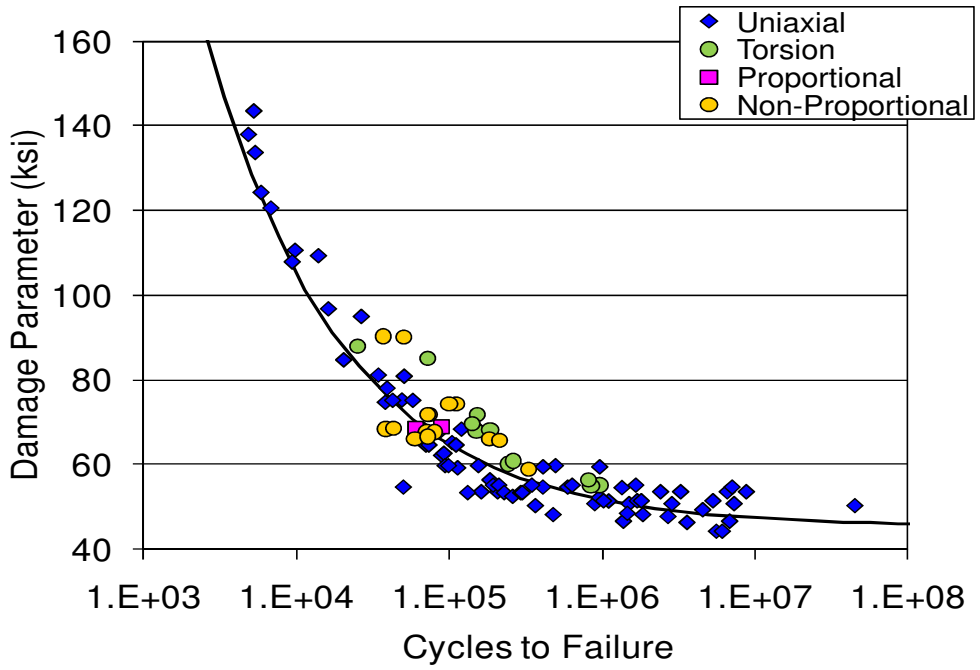

(e) Ti-6Al-4V (Data Set 1)

Figure 5.3(e): Damage Parameter vs. Life Using the Newly Developed Model (Ti-6Al-4V Data Set 1)

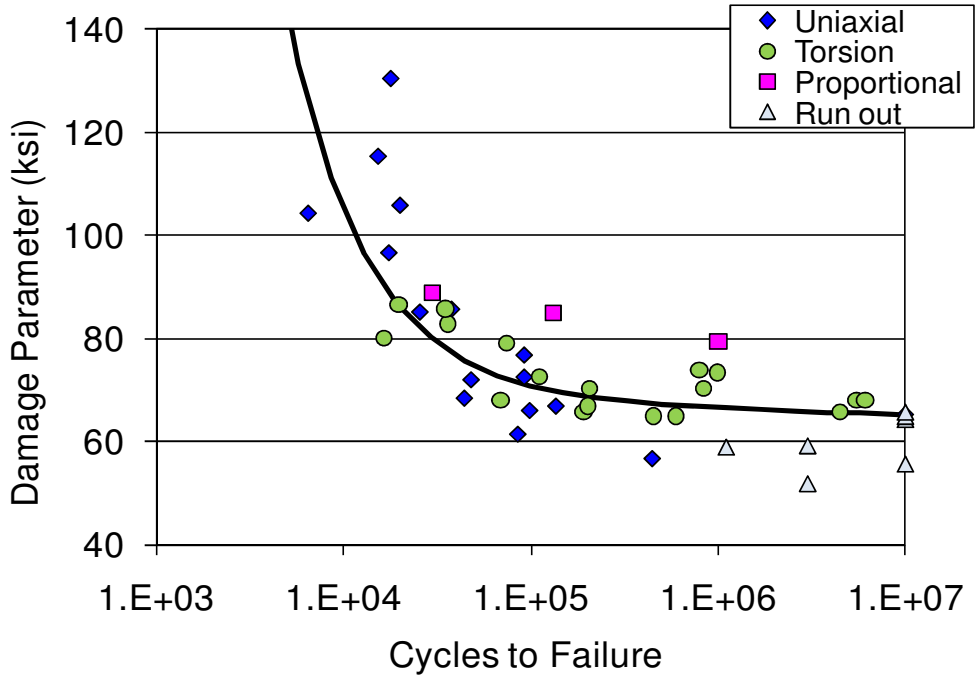

Figure 5.3(f): Damage Parameter vs. Life Using the Newly Developed Model (Ti-6Al-4V Data Set 2)

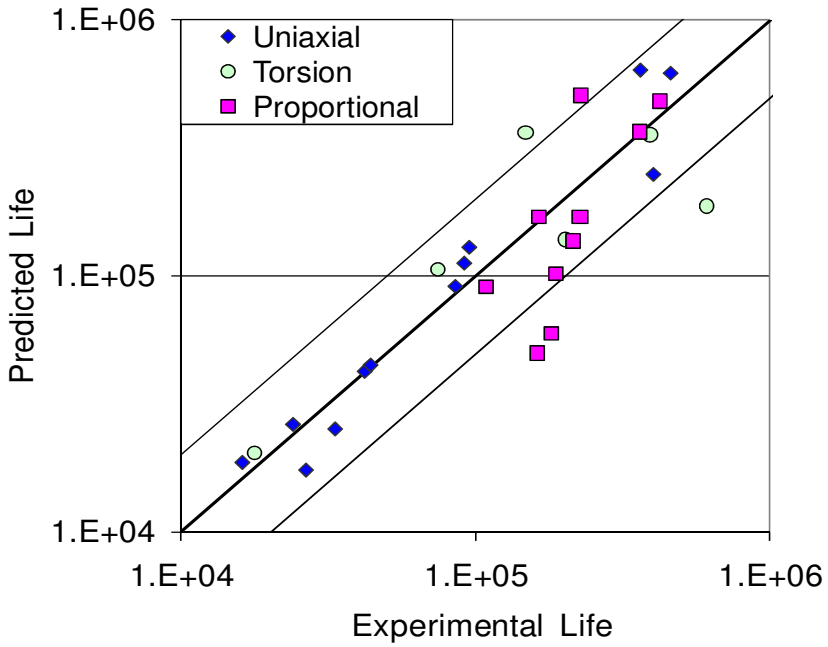

Figure 5.4(a): Predicted vs. Experimental Life Using the Newly Developed Model DA718 (Data Set 4)

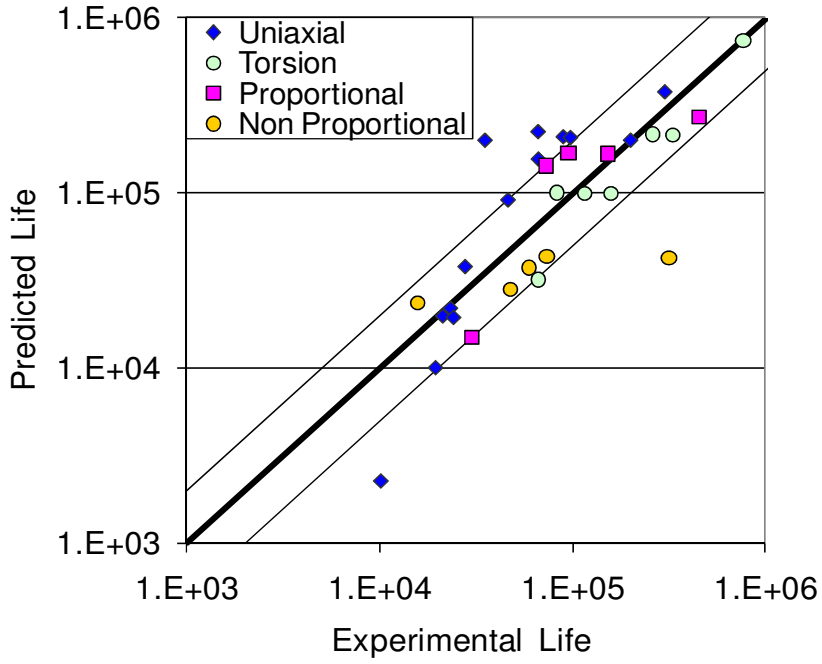

Figure 5.4(b): Predicted vs. Experimental Life Using the Newly Developed Model DA718 (Data Set 5)

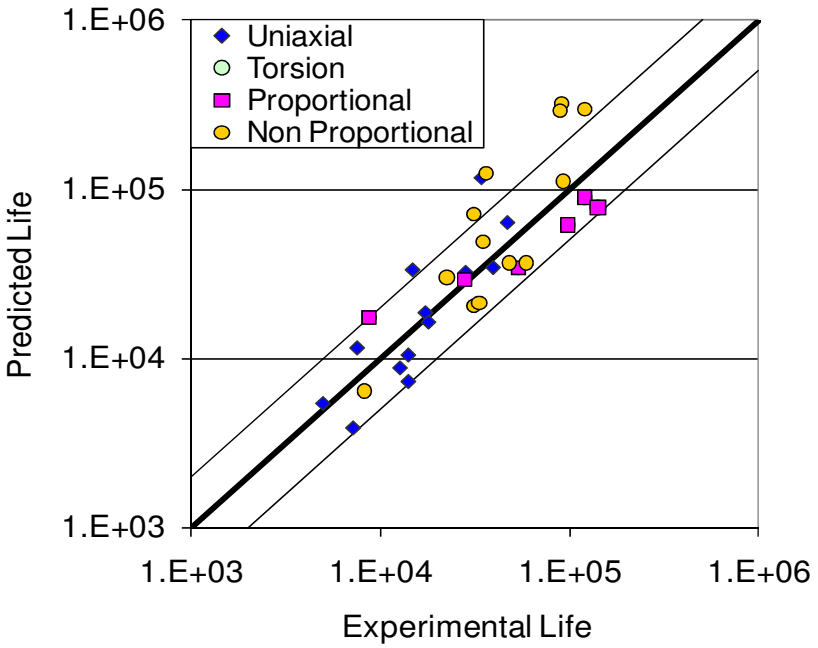

Figure 5.4(c): Predicted vs. Experimental Life Using the Newly Developed Model (Rene 88)

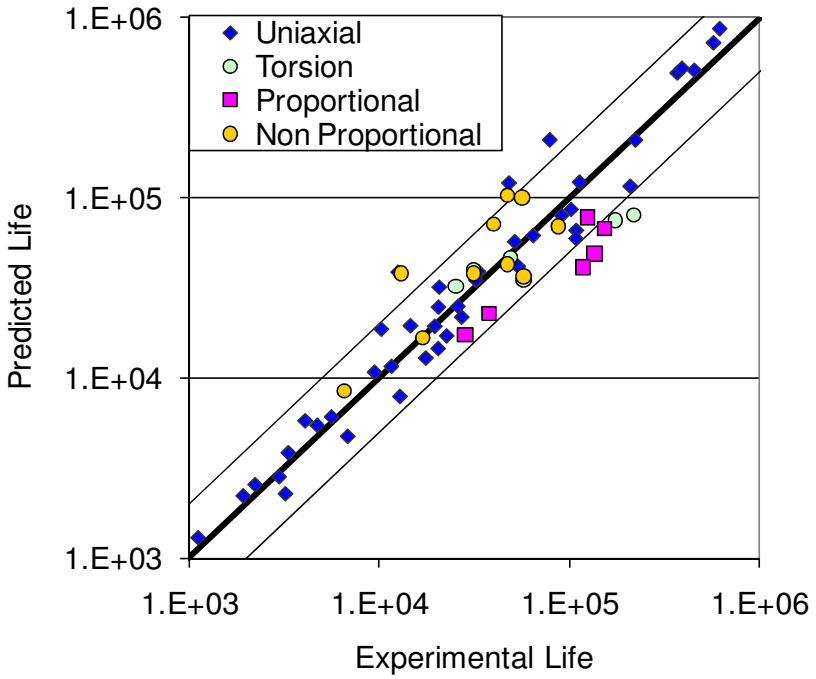

Figure 5.4(d): Predicted vs. Experimental Life Using the Newly Developed Model (Rene 104)

It can be observed from the plots shown in Fig. 5.3 that the newly developed damage parameter (Eq. 5.3) is well capable of modeling most of the uniaxial, torsional, proportional and non-proportional test data. In general, the data show fairly good correlation between experimental and predicted values of fatigue damage. The DA718 data at 1000^{o}F (Fig. 5.3 (c)) have a higher amount of scatter when compared with the same material data at 300^{o}F (Fig. 5.3 (a)) & 700^{o}FDA718 (Fig. 5.3 (b)). The uniaxial data at different stress ratios at 1000^{o}F (dataset-3) collapse along the fitting curve; however, some of the torsional data show significant scatter. This may be due to the absence of any explicit temperature term in Eq. 5.3, although temperature effects can be handled through the "w" and "k" terms in this equation. The microstructure of material changes at elevated temperatures and reacts to fatigue loads differently than at normal temperature. Nevertheless, in the overall trend in the data for each material data set follows typical S-N behavior, which can be taken as a measure to validate the proposed damage model (Eq. 5.3).

The IN718 data generated by Morrow [77] are shown in Fig. 5.3(d). The entire range of uniaxial, torsional, proportional and non-proportional data for this material has collapsed along the fitting curve. This data set is notable as it contains tests with three-dimensional stress states, and these data collapse very well along the fitting curve. Similarly, the two sets of data shown in Fig. 5.3 (e) and (f) also follow the typical S-N behavior, and most of these data in both the LCF and HCF range have been collapsed along the fitting curve.

The results of critical plane analysis for the remaining four material data sets are presented in the form of experimental versus predicted life plots in Fig. 5.4. A multiaxial fatigue analysis is often considered to be very good if the data points in the life-life plot fall within the

scatter bands representing a factor of two as can be seen in figures, most of the data for these materials fall within this accepted scatter range. These diagrams show a significant improvement in correlation when compared with other stress and strain- based critical plane models. As fatigue is an inherently unpredictable phenomenon with a high degree of scatter in experimental data, complete collapsing of all the data points cannot be expected from any damage model. However, comparative evaluations with other fatigue damage models (described in section 5.4) have shown the better capability of this newly developed model (Eq. 5.3) in handling fatigue data over the other models.

5.3.1. Optimization Technique for Determining Material Parameters

The materials constants k and w in the proposed damage model (Eq. 5.3) have been determined through an optimization process for each material data set. In this model, the value of w can be taken as a measure of the influence of the torsional(shear) mean stress, whereas k can be taken as a measure of the degree of interaction between the normal and shear stresses on the critical plane. To determine these constants, an optimization technique based on the "least square error" method was used. The technique required that an assumed form of the mathematical relationship between the damage parameter (DP) and fatigue life (N) be defined. In this study, a dual power-law relationship of the form shown in Eq. 5.4 was used, as this form of equation is very versatile and often used in fatigue studies. The constants A, b, C, and d in this equation are the curve-fitting parameters, and are optimized concurrently with the values of k and w.

$$DP_{predicted} = AN_f{}^{b} + CN_f{}^{d} \tag{5.4}$$

The optimization is performed by comparing the "predicted" values of the damage parameter (from Eq. 5.4) with the "experimental" values computed from Eq. 5.3. The squared relative error is then calculated for each data point using Eq. 5.5.

$$Squared\ relative\ error = \left(\frac{DP_{experimental} - DP_{predicted}}{DP_{experimental}}\right)^2 \tag{5.5}$$

As uniaxial and torsional tests are considered here to represent the baseline test for each material, the squared relative error values for all the torsional and uniaxial data of each material were summed, and the cumulative error value was minimized using a nonlinear numerical solver to calculate the optimal values of A, b, C, d, w and k. The values of w and k obtained from the optimization of the torsion and uniaxial data sets were subsequently used in the analysis of the proportional and non-proportional test data. Thus, w and k for each material were determined only through consideration of the uniaxial and torsion test data.

5.3.2. Material Parameters

The values of w and k were computed using the procedure explained in the previous section for all the material data sets. Values of these material dependent parameters are listed in Table 5.1. The values of these parameters for DA 718 data sets 3 and 4, Rene 88 and Rene 104 are not included here due to proprietary concerns.

The material dependent parameters listed in Table 5.1 can be considered as the signature for each material and the values of these parameters can easily be affected by a change in either

of the experimental conditions, crystal structure (FCC, BCC or HCP), sample preparation procedure, or material type. DA718 data set 1 through 3 were created using similar samples with only a variation of test temperature(300F,750F,1000F) during the experimentation. Although the value of w seems somewhat consistent over this range of temperatures, there is a clear trend of decreasing value of k, indicating a reduced influence of normal stress on crack initiation as temperature increases. However, given the small number of multiaxial data at the highest temperature, a definite conclusion cannot be deduced.

Table 5.1: Material Constants (w & k) for Selected Materials

Material	**w**	**k**
IN718	0.79	0.62
Ti-6Al-4V(data set-1)	0.65	1.53
Ti-6Al-4V(data set-2)	0.46	0.80
DA718(dataset-1)	0.55	0.63
DA718(dataset-2)	0.64	0.51
DA718(dataset-3)	0.56	0.01

Most of the nickel-based super alloys used in this research consist primarily of a FCC crystal structure, whereas Ti-6Al-4V consists of both BCC and HCP crystal structures. These crystal structures do not always exhibit similar fatigue behavior, and their effects should be examined under very strict experimental conditions. While the values of w do not exhibit significant differences between crystal structures, it does appear that the value of K is generally higher for the BCC/HCP structures than the FCC crystal structure. However, further data would be needed to verify this trend.

5.4. Comparative Evaluation of Proposed Damage Model

In order to evaluate the effectiveness of the proposed damage model (Eq. 5.3) relative to previously developed models, a direct comparison was made using the Ti-6Al-4V data set with the same optimization procedures described earlier. In this comparison, the new model was evaluated against the Findley [13] , Erickson et al. [5], and Fatemi-Socie [4] parameters. The Erickson parameter is shown in Eq. 5.1, and the Findley and Fatemi-Socie parameters are shown below in Eqs. 5.6 and 5.7, respectively. The resulting plots of damage parameter vs. fatigue life for each model are shown in Fig. 5.5.

$$\tau_a + k\sigma_{max} = f(N_f) \tag{5.6}$$

$$\frac{\Delta\gamma_{max}}{2}\left(1 + K\frac{\sigma_n^{max}}{\sigma_y}\right) = f(N_f) \tag{5.7}$$

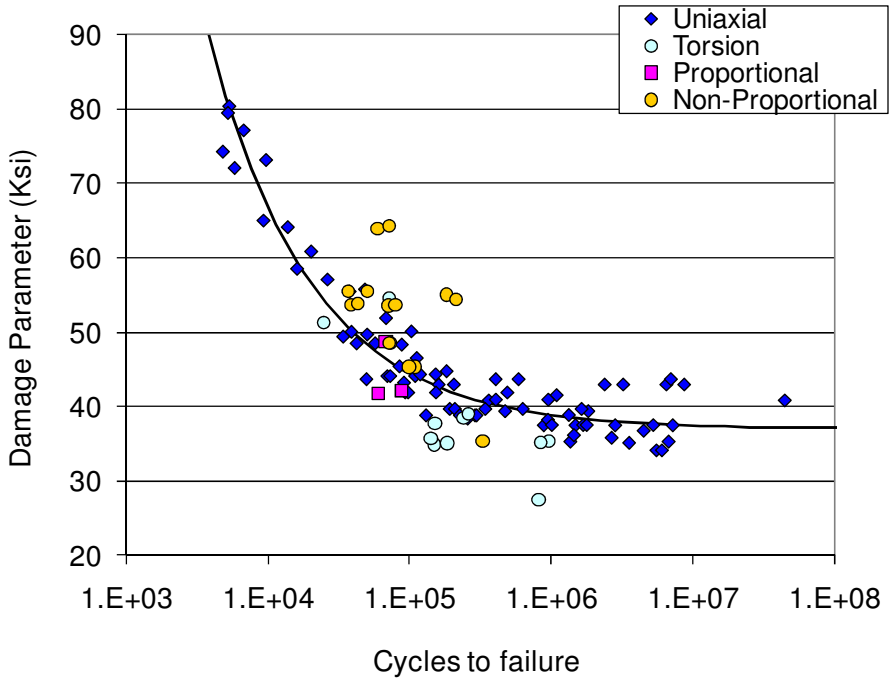

Figure 5.5(a): Comparative Evaluation of Critical Plane Models: Findley Model [13]

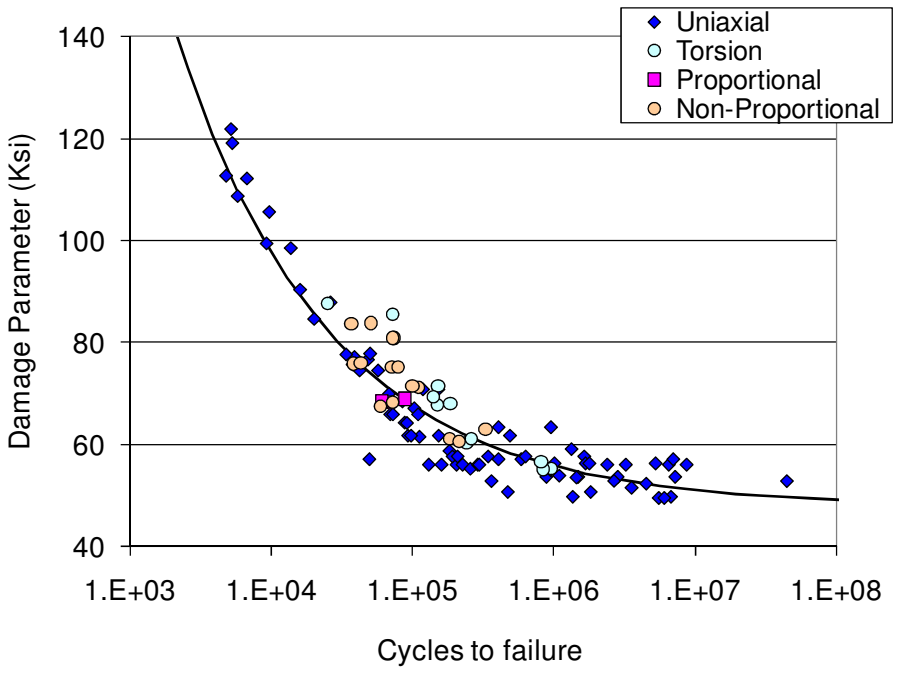

Figure 5.5(b): Comparative Evaluation of Critical Plane Models: Erickson et al. Model [5]

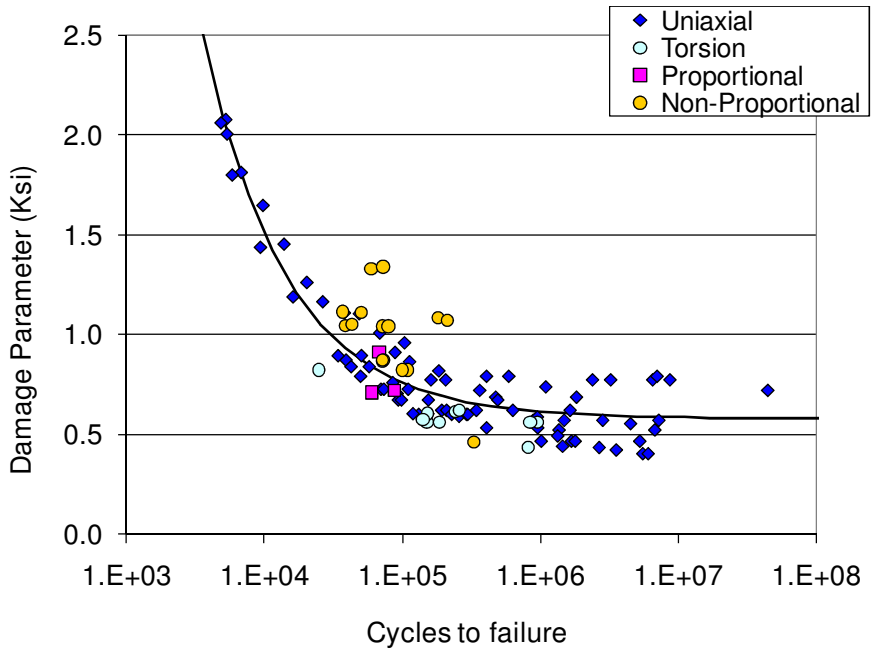

Figure 5.5(c): Comparative Evaluation of Critical Plane Models: Fatemi & Socie Model [4]

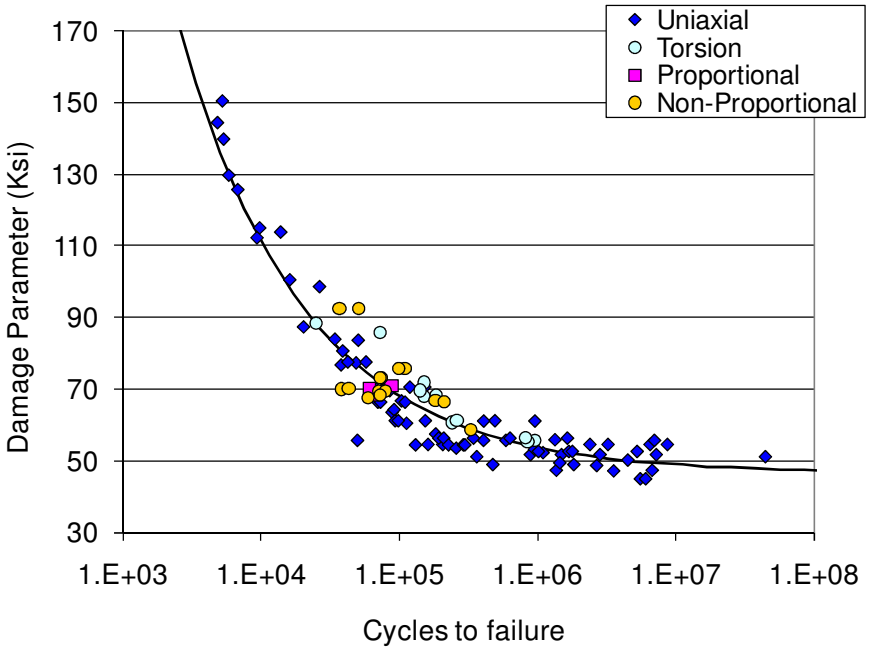

Figure 5.5(d): Comparative Evaluation of Critical Plane Models : Newly Developed Model

As can be seen in Fig. 5.5, the Erickson model provided a better correlation of the fatigue data than the Findley model, due in large part to the consideration of strain hardening effects caused by the normal stress. The Fatemi & Socie parameter modeled much of the uniaxial LCF data better than Findley's model due to the presence of the strain term, but it did not work very well in estimating the damage created by some of the non-proportional cycles. Erickson's (Eq.5.1) model collapsed the overall set of uniaxial and multiaxial data better than the Findley and Fatemi & Socie models. However, the best estimation of fatigue damage for both uniaxial and multiaxial data was observed using the proposed damage parameter of Eq. 5.3. In addition to the better predictive capability of the proposed model, it is also simple in formulation, with only two material dependent parameters. This is another important consideration when comparing this model with other multiaxial models.

CHAPTER 6. CUMULATIVE DAMAGE ANALYSIS

6.1. Variable Amplitude Loading

The critical plane damage parameter introduced in Chapter-5 can only model the damage that is created by constant amplitude uniaxial or multiaxial fatigue cycles. For variable amplitude loading, a cumulative damage analysis is required to predict the fatigue life of machine components. In this work, fatigue tests were carried out using mission histories "that were designed to that were designed to simulate actual service loading condition experienced by aircraft engine components. The "mission" or block loading basically consists of a combination of several load levels of LCF and HCF cycles designed to model severe service conditions. LCF cycles create larger deformations in the material due to their high stress amplitudes, whereas HCF cycles have predominantly elastic stress and strain levels, and thus are often considered to be insignificant in producing fatigue damage to machine components. To speed up the testing of structural components, many accelerated mission testing procedures ignore these small cycles. However, it has been observed during the experiments in this study, that the fatigue life of a specimen subjected to both LCF and HCF cycles may be significantly less than the corresponding LCF life, indicating that HCF cycles may contribute significant damage when coupled with LCF cycles.

A cumulative damage model based upon the consideration of both LCF and HCF damage has been developed in this work. The newly developed damage model is based upon the assumption that the fatigue damage under variable amplitude loading is caused by both LCF & HCF cycles as well as due to their interactions.

In a previous study [71] two level mission tests were conducted on Ti-6Al-4V specimens. As illustrated schematically in Fig. 6.1, LCF life levels were in the range of 40,000-70,000 cycles, while HCF load levels were selected to be below threshold levels (resulting in fatigue lives greater than 10^8 cycles). The results of this test program, summarized in Table 6.1, indicate a significant life reduction was observed in these mission tests, relative to the LCF lives. A life reduction factor has been defined in this table as the ratio of mission life (where a mission consists of 1 LCF cycle and 50 HCF cycles) and the corresponding LCF life. Life reduction factors ranging from 1 (No-reduction) to nearly 25 were observed during these tests, depending on the load level and loadpath (Table 6.1). The loadpaths for these tests were designed using different combinations of torsion, axial, proportional and non-proportional fatigue cycles. The mission histories were also created using various combinations of LCF and HCF cycles to observe the multiple load interactions. Most of the data in Table 6.1 strongly emphasize the importance of HCF cycles when interacting with LCF cycles. However, the amounts of life reductions and LCF-HCF interactions have shown a high level of dependency on the load values and type of load-path. A detailed investigation of all the cumulative damage related issues have been performed in this work to analyze the effects of smaller HCF cycles on the overall fatigue life of titanium alloys subjected to variable amplitude loads.

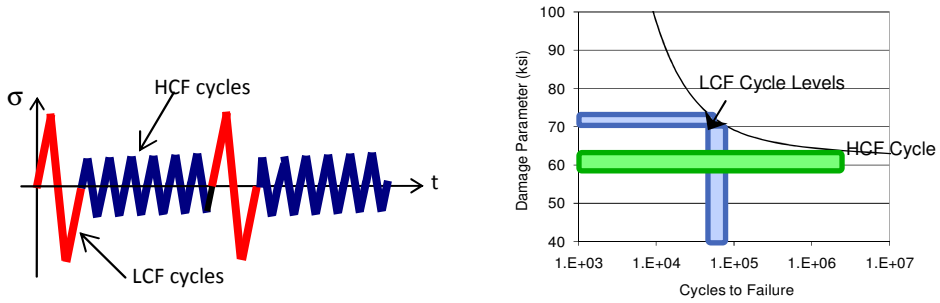

Figure 6.1: Illustration of LCF and HCF Levels Used in the Mission Histories

Table 6.1: Mission Test Results for Ti-6Al-4V (Data Set 1)

History	**LCF/HCF**	**Average LCF life level**	**Predicted HCF life**	**Average Mission life**	**$N_{LCF}/N_{Mission}$**
Box-1	1-LCF/50-HCF	68721	$> 10^8$	20446	3.36
Check-1	1-LCF/50-HCF	43744	$> 10^8$	47160	0.92
Box-2	1-LCF/50-HCF	68721	$>10^8$	10927	6.28
Check-2	1-LCF/50-HCF	43744	$> 10^8$	7250	6.03
Torsion axial-1	1-LCF/50-HCF	72926	$> 10^8$	3688	19.77
Torsion-proportional	1-LCF/50-HCF	72926	$> 10^8$	2944	24.77

6.2. LCF-HCF Interactions in Ti-6Al-4V (Data Set 1)

The set of Ti-6Al-4V data shown in Table 6.1 was analyzed in this study in an attempt to identify the correlating factors for strong LCF/HCF interactions. Two important observations can be deduced from these test results. The first one relates to the orientations of the maximum shear stress and maximum tensile stress planes in the vicinity of the crack initiation sites, and the other pertains to the amount of damage created by the particular LCF and HCF stress levels on those planes. The relative orientations of the maximum shear stress and normal stress planes between the LCF and HCF cycles are thought to influence the degree of interaction between these cycles, whereas the analysis of their stress levels and the damage created by them would influence the

overall magnitude of reduction in fatigue life. The orientations and cyclic stress levels on the planes of maximum shear and normal stress for the LCF and HCF cycles in each test are shown in Table 6.2.

Table 6.2: Maximum Shear and Tensile Planes and Corresponding Stress Levels for Ti-6Al-4V (Data Set 1)

History	LCF/HCF	Specimen ID	Max Shear Plane (degrees)	Max Tensile Plane (degrees)	$\Delta\tau$ (ksi)	$\Delta\sigma$ (ksi)
Box 1	LCF	142-7	22	68	73.82	125.81
	HCF		0	44	32.01	31.99
Check 1	LCF	178-4	86	40	76.27	88.53
	HCF		12	58	24.61	35.14
Box 2	LCF	03-609	68	68	73.68	124.69
	HCF		44	0	30.13	60.30
Check 2	LCF	03-612	86	40	76.27	88.53
	HCF		78	32	42.18	60.55
Torsion-Axial	LCF	04-195	0	46	86.67	86.62
	HCF		45	0	32.38	64.80
Torsion-Proportional	LCF	04-A93	0	46	88.37	88.49
	HCF		70	26	40.47	66.43

A fundamental hypothesis in this study is that fatigue cracks are initiated by cyclic shear stresses from the LCF cycles, and then cyclic tensile stresses from the HCF cycles contribute to accelerate the growth of the microcracks. To evaluate this hypothesis, an analysis was performed to compare the stress levels and plane orientations between LCF max shear planes and HCF max tension planes. Load paths which produce high cyclic tensile stresses in the HCF cycles on planes oriented close to LCF max shear planes would be expected to result in greater LCF/HCF interactions, and hence shorter mission lives, than other load paths.

Thorough examination of Tables 6.1 and 6.2, three levels of LCF-HCF interactions can be observed in these data. A relatively small LCF-HCF interaction effect can be observed in the Box-1 and Check-1 loadpaths, with life reductions of a factor of 1 to 3.4. The shift from the LCF maximum shear plane to the HCF maximum tensile plane in the Box-1 and Check-1 loadpaths is 22 and 28 degrees respectively (Table 6.2). However, a moderate interaction between LCF and HCF cycles was observed in the Box-2 and Check-2 loadpaths with life reductions of more than a factor of 6. In these loadpaths, the shift in orientation between the LCF max shear plane and HCF max tensile plane was 68 and 54 degrees, respectively. Thus, a greater interaction (life reduction) was observed despite a greater difference in plane orientations. Finally, a high level of LCF/HCF interaction was observed in the torsion-axial and torsion-proportional loadpaths (Table-6.2). The shift in planes between the LCF maximum shear stress and HCF maximum normal stress is 0 degrees for the torsion-axial load-path and 26 degrees for the torsion-proportional loadpath. For these loadpaths, life reduction factors of 20 and 25 were observed. These results indicate a mixed influence of plane orientation between the LCF and HCF cycles on the level of interaction. Hence, the plane orientation concept alone cannot explain the observed life reductions indicating that the level of cyclic stresses on these planes must also be considered.

Examination of Table 6.2 reveals a much stronger correlation between LCF/HCF interactions and the magnitudes of the HCF cyclic tensile stresses, rather than the relative plane orientations. For example, in the Box-1 and Check-1 loadpaths (which produced fairly small life reduction factors), the maximum cyclic HCF tensile stress magnitudes were approximately 32 and 35 ksi, respectively. For the Box-2 and Check-2 loadpaths (with moderate life reductions),

the stress magnitudes were approximately 60 ksi. Finally, for the two loadpaths with high life reductions (torsion-axial and torsion-proportional), the stress magnitudes were 65-66 ksi.

The maximum tensile stress level in the HCF cycles appears to explain the effect of the HCF loads on damage accumulation with a secondary effect attributed to the orientation of the HCF max tensile plane relative to the LCF max shear plane. Hence, it can be deduced from these tests, that the complete LCF-HCF interaction effect is not only dependent upon one factor but is influenced by many factors like type of loadpath, plane orientation and load levels. The loadpaths with high HCF tensile stresses on planes near LCF max shear planes have resulted in greater life reductions due to the introduction of HCF cycles when compared to other loading conditions.

An explanation for this observed phenomenon is that fatigue cracks, once initiated by cyclic shear stresses in the LCF cycles, are subsequently propagated by tensile stresses in the HCF cycles. In this case, the LCF cycles would have a greater influence on the fatigue damage in the early stages of the life, and the HCF cycles would have a greater influence on damage later in the life. However, additional tests are required to support this hypothesis, as described in the next section.

6.3. LCF-HCF Interactions in Ti-6Al-4V (Data Set 2)

On the basis of the results obtained from the Ti-6Al-4V Data set-1, additional mission tests were designed and conducted in this study on specimens of Ti-6Al-4V Data set 2. As shown in Tables 6.3 (a) and 6.3 (b), these new mission tests have demonstrated similar types of LCF-HCF interactions as those seen in Data set-1. Notably, strong LCF-HCF interactions were observed in the mission histories with torsional LCF and tensile or proportional HCF cycles. A

moderate amount of interaction was observed in mission histories with LCF torsion and HCF torsion cycles and almost no interaction was observed in the histories with tensile LCF cycles coupled with tensile HCF cycles. However, it should be noted that, there are a few mission tests with torsional HCF cycles that showed a significant life reduction in spite of lower tensile stress levels. This is somewhat contradictory to the earlier hypothesis of tensile-based HCF damage. The detailed analysis of these mission histories is presented in the later sections of this chapter.

Table 6.3(a): Mission Test Results for Ti-6AL-4V (Data Set 2)

Spec.	**Mission**	**LCF and HCF cycles**	N_{LCF}	N_{HCF}	$N_{Mission}$	$N_{LCF}/N_{Mission}$
S-9	Torsion-Axial	1 LCF Cycle: R = 0 Torsion (τ_{max}=87 ksi) 50 HCF Cycles: R = 0 Axial (σ_{max}=98.9 ksi)	118500	$>10^8$	5842	20.28
S-12	Torsion-Axial	1 LCF Cycle: R = 0 Torsion (τ_{max}=87.40 ksi) 50 HCF Cycles: R = 0 Axial (σ_{max}=88.50 ksi)	118500	$>10^8$	6780	17.47
S-1	Torsion-Proportional	1 LCF Cycle: R = 0 Torsion (τ_{max}=88.7 ksi) 50 HCF Cycles: R = 0 Proportional, (σ_{max}=58 ksi, τ_{max}=31.60 ksi))	118500	$>10^8$	37286	3.17
S-4	Torsion-Torsion	1 LCF Cycle: R = 0 Torsion (τ_{max}=88.6 ksi) 50 HCF Cycles: R = 0 Torsion (τ_{max}=57.9 ksi)	118500	$>10^8$	11068	10.7
T-7	Axial-Axial	1 LCF Cycle: R = 0 Axial (σ_{max}=109 ksi) 50 HCF Cycles: R = 0 Axial (σ_{max}=89.50 ksi)	135800	$>10^8$	403150	0.33
T-9	Torsion-Torsion	1 LCF Cycle: R = 0 Torsion (τ_{max}=70.50 ksi) 50 HCF Cycles: R = 0 Torsion (τ_{max}=43.9 ksi)	36028	$>10^8$	9201	3.91
T-48	Axial-Axial	1 LCF Cycle: R = 0 Axial (σ_{max}=108.80 ksi) 50 HCF Cycles: R = 0 Axial (σ_{max}=100.1 ksi)	135800	$>10^8$	331841	0.409
T-37	Torsion-Torsion	1 LCF Cycle: R = 0 Torsion (τ_{max}=70.70 ksi) 50 HCF Cycles: R = 0 Torsion (τ_{max}=39.8 ksi)	36028	$>10^8$	9488	3.79
T-42	Torsion-Torsion	1 LCF Cycle: R = 0 Torsion (τ_{max}=70.31 ksi) 50 HCF Cycles: R = 0 Torsion (τ_{max}=38.93 ksi)	36028	$>10^8$	9920	0.63
T-47	Torsion-Torsion	1 LCF Cycle: R = -1 Torsion (τ_{max}=47.58 ksi) 50 HCF Cycles: R = -1 Torsion (τ_{max}=32.72 ksi)	68928	$>10^8$	3408	20.22
T-32	Axial-Axial	1 LCF Cycle: R = 0 Axial (σ_{max}=127.72 ksi) 50 HCF Cycles: R = 0 Axial (σ_{max}=36.29 ksi)	17393	$>10^8$	9216	1.88

Table 6.3(b): Mission Test Results for Ti-6Al-4V (Data Set 2)

Spec.	Mission	LCF/HCF	N_{LCF}	N_{HCF}	$N_{Mission}$	$N_{LCF}/N_{Mission}$
U-T1	Torsion Axial	1 LCF Cycle: R = 0 Torsion (τ_{max}=86.65 ksi) 50 HCF Cycles: R = 0 Axial (σ_{max}=89.64 ksi)	74151	 $>10^8$	2805	26.43
U-T2	Torsion Axial	1 LCF Cycle: R = 0 Torsion (τ_{max}=86.65 ksi) 50 HCF Cycles: R = 0 Axial (σ_{max}=74.97 ksi)	74151	 $>10^8$	16867	4.39
U-T3	Torsion- Proportion	1 LCF Cycle: R = 0 Torsion (τ_{max}=86.65 ksi) 50 HCF Cycles: R = 0 Prop (σ_{max}=58.67 ksi, τ_{max}=52.95 ksi)	74151	 $>10^8$	9962	7.44
U-T4	Torsion Proportion	1 LCF Cycle: R = 0 Torsion (τ_{max}=86.65 ksi) 50 HCF Cycles: R = 0 Proportional (σ_{max}=48.89 ksi, τ_{max}=44.53 ksi)	74151	 $>10^8$	25090	2.95
U-T5	Torsion Torsion	1 LCF Cycle: R = 0 Torsion (τ_{max}=86.65 ksi) 50 HCF Cycles: R = 0 Torsion (τ_{max}=63.786 ksi)	74151	 $>10^8$	2805	26.44
U-T6	Proportional Axial	1 LCF Cycle: R = 0 Prop (τ_{max}=66.193 ksi, σ_{max}=74.96 ksi) 50 HCF Cycles: R = 0 Axial (σ_{max}=89.636 ksi)	132237	 $>10^8$	16867	7.84
U-T7	Proportional Proportioal	1 LCF Cycle: R = 0 Prop (τ_{max}=66.193 ksi, σ_{max}=74.96 ksi) 50 HCF Cycle: R = 0 Proportional (τ_{max}=52.95 ksi, σ_{max}=58.671 ksi)	132237	 $>10^8$	9962	13.27
U-T8	Proportional Torsion	1 LCF Cycle: R = 0 Prop (τ_{max}=66.193 ksi, σ_{max}=74.96 ksi) 50 HCF Cycles: R = 0 Torsion (τ_{max}=63.786 ksi)	132237	 $>10^8$	25090	5.27
U-T9	Axial Axial	1 LCF Cycle: R = 0 Axial (σ_{max}=130.38 ksi) 50 HCF Cycles: R = 0 Axial (σ_{max}=89.636 ksi)	37602	 $>10^8$	29958	1.26
U-T10	Axial Torsion	1 LCF Cycle: R = 0 Axial (σ_{max}=130.38 ksi) 50 HCF Cycles: R = 0,Torsion (τ_{max}=63.786 ksi)	37602	 $>10^8$	2975	12.64
U-T11	Axial Proportional	1 LCF Cycle: R = 0 Axial (σ_{max}=130.38 ksi) 50 HCF Cycle: R = 0 Proportional (τ_{max}=52.95 ksi, σ_{max}=58.671)	37602	 $>10^8$	18762	2
U-T12	Torsion Axial Proportional	1 LCF Cycle: R = 0 Torsion (τ_{max}=86.65 ksi) 50 HCF Cycles: R = 0 Axial (σ_{max}=74.97 ksi) 50 HCF Cycle: R = 0 Proportional (τ_{max}=48.89 ksi, σ_{max}=44.53)	74151	 $>10^8$ $>10^8$	17161	4.32
U-T13	Torsion Proportional Axial	1 LCF Cycle: R = 0 Torsion (τ_{max}=86.65 ksi) 5 MCF Cycle: R = 0 Proportional (τ_{max}=62.58 ksi, σ_{max}=74.96 ksi) 50 HCF Cycles: R = 0 Axial (σ_{max}=48.892 ksi)	74151	 $>10^5$ $>10^8$	196078	0.38
U-T14	Proportional Torsion Axial	1 LCF Cycle : R=0 Proportional (τ_{max}=66.193 ksi, σ_{max}=74.96 ksi) 25 HCF Cycles: R = 0,Torsion (τ_{max}=63.786 ksi) 25 HCF Cycles: R = 0 Axial (σ_{max}=89.636 ksi)	132237	 $>10^8$ $>10^8$	50299	2.63
U-T15	Torsion Axial	1 LCF Cycle: R = 0 Torsion (τ_{max}=86.65 ksi) 50 HCF Cycles: R = 0 Axial (σ_{max}=74.97 ksi)	74151	 $>10^8$	27863	2.66

6.4. Critical Plane Analysis of Ti-6Al-4V (Data Set 2)

A critical plane analysis of the mission loadings was performed by separately considering each cyclic load level in the mission histories. As discussed in previous chapters, the critical plane is defined as the plane in a specimen or component where a fatigue crack initiates. However, for the life prediction purposes, the definition of the crack initiation plane varies among different fatigue researchers. Many researchers [17] have considered the plane on which the damage parameter reaches a maximum value as the critical plane. This definition has resulted in good correlations with test data, however; it often requires a significant number of computations for complex load histories due to the requirement to calculate the damage parameter on multiple planes in order to determine the plane of maximum damage. Hence, a study was conducted as part of this research to define the critical plane in a more efficient way. This study led to the conclusion that the plane of maximum alternating shear stress can be considered as the critical plane for fatigue analysis, in comparison to the plane of maximum damage parameter value, with only a small compromise in precision and a substantial saving in computation time. As a result, all the subsequent analysis in this work is based upon the definition that the plane of maximum cyclic shear stress is the critical plane on which the fatigue crack initiates. Findley [13] also postulated that the fatigue crack is initiated by the cyclic shear stresses between crystallographic planes, and any additional tensile stresses applied on that plane help in the propagation of these micro-cracks. However, a new definition of this concept is proposed in this work, and the experimental validation is presented.

Low cycle fatigue (LCF) stress amplitudes are normally large in comparison to high cycle fatigue (HCF) stress levels. Hence, it is reasonable to conclude that the fatigue crack

initiation process is primarily dictated by the LCF amplitudes. However, it would be irrational to assume, that there is little or no contribution from the HCF cycles in the fatigue damage accumulation process. Thus, an analysis of both tensile and shear stress plane locations in the HCF loading has been done in this work. Table 6.4 lists the orientation of the maximum tensile and shear stress planes for each cyclic load level applied during the mission testing of Ti-6Al-4V Data Set 2.

Table 6.4(a): Critical Plane Orientations (Ti-6Al-4V Data Set 2)

Spec.	**Mission**	**LCF and HCF Cycles**	**Max Tensile Plane Orientation (Deg)**	**Max Shear Plane Orientation (Deg)**	$N_{Mission}$	$N_{LCF}/N_{Mission}$
S-9	Torsion-Axial	1 LCF Cycle: R = 0 Torsion (τ_{max}=87 ksi) 50 HCF Cycles: R = 0 Axial (σ_{max}=98.9 ksi)	45 0	0 45	5842	20.28
S-12	Torsion-Axial	1 LCF Cycle: R = 0 Torsion (τ_{max}=87.40 ksi) 50 HCF Cycles: R = 0 Axial (σ_{max}=88.50 ksi)	45 0	0 45	6780	17.47
S-1	Torsion-Proportional	1 LCF Cycle: R = 0 Torsion (τ_{max}=88.7 ksi) 50 HCF Cycles: R = 0 Proportional, (σ_{max}=58 ksi, τ_{max}=31.60 ksi))	45 12	0 74	37286	3.17
S-4	Torsion-Torsion	1 LCF Cycle: R = 0 Torsion (τ_{max}=88.6 ksi) 50 HCF Cycles: R = 0 Torsion (τ_{max}=57.9 ksi)	45 45	0 0	11068	10.7
T-7	Axial-Axial	1 LCF Cycle: R = 0 Axial (σ_{max}=109 ksi) 50 HCF Cycles: R = 0 Axial (σ_{max}=89.50 ksi)	0 0	45 45	403150	0.33
T-9	Torsion-Torsion	1 LCF Cycle: R = 0 Torsion (τ_{max}=70.50 ksi) 50 HCF Cycles: R = 0 Torsion(τ_{max}=43.9 ksi)	45 45	0 0	9201	3.91
T-48	Axial-Axial	1 LCF Cycle: R = 0 Axial (σ_{max}=108.80 ksi) 50 HCF Cycles: R = 0 Axial(σ_{max}=100.1 ksi)	0 0	45 45	331841	0.409
T-37	Torsion-Torsion	1 LCF Cycle: R = 0 Torsion (τ_{max}=70.70 ksi) 50 HCF Cycles: R = 0 Torsion(τ_{max}=39.8 ksi)	45 45	0 0	9488	3.79
T-42	Torsion-Torsion	1 LCF Cycle: R = 0 Torsion (τ_{max}=70.31 ksi) 50 HCF Cycles: R = 0 Torsion (τ_{max}=38.93 ksi)	45 45	0 0	9920	3.63
T-47	Torsion-Torsion	1 LCF Cycle: R = -1 Torsion (τ_{max}=47.58 ksi) 50 HCF Cycles: R = -1 Torsion (τ_{max}=32.72 ksi)	45 45	0 0	3408	20.22
T-32	Axial-Axial	1 LCF Cycle: R = 0 axial (σ_{max}=127.72 ksi) 50 HCF Cycles: R = 0 Axial (σ_{max}=36.29 ksi)	0 0	45 45	9216	1.88

Table 6.4(b): Critical Plane Orientations (Ti-6Al-4V Data Set 2)

Spec.	Mission	LCF/HCF	Max Tensile	Max Shear	$N_{Mission}$	$N_{LCF}/N_{Mission}$
U-T1	Torsion- Axial	1 LCF Cycle: R = 0 Torsion (τ_{max}=86.65 ksi) 50 HCF Cycles: R = 0 Axial (σ_{max}=89.64 ksi)	45 0	0 45	2805	26.43
U-T2	Torsion- Axial	1 LCF Cycle: R = 0 Torsion (τ_{max}=86.65 ksi) 50 HCF Cycles: R = 0 Axial(σ_{max}=74.97 ksi)	45 0	0 45	16867	4.39
U-T3	Torsion- Proportional	1 LCF Cycle: R = 0 Torsion (τ_{max}=86.65 ksi) 50 HCF Cycles: R = 0 Prop (σ_{max}=58.67 ksi, τ_{max}=52.95 ksi)	45 28	0 76	9962	7.44
U-T4	Torsion- Proportional	1 LCF Cycle: R = 0 Torsion (τ_{max}=86.65 ksi) 50 HCF Cycles: R = 0 Prop (σ_{max}=48.89 ksi, τ_{max}=44.53 ksi)	45 28	0 76	25090	2.95
U-T5	Torsion Torsion	1 LCF Cycle: R = 0 Torsion (τ_{max}=86.65 ksi) 50 HCF Cycles: R = 0,Torsion (τ_{max}=63.786 ksi)	45 45	0 0	29958	2.47
U-T6	Proportional Axial	1 LCF Cycle: R = 0 Prop (τ_{max}=66.193 ksi, σ_{max}=74.96 ksi) 50 HCF Cycles: R = 0 Axial (σ_{max}=89.636 ksi)	30 0	76 45	2975	44.44
U-T7	Proportional Proportional	1 LCF Cycle: R = 0 Prop(τ_{max}=66.193 ksi, σ_{max}=74.96 ksi) 50 HCF Cycle: R = 0 Prop (τ_{max}=52.95 ksi, σ_{max}=58.671)	30 28	76 76	18762	7.05
U-T8	Proportional Torsion	1 LCF Cycle: R = 0 Prop (τ_{max}=66.193 ksi, σ_{max}=74.96 ksi) 50 HCF Cycles: R = 0,Torsion (τ_{max}=63.786 ksi)	30 45	76 0	17161	7.71
U-T9	Axial Axial	1 LCF Cycle: R = 0 Axial (σ_{max}=130.38 ksi) 50 HCF Cycles: R = 0 Axial (σ_{max}=89.636 ksi)	0 0	45 45	196078	0.00
U-T10	Axial Torsion	1 LCF Cycle: R = 0 Axial (σ_{max}=130.38 ksi) 50 HCF Cycles: R = 0 Torsion (τ_{max}=63.786 ksi)	0 45	45 0	50299	0.00
U-T11	Axial Proportional	1 LCF Cycle: R = 0 Axial (σ_{max}=130.38 ksi) 50 HCF Cycle: R = 0 Prop (τ_{max}=52.95 ksi, σ_{max}=58.671)	0 28	45 76	27863	1.35
U-T12	Torsion Axial Proportional	1 LCF Cycle: R = 0 Torsion (τ_{max}=86.65 ksi) 50 HCF Cycles: R = 0 Axial (σ_{max}=74.97 ksi) 50 HCF Cycle: R = 0 Prop (τ_{max}=48.89 ksi, σ_{max}=44.53)	45 0 28	0 45 76	39199	1.89
U-T13	Torsion Proportional Axial	1 LCF Cycle: R = 0 Torsion (τ_{max}=86.65 ksi) 5 MCF Cycle: R = 0 Prop(τ_{max}=62.58 ksi, σ_{max}=74.96 ksi) 50 HCF Cycles: R = 0 Axial (σ_{max}=48.892 ksi)	45 28 0	0 78 45	7609	9.75
U-T14	Proportional Torsion Axial	1 LCF Cycle : R=0 Prop (τ_{max}=66.193 ksi, σ_{max}=74.96 ksi) 25 HCF Cycles: R = 0 Torsion (τ_{max}=63.786 ksi) 25 HCF Cycles: R = 0 Axial (σ_{max}=89.636 ksi)	30 45 0	76 0 45	16168	8.17
U-T15	Torsion Axial	1 LCF Cycle: R = 0 Torsion (τ_{max}=86.65 ksi) 50 HCF Cycles: R = 0 Axial (σ_{max}=74.97 ksi)	45 0	0 45	38384	1.93
UT16	Axial Proportional Torsion	1 LCF Cycle: R = 0 Axial (σ_{max}=130.38 ksi) 5 HCF Cycle: R = 0 Prop (τ_{max}=62.58 ksi, σ_{max}=74.96 ksi) 50 HCF Cycles: R = 0 Torsion (τ_{max}=63.786 ksi)	0 28 45	45 78 0	5813	6.47

6.4.1. Tests with Tensile Dominant HCF Cycles

As can be seen in Table 6.4, a high level of LCF-HCF interaction was observed in the solid specimens (S-9 and S-12) that were loaded with the torsional LCF cycles and tensile HCF cycles. Life reduction factors of 20.28 and 17.47 were found in these samples. A similar result was observed in the tubular specimen (UT-1), with a life reduction factor of around 26. In all of these fatigue tests, the LCF critical shear plane and HCF maximum tensile plane were both oriented at 0^0 , thus, the damage concept of shear-based crack initiation followed by tensile propagation would be expected to cause maximum interaction here, since the LCF max shear and HCF max tensile planes coincide. In comparison, a moderate amount of LCF-HCF interaction was observed in tubular samples UT-3 and UT-7, with the life reduction ratios of 7.4 & 13.27 respectively. The orientations of the LCF critical shear plane and HCF maximum tensile plane for these tests were approximately 30 degrees apart from each other. Hence, it can be assumed that the fatigue cracks initiated on the LCF critical shear plane and further propagated to the plane HCF maximum tensile plane 30^0 away. Finally, a very low effect of the HCF cycles can be observed in the tubular tests T-7, T-32, and UT-9. All of these tests had tensile LCF cycles followed by tensile HCF cycles, resulting in a 45^0 difference between the LCF max shear plane and the HCF max tensile plane. Thus, when the orientation of these planes differed by a large amount, the effect of LCF-HCF interaction was reduced.

6.4.2. Tests with Shear Dominant HCF Cycles

The concept of shear-based crack initiation and tensile-based micro-crack propagation was found to be not valid for the fatigue tests labeled S-4, T-9, T-47, UT-5 and UT-10. Most of these tests were loaded by torsional LCF cycles followed by torsional HCF cycles,

and resulted in a very high level of life reduction due to the LCF-HCF interactions. This indicates that when the LCF and HCF cycles have similar shear dominant mechanisms, the crack initiate and subsequently propagate in a fully shear mode, rather than relying on tensile propagation mechanisms. Hence, a different damage growth concept is required to handle this specific type of LCF/HCF loading.

6.5. Development of Cumulative Damage Methodology

From the experimental results of Ti-6Al-4V (Data Set-1 and Data Set-2), it can be noticed that the fatigue damage is highly influenced by the magnitude and nature of both the LCF and HCF cycles. Consideration of only tensile or shear stress levels in the LCF or HCF cycles is insufficient for fatigue life estimation. Rather, the fatigue damage accumulation appears to depend on the different types of damage mechanisms (shear vs. tensile) inherent in the LCF and HCF cycles. Hence, the damage analysis of each fatigue cycle in the entire mission should be performed separately, and in general cannot be analyzed by any single model. Each cyclic load-level, applied for a certain number of cycles, creates a certain fraction of the total damage, and the final failure will occur, when the value of the total fractional damage equals one. Thus, a cumulative damage analysis is required to predict the fatigue life of machine components subjected to realistic mission histories with variable amplitude fatigue loading.

The most widely accepted and simple way to estimate the cumulative fatigue damage is through a linear summation of cycle ratios commonly referred to as the Palmgren-Miner linear damage rule or Miner's rule [7], as shown in Eq. 6.1. According to this rule, when the summation of ratios of applied cycles (n_i) to failure cycles (N_i) at each levels equals one, the component will fail due to the nucleation of a fatigue crack. However, experimental data have

shown (here and elsewhere) that a linear damage summation is often insufficient to predict lives in complex load histories consequently, several nonlinear cumulative damage models [53-68] have been proposed by other researchers in an effort to provide satisfactory and reliable methodology for the life prediction of machine components subjected to a wide range of variable amplitude fatigue loading conditions.

$$D_i = \sum_{i=1}^{j} \frac{n_i}{N_i} \tag{6.1}$$

Among the many proposed cumulative damage theories, the "Damage Curve Approach" developed by Manson and Halford [53-54] has received significant attention among researchers due to its simplicity and ability to account for many of the shortcomings of Miner's linear damage rule. This approach is based upon the concept of a family of "damage curves", in which the fatigue damage caused by an applied number of cycles at a particular load level is calculated by following the specific curve associated with that load (or life) level, illustrated in Fig. 6.2.

As shown in Fig 6.2, for each load (life) level, the damage accumulation rate follows a particular nonlinear curve. The damage accumulation caused by a number of applied cycles (n_i) at a load level associated with life of N_i is illustrated by the red lines in this figure. When the load level changes, the damage accumulation rate calculation shifts (horizontally) to the curve associated with the new load level, and the damage (D) continues to accumulate until a value of D =1 is reached. The model developed by Manson & Halford [52-54] to compute this damage is

shown in equation form in Eq. 6.2. The value of α in this model is a material dependent parameter. The value of N_{ref} represents the life level at which damage is assumed to accumulate linearly. Lacking specific data, the value of N_{ref} is normally taken as unity.

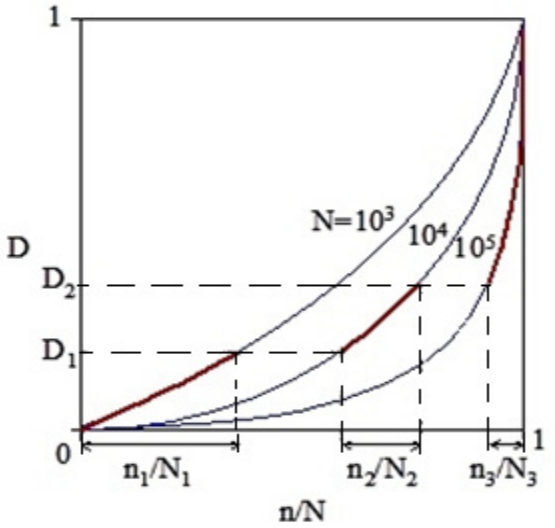

Figure 6.2: Illustration of the Damage Curve Approach [53-54]

$$D = \left(\frac{n}{N_f}\right)^{\left(\frac{N_f}{N_{Ref}}\right)^{\alpha}} \tag{6.2}$$

The model developed by Manson and Halford has several benefits over Miner's linear damage rule. Notably, this model can account for the sequence effects commonly observed under block loading conditions, as the rate of damage accumulation changes with each applied load level. In addition, the model is defined solely in terms of the life (N_f) associated with a particular load level, and is thus independent of the fatigue damage parameter utilized to estimate the life

from the applied stress/strain values. This also allows for the use of different damage parameters to represent LCF and HCF cycles.

6.5.1. Consideration of HCF Damage

Most of the cumulative fatigue damage theories developed by Miner, Manson & Halford, and others, cannot model any potential damage contributed by HCF cycles with an infinite fatigue life level; i.e., at load levels below the fatigue limit. These models predict zero value of damage for any HCF cycles with a life level (N_f) of infinity, and thus result in no calculated reduction in the mission life with the introduction of such HCF cycles during the mission loading. However, the tests conducted for this study have shown significant life reductions due to sub-threshold HCF cycles in the mission histories. By ignoring the effects of these HCF cycles, the amount of fatigue damage created by the mission histories will certainly be underestimated. A more accurate life prediction can be made if these cycles can be modeled properly. Hence, a new damage concept is needed to explain the life reductions shown in Table 6.3 and 6.4. Based upon the damage curve approach, a new cumulative damage concept has been developed in this work to explain and model the significant amount of damage that may be contributed by cycles with infinite life levels (HCF). The conceptual presentation of this newly developed damage model is shown in Fig 6.3.

Fig. 6.3 shows the basic concept of damage accumulation due to HCF cycles. The cumulative damage estimation concept in this work is developed based on the analysis of experimental data and modification of the damage curve approach. Through detailed analysis of the test results, it has been observed that sub-threshold (infinite life) HCF cycles may create fatigue damage if they follow larger (LCF) cycles that cause a certain amount of “predamage”.

Hence, if the required amount of pre-damage or damage threshold level, of the HCF cycles can somehow be modeled, a curve similar to the red line (Fig 6.3), can be drawn to represent the accumulation of subsequent damage caused by these HCF cycles. This red line represents the "infinite life" damage curve in the damage curve approach developed by Manson & Halford. However, the specific nature of this curve will depend on the applied load (stress or strain) level of the HCF cycles. Hence, emphasis in this study has been given to modeling the threshold damage level (D_{th}) corresponding to each HCF load level.

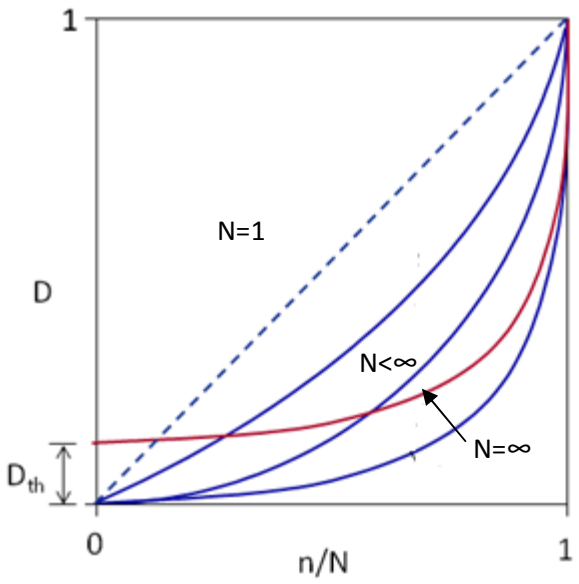

Figure 6.3: Conceptual Illustration of the Proposed Damage Model

This new conceptual damage model takes care of many of the shortcomings of the damage curve approach, and provides a method for modeling the damage created by HCF cycles with an infinite life level. Using this approach, every HCF cycle can be defined by its load level and its threshold damage level (D_{th}). D_{th} represents the amount of pre-damage required by the corresponding HCF cycle before it will start contributing in the damage accumulation process.

This pre-damage might come from prior LCF cycles alone or from the mixed effects of previous LCF and HCF damage. The damage created by the HCF cycles cannot be taken into consideration until the corresponding amount of pre-damage, defined by the damage threshold level (D_{th}), load (stress or strain) level of the HCF cycles. At the same time, the over all process of damage accumulation at each load level is assumed to occur at a nonlinear rate, as in the original damage curve approach.

The graphical representation of this damage accumulation concept for multiple HCF load levels is presented in Fig. 6.4. As shown in this figure, the damage threshold level (the value at which damage will begin to accumulate) increases as the applied HCF load level decreases; i.e., a greater amount of predamage is required for smaller HCF cycles, before they begin to contribute to the damage accumulation process. The conceptual diagram shown in Fig 6.4 also shows the finite-life level damage curves drawn by Manson & Halford [53, 54]. The linear diagonal line in this figure represents Miner's damage rule (Eq. 6.1). Different D_{th} level lines (Fig. 6.4) are shown to illustrate the proposed concept developed in this work for nonlinear damage accumulation by various HCF load levels; i.e. D_{th} increases as the HCF load level decreases.

The test results from the two sets of Ti-6Al-4V data (Table 6.2 & 6.3) show that the life reduction ratio ($N_{LCF}/N_{Mission}$) is strongly influenced by the load level of the HCF cycles. The cyclic tests with similar LCF load levels and different HCF load levels resulted in different experimental life values. Hence, both LCF and HCF damage, along with their corresponding interactions, have been modeled in the newly developed cumulative damage concept.

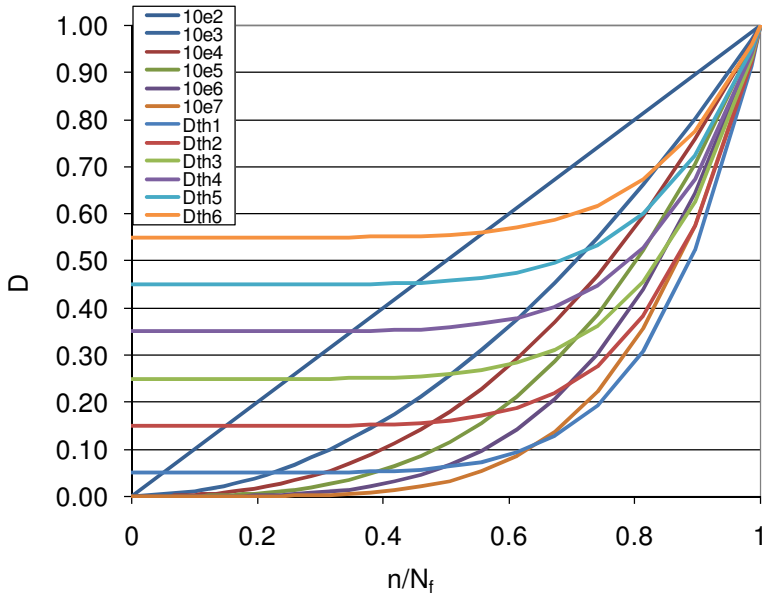

Figure 6.4: Modified Damage Curve Approach Showing Infinite Life Damage Curves with Increasing Threshold Level Corresponding to Decreasing Load Level

The cumulative fatigue damage model developed in this study is nonlinear in nature and addresses a wide variety shortcomings associated with other cumulative damage models. The new model presented in the following sections, can account for load-sequence, load-interaction, and other nonlinear effects in the damage accumulation process

6.6. Damage Analysis of HCF Cycles: Shear vs Tensile Damage

As previously discussed in section 6.4, it was found that different mechanisms (shear vs tensile) may be responsible for causing the LCF/HCF interactions observed in the Ti-6Al-4V data. Thus, when analyzing the effects of the HCF cycles, consideration must be given to both tensile and shear stress levels on the corresponding critical planes. This is most noticeable in the second set of Ti-6Al-4V data presented in Table 6.3 and 6.4. For example, for tensile dominated HCF cycles (e.g., axial cycles with high tensile stress levels on maximum tensile planes), the

microcracks propagate in a tensile manner similar to classical long-crack growth mechanisms. On the other hand, for HCF cycles which are dominated by shear stresses (e.g., torsion cycles with high shear stress levels on maximum shear planes), the microcracks continue to propagate through shear mechanisms, similar to the crack nucleation mechanisms exhibited by the LCF cycles. As a result, it is necessary to develop a model capable of accounting for both types of mechanisms in the HCF cycles, as well as one that is capable of distinguishing between the two types of cycles so that the appropriate methodology can be applied.

A detailed investigation of several tensile and shear based damage parameters was undertaken to correlate the test data in this study. After reviewing numerous parameters, a "Walker" type of damage parameter (Eq. 6.3) was found to provide a good correlation of the test data for the tensile HCF cycles, while the strain-based damage parameter used to model the LCF cycles (Eq. 6.4) was found to provide good results in modeling the shear-based damage mechanisms in the HCF cycles. The "Walker" parameter shown in Eq. 6.3 is a commonly used form of parameter to model mean stress effects in crack growth studies [83].

$$Walker\ DP = \sigma_{max}\left(1 - \frac{\sigma_{min}}{\sigma_{max}}\right)^{w} \tag{6.3}$$

$$DP\ = (G \times \Delta\gamma)^{w} \times \tau_{max}^{(1-w)}\left(1 + k\frac{(\sigma \times \tau)_{max}}{\sigma_o^2}\right) \tag{6.4}$$

The two damage parameters shown in Eq. 6.3 and Eq. 6.4 were applied to the uniaxial Ti-6Al-4V fatigue data from data set 1 to optimize the material constants for each parameter, using the same process to minimize the least squared errors as described in chapter-5. The results of

this analysis are shown in Fig 6.5, with (a) showing the plot for the strain-based parameter of Eq. 6.4 and (b) showing the plot using the Walker parameter of Eq. 6.3. As can be seen in these plots, both parameters successfully collapsed the uniaxial data at different stress ratios into a single curve, which leveled off at high life values corresponding to the "fatigue limit" of the material. This " fatigue limit" taken here as approximately 100 ksi using Eq. 6.4 and 60 ksi using Eq.6.3, represents the "threshold" level of the corresponding damage parameter, DP_{th} , below which fatigue damage will not occur in the absence of prior damage caused by larger (LCF) cycles applied before the HCF cycles. Thus, these two damage parameters may be used to model the HCF damage in the mission histories, provided a method can be identified for distinguishing the conditions in which the tensile parameter (Eq. 6.3) should be used vs. the shear parameter of Eq. 6.4; i.e., how to determine when the HCF cycles should be considered as causing shear-dominant damage as opposed to causing tensile-dominant damage.

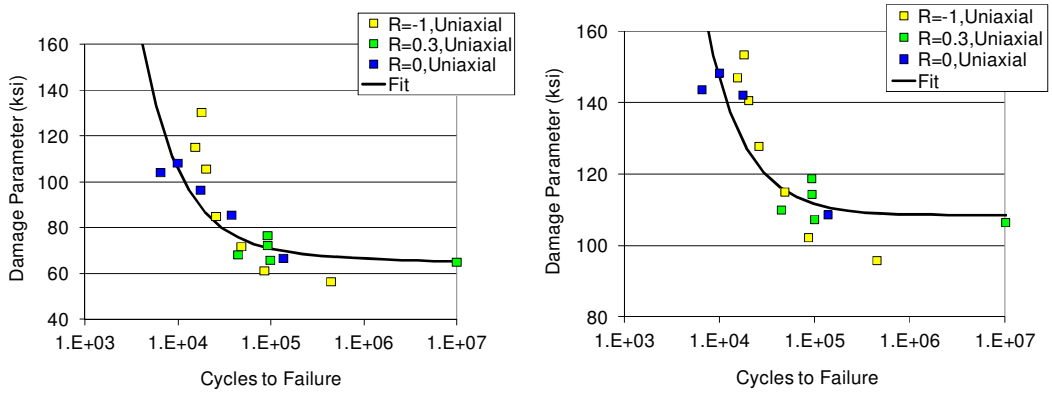

(a) Shear-Based Parameter (Eq. 6.4) (b) Tensile-Based "Walker" Parameter (Eq. 6.3)

Figure 6.5: DP vs Life Curves for Ti-6AL-4V (Data Set 1) Data Using Eq. 6.3 and Eq. 6.4, Showing the Threshold Damage Parameter Levels

By comparing the HCF damage contribution, as calculated from Eq. 6.3 and Eq. 6.4, to the experimental mission lives, it was found that the maximum value of the calculated tensile (Walker) parameter (Eq. 6.3) could be used to distinguish between the conditions for tensile vs. shear damage. Specifically, for a given HCF cycle, if the maximum value of the walker parameter (calculated on the maximum tensile plane) exceeded 50% of the "threshold" level (100 ksi in Fig 6.5), that cycle can be considered to be tensile dominant, and the Walker parameter should be used to calculate the HCF damage in the cumulative damage model. However, if the maximum calculated value of the Walker parameter was less than 50% of the threshold level, the HCF cycle should be considered shear dominant, requiring Eq. 6.4 to be used for calculation of HCF damage.

To demonstrate the influence of HCF damage on the overall mission life, the value of the Walker damage parameter is plotted against the life reduction ratio for the Ti-6Al-4V mission histories (data set 2) in Fig 6.6 (a). A similar plot is shown in Fig. 6.6 (b) for the shear based HCF damage calculated from Eq. 6.4. The increasing trend of life reduction ratio with increasing value of tensile and shear based damage parameters supports the concept of this critical-plane based cumulative damage methodology for the analysis of LCF-HCF interactions.

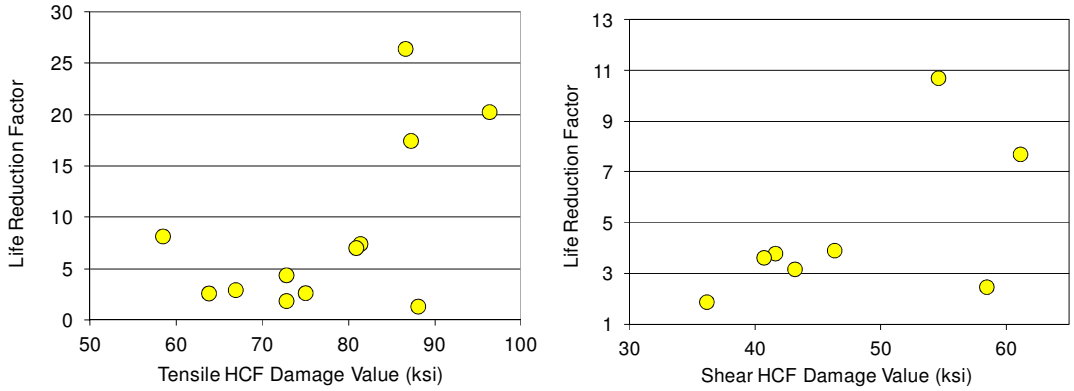

(a) Walker Damage Parameter (Eq. 6.3) (b) Shear Damage Parameter (Eq.6.4)

Figure 6.6: HCF Damage Parameter Value vs. Mission Life Reduction for Ti-6Al-4V

It has been observed that the threshold damage value (D_{th}) for each HCF cycle depends upon the material type and loading level as determined from the corresponding damage parameter versus life curve. The value of the "fatigue limit" for both the tensile (Eq. 6.3) & shear based damage parameters (Eq. 6.4) can be taken as the threshold value of the damage parameter (DP_{th}) for a particular material data set. On the basis of this threshold damage parameter value and analysis of the available data, a non-linear model (Eq. 6.5) is formulated to estimate the threshold damage level (D_{th}) for each HCF cycle. This model relates the calculated value of the HCF damage parameter (DP), relative to the limit level (DP_{th}) to the threshold damage level that is used in Fig. 6.4. In Eq. 6.5, if the calculated value of DP equals or exceeds DP_{th}, then D_{th} is taken as zero. However, for any value of DP less than DP_{th}, a positive value of D_{th} is calculated. The constant β used in this model (Eq. 6.5) is assumed to be a material dependent parameter, and must be evaluated for each data set. The ratio of DP and DP_{th} in Eq. 6.5 represents the relative HCF load level below the "infinite life" level of any material.

$$D_{th} = \left(1 - \frac{DP}{DP_{th}}\right)^{\beta} \tag{6.5}$$

It should be noted that the value of DP_{th} for tensile and shear dominant HCF cycles cannot be directly compared as both of these values are dependent upon separate damage parameters (Fig. 6.6). With these values of $DP_{th,}$ the amount of pre-damage (D_{th}) required before each HCF cycle begins contributing to the overall damage accumulation can be estimated using Eq. 6.5.

6.7. Development of Cumulative Damage Model

Using the definition of the HCF damage threshold shown in Eq. 6.5, a modified form of the Manson and Halford's damage curve model (Eq. 6.2) was developed to represent the red curve illustrated in Fig. 6.3. The modified damage curve model is defined in Eq. 6.6. The first part of this equation represents the pre-damage level required for the HCF cycle, and the second part estimates the cumulative fatigue damage for the particular number of applied cycles at this level. Note that, if $D_{th} = 0$ (e.g., for an LCF cycle), Eq. 6.6 reduces to the original expression of Manson and Halford shown in Eq. 6.2.

The threshold value of damage (D_{th}) estimated from Eq. 6.5 represents the amount of pre-damage required for a particular HCF cycle to significantly contribute in the damage accumulation process. Once calculated, the current value of cumulative damage in the load history (D) is checked against the damage threshold value (D_{th}) for the applied HCF load level. If $D<D_{th}$, the applied HCF cycle is assumed to cause no damage, and hence D is not increased due to that cycle. Conversely, if $D>D_{th}$, the applied HCF cycle is assumed to contribute damage, and

the value of D is increased according to Eq. 6.6. Note that this process of incrementing the damage value is independent of the definition of the damage parameter itself. Thus the cumulative damage model of Eq. 6.6 is applicable to any stress or strain based damage parameter model. The algorithm used to develop the iterative set of mathematical calculations, is shown in Fig 6.7.

$$D = D_{th} + (1 - D_{th})^{\beta} \times \left(\frac{n}{N_f}\right)^{(N_f)^{\alpha}} \tag{6.6}$$

The cumulative damage estimation process using the newly developed methodology requires an iterative process, in which each iteration represents the damage computation for one cycle (HCF or LCF) in the mission history. Starting with a damage level of zero, each applied cycle is first checked to determine if it is an LCF or HCF cycle. If it is an LCF, the damage for that cycle, or group of n cycles, is calculated from Eq. 6.2 and added to the total accumulating damage. In this case, the life N_f is determined from the LCF damage parameter as calculated in Eq. 6.4. If the applied load level corresponds to an HCF cycle, the threshold damage level, D_{th}, corresponding to that load level must be calculated from Eq. 6.5. The value of DP in this equation is computed from either eq. 6.3 (for tensile-dominant damage) or Eq. 6.4 (for shear dominant damage). If $DP < DP_{th}$ for the appropriate loading type, then D_{th} is computed from Eq. 6.5. The HCF damage only contributes once the current accumulated damage level has exceeded the value of D_{th} for that particular HCF cycle. In this case ($D > D_{th}$), the value of damage due to that HCF cycle is computed using Eq. 6.6, and then added to the total accumulated damage. Conversely, if the level of accumulated damage is less than the threshold damage level for any

HCF cycle (i.e., $D < D_{th}$), that particular HCF cycle can be omitted from the calculation. In other words, for each HCF cycle, there must be a certain pre-damage level that has been attained before that cycle may contribute to the overall damage process. The symbols n and N_f in Eq. 6.2 and Eq. 6.6 represent the applied number of cycles and the cycles to failure respectively, for a particular load level. The values of α and β account for the level of nonlinearity present in the damage accumulation process, and must be determined experimentally for each material data set.

The newly-developed nonlinear damage accumulation model was used to estimate the "mission lives" for the Ti-6Al-4V (Data Set 2) test results shown in Table 6.3 and 6.4. These results were compared to the fatigue lives calculated using the conventional Palmgren-Miner linear damage rule. For the new model, the value of α and β (Eqs. 6.2, 6.5 and 6.6) had to be determined for this material. These values were estimated through an incremental procedure that resulted in the best overall correlation between predicted and experimental lives. For Ti-6Al-4V alloy, from this analysis, the value of $\alpha = 0.0058$ and $\beta = 0.98$ were optimally determined for the fatigue damage influenced by tensile dominant HCF cycles. These values were calculated as $\alpha = 0.0088$ and $\beta = 0.91$ for the fatigue damage influenced by shear dominant HCF cycles.

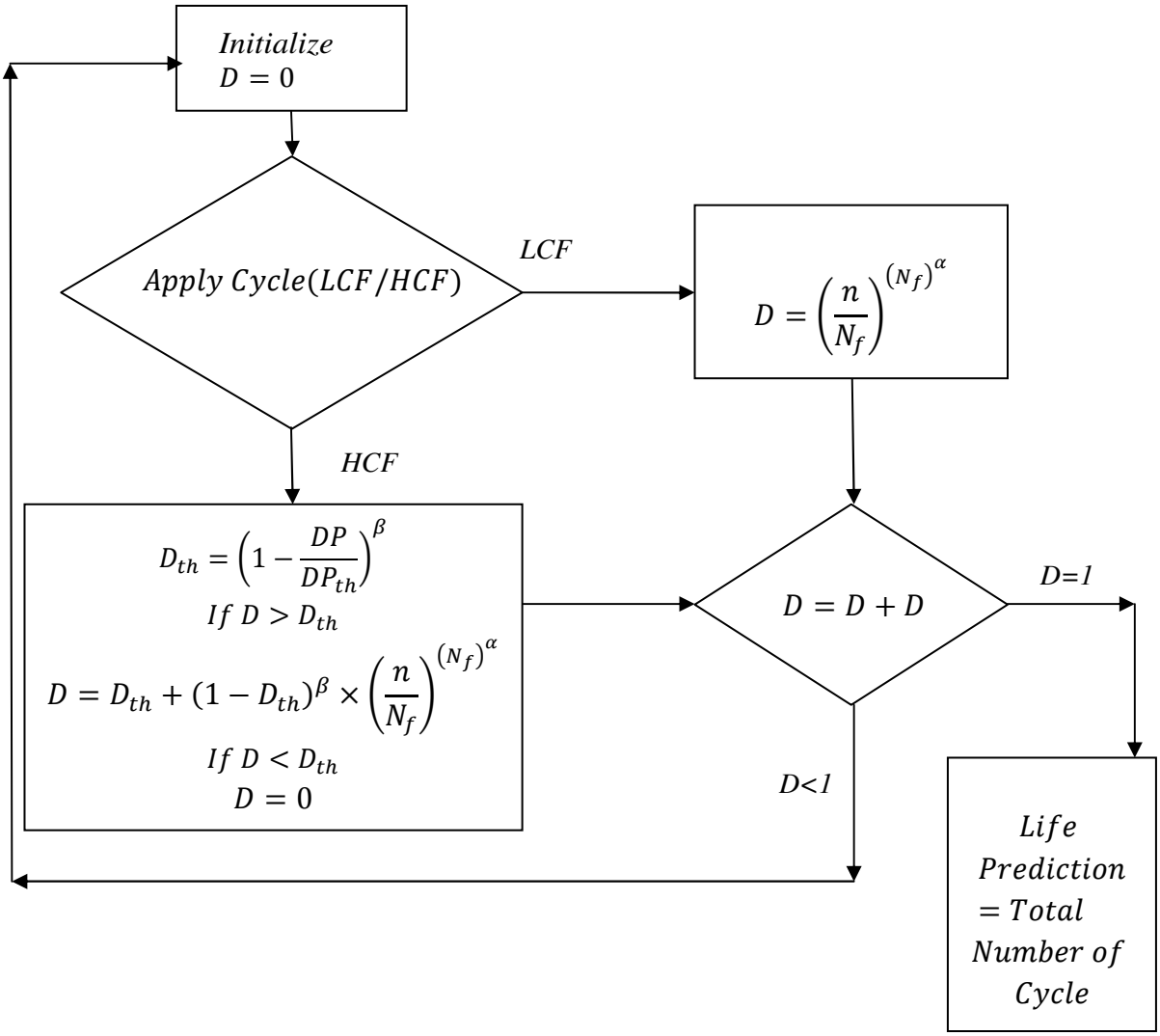

Figure 6.7: Cumulative Damage Computation Process

Fig. 6.8 shows a plot of predicted (calculated) life vs. experimental life for Ti-6Al-4V using Miner's linear rule and the new nonlinear damage model. The yellow data points represent the value of life predicted by Miner's linear model, while the green and blue data points in the plot represent the life predictions calculated by the newly developed damage concept. The green

data points represent the mission lives with tensile-dominant HCF damage mechanisms and the blue data points represent the fatigue tests with shear-dominant damage mechanisms. In this plot, a perfect correlation would be represented by the data points lying on the diagonal solid line, indicating the predicted lives equal the experimental lives. Also shown on this plot are scatter bands representing a factor of two (dashed lines) and a factor of four (red lines). In fatigue analysis, life predictions within a factor of two are generally considered to be very good, given the high degree of scatter often observed in experimental lives.

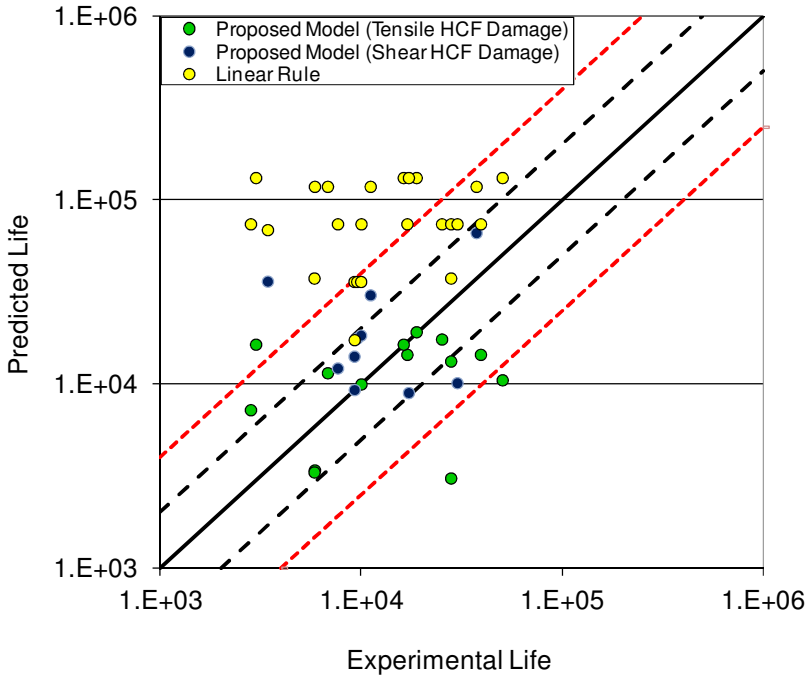

Figure 6.8: Predicted Life vs Experimental Life For the Ti-6AL-4V (Data Set 2) Mission Histories.

As can be seen in Fig 6.8, the new nonlinear damage model produced a significant improvement in calculated fatigue lives relative to Miner's linear damage rule. Notably, in most cases, the linear rule predicted no decrease in fatigue life due to HCF cycles in the mission histories, as the HCF magnitudes were below the fatigue limit. Consequently, the calculated mission lives were equal to the LCF lives, resulting in highly non-conservative life predictions. As is evident in Fig 6.8 most of the yellow points stay outside the "factor of four" scatter bands and only three points fell inside the "factor of two" scatter bands. All lives using this model were over-predicted. In contrast, using the new model, only four points fell outside the factor of four scatter bands, and the majority of calculated lives were within a factor of two of experimental lives. In addition, the calculated lives did not exhibit a strong bias towards over or under-prediction.

The newly developed cumulative damage model presents a significant improvement for cumulative fatigue damage analysis due to its better life prediction capability. Once the required material constants have been determined, the model can be easily programmed to estimate fatigue lives under any complex loading conditions, including multiaxial stress states and highly variable load levels. In addition, the ability of the new model to account for damage caused by very small HCF cycles represents another substantial improvement over the original damage curve approach developed by Mansion & Halford [53 & 54].

CHAPTER 7. CONCLUSIONS & RECOMMENDATION

7.1. Conclusions

The intent of this study was to gain a deeper understanding of fatigue damage accumulation mechanisms and develop an improved critical-plane based fatigue life prediction methodology for aircraft engine components subjected to multiaxial variable-amplitude cyclic loading conditions. The findings of this work may eventually improve aircraft engine design methodologies and reduce field failures of components that risk human life and expensive aircraft. Although this study was focused on the materials used for aircraft applications, the results and findings are equally important for the entire mechanical engineering community.

Fatigue behavior is highly dependent upon the properties of the material, processing conditions loading and part geometry. Hence, efforts were made in this study to indentify and examine several of these parameters among different material data sets. Notably, multiaxial loadpaths were designed using finite-element based simulations and experiments were carried out with loadings similar to actual service conditions experienced by the aircraft engine components. Both constant-amplitude and variable-amplitude fatigue tests were conducted using a variety of loadpaths and load levels.

For the analysis of constant-amplitude loading conditions, a large number of data sets were examined that included a wide variety of service and temperature conditions. Additional data sets from nickel-based super alloys (DA 718, Rene 88 and Rene 104) were provided by GE to validate the developed fatigue life prediction methodology. For the variable-amplitude fatigue analysis, Ti-6Al-4V data from a USAF-HCF program were taken as baseline data, and further tests were also conducted on this material from separate source. All the multiaxial tests were

designed by performing an elastic-plastic finite element analysis for each load levels. Stress and strain values on the surface of specimens were determined from the finite element analyses, and subsequently used in the fatigue damage models.

7.1.1. Development of Critical Plane Damage Parameter

Several critical plane damage parameters were evaluated to determine the best correlation between experimental and predicted values of fatigue damage and life. Fatigue damage models developed by Erickson et al. [5], Fierabend [82], Findley [13], and Fatemi & Socie [4] were investigated in detail for their potential to accurately predict the fatigue life of aircraft engine materials. After evaluating these damage parameters against a significant amount of experimental fatigue data, it was concluded that the models proposed by Erickson et al [5] and Fierabend [82] estimate multiaxial fatigue damage better than those proposed by Findley [13] and Fatemi & Socie [4]. However, Erickson et al.'s [5] damage model is not very easy to implement due to its complexity in formulation. Fierabend [82] proposed some significant improvements in Erickson et al.'s [5] model by conducting additional fatigue tests with multiple normal stress sub-cycles and found that the summation term presented in Erickson et al.'s [5] model can be eliminated. This certainly reduces the computational effort; however, the model proposed by Fierabend [82] is still complex in its formulation and has six material dependent parameters. This parameter [82] also lacks terms for modeling low cycle fatigue test data with a significant amount of material plasticity involved. In addition, this model [82] ignores any interactions between normal and shear stresses on the critical plane.

A new critical plane damage parameter has been developed in this work which includes a strain term to model the plasticity that may occur in low cycle fatigue data as well as term

involving the product of normal and shear stresses to account for the interaction between these stress components. The newly developed damage parameter has only two material-dependent constants which makes the damage estimation process significantly easier to implement for large volumes of fatigue data.

7.1.2. Development of Cumulative Damage Model for Variable Amplitude Loading

Experiments consisting of two or three levels of fatigue loading were carried out for this research to understand the damage mechanisms under variable amplitude loading conditions. The experiments were performed with the intent to understand and analyze the effects of different load paths, load sequences, and other nonlinearities involved with variable amplitude loading. A number of different load levels of torsional, axial and proportional fatigue cycles were combined to form the simulated mission histories. The design of the mission histories was intended to highlight differences among the various factors studied in this research.

It was observed that the presence of HCF cycles in the mission histories significantly influenced the overall fatigue life of the material, even when the HCF load levels were below the fatigue threshold for the material. In some cases, life reductions of up tp a factor pf 26 were observed due to the inclusion of these very small HCF cycles. However, the damage contributions due to the HCF cycles were highly dependent upon the load levels and load-paths of the LCF and HCF cycles in the mission histories.

Several cumulative damage approaches were studied to model the observed behavior. The most commonly used model, the Palmgren-Miner linear damage rule could not account for the damage caused by the HCF cycles nor the nonlinearities observed in the experiments. The damage curve approach had the capability of modeling nonlinear damage accumulation, but was

incapable of accounting for sub-threshold damage caused by the HCF cycles. Hence, a new cumulative damage model was developed in this work to address the shortcomings of the previously developed cumulative damage theories. The iterative damage estimation process developed in this work computes the LCF damage on the basis of the number of cycles applied at a particular load level, and the HCF damage on the basis of the existing total damage level and the nature of the HCF loading.

After extensive analysis of experimental data, it was concluded that, HCF cycles below the fatigue threshold (fatigue limit) may still cause damage if prior fatigue damage has already been incurred through application of LCF cycles. The subsequent growth of HCF damage depends on the magnitude and load path of the HCF cycles, as well as the level of prior damage incurred. In addition two different HCF damage mechanisms were noticed in the test data. Some data revealed a tensile nature of HCF damage and others showed a shear type of damage contribution. Hence, two different damage parameters were used to estimate the tensile and shear fatigue damage from HCF cycles. The separation of tensile and shear dominant HCF cycles was performed on the basis of their damage parameter values with respect to the saturation damage level for that particular data set.

A significant improvement in the correlation between experimental and predicted values of fatigue life of Ti-6Al-4V samples was found when the cumulative damage was estimated by the newly developed damage concept. The capability of estimating the damage contribution from sub-threshold HCF cycles can be considered as another significant achievement of this research.

7.2. Recommendations

The research conducted for this work was very thorough, and several hundred of fatigue data points were analyzed to develop the fatigue damage models. However, fatigue is a very unpredictable phenomenon, and further exploration in several areas is required to fully evaluate the capabilities of the proposed models.

7.2.1. Study of Variable Amplitude Fatigue Histories Containing More Three Load Level

The variable amplitude mission histories analyzed in this fatigue study had only two and three load level. Significant amount of further work is needed to be done to test the developed methodology under more realistic loading scenario with mission histories that have more than three load levels.

7.2.2. High Temperature Fatigue Study

Most of the fatigue data used in this research was generated from common aircraft engine materials tested at temperatures of 300^0F or less, with only a small amount of data at 700-1000^0F. Both nickel-based steel and titanium alloys are often used in components that are subjected to very high temperatures during service conditions, which may significantly change the fatigue response of the material. Due to the difficulties in conducting experiments in high temperature environments, fatigue data were not analyzed in much detail in terms of these high temperature applications. Hence, a detailed study of fatigue response at high temperatures would add significant value to this research.

7.2.3. Microscopic Analysis of Fatigue Behavior

This research focused on the fatigue analysis of material samples at the macroscopic level and no microscopic examinations were conducted. This study can further be extended to the microscopic and nano levels to better understand the details of fatigue science. Many of the macroscopic law of physics lose their validity at the microscopic and nano levels. Hence, further detailed analysis can provide some guidance to understand these limitations leading to the development of models with improved life-prediction capabilities.

7.2.4. Fatigue in Composite Materials

Another important area of fatigue research is in the exploration of composite materials. This study was strictly limited to metals and no composite materials were analyzed. Many high-performance applications are now using composite materials due to the ability to tailor their physical and chemical properties. However, this presents complexities from a design standpoint since the material properties in all directions do not remain same in composite materials. While a significant amount of uniaxial fatigue data exists for composite materials, very few studies have focused on the multiaxial fatigue response of materials with bidirectional and tri-directional properties. Such information would be very useful for design purposes..

REFERENCES

1. "Standard Terminology Relating to Fatigue and Fracture", Testing ASTM Designation E1823,Vol 03.01,ASTM,West Conshohocken, PA,P 1034,(2000)
2. Findley, W. "A theory for the effect of mean stress on fatigue of metals under combined torsion and axial load or Bending." Journal of Engineering for Industry, pp 301-306 (1959)
3. Brown MW and Miller KJ, "A theory for fatigue under multiaxial stress-strain conditions", Proceeding of the Institute of Mechanical Engineers, Vol 187,pp 745-755,(1973)
4. Fatemi, A., Socie, D. " A critical plane approach to multi-axial fatigue damage including out-of-phase loading" Journal of Fatigue and Fracture of Engineering Materials and Structures ,vol l1-3, pp. 149-165,(1988)
5. Erickson M, Kallmeyer AR, Van stone RH, Kurath P, "Development of a multiaxial fatigue damage model for high strength Alloys using critical plane methodology", Journal of Engineering Materials and Technology, Vol 130,pp 041008-1:9,(2008)
6. Palmgren, "Die Lebensdauer von Kugellagern, Verfahrenstechinik", Berlin, vol-68, pp. 339–341(1924)
7. Miner M.A., "Cumulative damage in fatigue", Journal of Applied Mechanics,vol-67 pp. A159–A164, (1945)
8. Ewing, J.A. and Humfrey, J C W., "The fracture of metals under repeated alteration of stress", Philosophical Transactions of Royal society,London,vol-210,pp 241-253, (1903)
9. Stephens R.I., Fatemi A, Stephenes R R, Fuchs H O, "Metal fatigue in Engineering" second edition ,John Wiley & sons , (2001)
10. Smith KN, Watson P, Topper TH, "A stress-strain function for the fatigue of metals", Journal of Materials, vol 5-4,pp 767,(1970)

11. Fatemi, A. Kurath, P. “Multi-axial fatigue life predictions under the influence of mean-Stresses” Journal of Engineering Materials and Technology, vol 110, pp 380 -388, (1998)
12. Fatemi A and Stephens R.I., “Biaxial fatigue of 1045 steel under in-phase and out of phase loading condition to appear in multiaxial fatigue” Analysis and Experiment, SAE AEXX (1988)
13. Findley W N, “Fatigue of Metals under combination of stresses”, Transaction of ASME, vol 79, pp 1337-1348,(1957)
14. Findley W.N, Mitchell W.I., “Two Machines for Combined Bending and Torsion Fatigue”, Proceedings, SESA, vol 11-1, pp 203-212,(1953)
15. Findley W.N, “Fatigue of 76S-T61 Aluminum Alloy under Combined bending and Torsion”, Proceedings of ASTM , vol 52,pp 818-835(1952)
16. Brown M, Miller K, “A theory for fatigue failure under multiaxial stress-strain condition”, Proceedings of the IME,vol-187,pp 745-755,(1973)
17. Socie D, “Multiaxial fatigue damage models”, Journal of Engineering Material and Technology, Vol 109,pp 293-298,(1987)
18. You BR, Lee SB, “A critical review on multiaxial fatigue assessments of metals”, International Journal of Fatigue, Vol 18-4,pp 235-244,(1996)
19. F. Ellyin and K. Golos, “Multiaxial Fatigue Damage Criterion”, Journal of Engineering Material and Technology, Trans. ASME, vol-110, pp. 63-68, (1988)
20. Bhat S.P ,Morris E. Fine, “Fatigue crack nucleation in iron and a high strength low alloy steel”, Journal of Material science and Engineering, vol-A314,pp 90-96, (2001)

21. Connor ZM, Li W, Fine ME, Achenbach JD, “Fatigue crack initiation and growth in riveted specimens; an optical and acoustic microscopic study”, International Journal of Fatigue, Vol 19.-1, pp S331-S338,(1997)
22. McDowell DL, Multiaxial small fatigue crack growth in metals, International Journal of Fatigue,Vol-19,No 1, pp S127-S135,(1997)
23. Kanazawa K, Miller K J, Brown M W, “Low cycle fatigue under out of phase loading conditions”, Journal of Engineering Material Technology, Vol 8, pp 99- 222,(1977)
24. Wu HC, Yang CC, “On the influence of strain-path in multiaxial fatigue failure, Journal of Engineering Matarials and Technology, Vol 109, pp 107-113,(1987)
25. Garud YS, “A new approach to the evaluation of fatigue under multiaxial loadings”, Transaction of ASME, Vol 103, pp 118-125,(1981)
26. Ellyin F. and Golos K., “Multiaxial fatigue damage criterion”, Journal of Engineering Materials and Technology, Trans. ASME,vol-110, pp 63-68, (1988)
27. Shariyat M, “A fatigue model developed by modification of Gough’s theory, for random non proportional loading conditions and three dimensional stress fields”, International Journal of Fatigue, vol 30,pp 1248-1258,(2008)
28. Gough,H.J.,Polland, H.V. and Clenshaw, W.J. “Some experiment on the resistance of metals under combined stress,” Ministry of Supply, Aeronautical Research Council Report and Memoranda no.2522,HMSO,London (1951)
29. Lee, S.B., “A criterion for fully reversed out-of-phase torsion and bending” American Society for Testing and Materials, STP 853,PA, pp 553, (1985)
30. Mowbray D F, “A hydrostatic stress sensitive relationship for fatigue under biaxial stress conditions”, Journal of Testing and Evaluation, vol 8-1,pp 3-8,(1980)

31. Findley WN, “Effect of range of stress on fatigue of 76S-T61 aluminum alloy under combined stresses which produce yielding”, Journal of Applied Mechanics, pp 365-374,(1953)
32. Glinka G, Wang G, Plumtree A, “Mean stress effect in multiaxial fatigue”, Journal of Fatigue and Fracture of Engineering Materials and Structures, vol 18,pp755-64, (1995)
33. Farahani AV, “A new energy critical plane parameter for fatigue life assessment of various metallic materials subjected to in-phase and put of phase multiaxial fatigue loading conditions” International Journal of Fatigue,Vol 22,pp 295-305, (2000)
34. Pan WF, Hung CY, Chen LL, “Fatigue life estimation under multiaxial loadings” International Journal of Fatigue, Vol 21, pp 3-10,(1999)
35. Wang YY, Yao W X, “Evaluation and comparison of several multiaxial fatigue criteria”, International Journal of Fatigue, vol- 26,pp 17-25,(2004)
36. McDiarmid D.L.,"A general criterion for high cycle multiaxial fatigue failure", Journal of Fatigue and Fracture of Engineering Materials and Structures , vol-14, pp 429-453, (1991)
37. Matake T, “Explanation of fatigue limit under combined stress”, Bull JSME vol 20-141, pp 257-264,(1977)
38. Carpinteri A, Spagnoli A, “Multiaxial high cycle fatigue criterion for hard metals”, International Journal of Fatigue , vol 23, pp 135-145,(2001)
39. Ninic D and Stark H L, “A multiaxial fatigue damage function”, International Journal of Fatigue ,vol 29,pp 553-548,(2007)
40. Fischer F D, Reisner G, Werner E, Tanaka K, Cailletaud G, Antretter T., “A new view on transformation induced plasticity (TRIP),International Journal of Plasticity, vol 16, pp 723–748, (2000).

41. Zhao T, Jiang Y, " Fatigue of 7075-T651 aluminum alloy", International Journal of Fatigue, vol-30,pp 834–849,(2008)

42. Sines G. and Ohgi G., "Fatigue criteria under combined stresses or strains", Journal of Engineering Material and Technology. Tranactions of ASME,Vol103-2, pp. 82.,(1981)

43. Crossland, B., "Effect of large hydrostatic pressures on the torsional fatigue strength of an alloy steel". Proceedings of IME, , pp. 138-49, London, (1956)

44. Socie D, D.L. McDowell , " Critical plane approaches for multiaxial fatigue damage assessment" Advances in Multiaxial fatigue, American society for testing and materials, Philadelphia, pp 7-36, (1993)

45. UematsuY,AkitaM,NakajimaM,Tokaji K, "Effect of temperature on high cycle fatigue behavior in 18 Cr-2Mo ferritic stainless steel", International Journal of Fatigue, vol-30,pp 642-648,(2008)

46. Xu S., Wu X.Q., Han E.H., Ke W. and Katada Y., "Crack initiation mechanisms for low cycle fatigue of type 316Ti stainless steel in high temperature water", Journal of Materials Science and Engineering: A,Vol-490, pp16-25(2008)

47. Dowling N.E., "Fatigue life predictions for complicated stress strain histories", Journal of Materials, ASTM, vol 7, No 1,pp 71:87,(1972)

48. Fatemi A. and Yang L., "Cumulative fatigue damage and life prediction theories: a survey of the state of the art for homogeneous materials",International Journal of Fatigue, vol-20-1,pp 9-34,(1998)

49. Lim L.C., Tay Y.K., Fong H.S., "Fatigue damage and crack nucleation mechanisms at intermediate strain amplitudes", ActaMetallurgica et Materialia, vol-38-4,pp. 595–601, (1990)

50. Coffin L.F., “Design aspects of high-temperature fatigue with particular reference to thermal stresses”, Transactions of the ASME, vol-78 ,pp. 527–532, (1956)

51. Topper T.H., Biggs W.D., “The cyclic straining of mild steel”, Journal of Applied Materials Research, pp. 202–209, (1996)

52. Grover H.J., “An observation concerning the cycle ratio in cumulative damage, Symposium on Fatigue of Aircraft Structures”, American Society for Testing and Materials, Philadelphia, PA, pp. 120–124., (1960)

53. Manson S.S., Interfaces between fatigue, creep, and fracture, International Journal of Fracture Mechanics vol-2, pp. 328–363, (1966)

54. Manson S.S.,Halford G R, “Re-examination of cumulative fatigue damage analysis-An Engineering Perspective” Engineering fracture mechanics Vol-25,pp 539-571,(1986)

55. F.E. Richart and N.M. Newmark, “A hypothesis for the determination of cumulative damage in fatigue”, Proceedings of American Society for Testing and Materials, vol-48, pp. 767–800, (1948)

56. Marco SM, Starkey WL , “A concept of fatigue damage”, Transaction of ASME,vol-76-1,pp 627,(1954)

57. Goodin, E., Kallmeyer, A., and Kurath, P. "Evaluation of Nonlinear Cumulative Damage Models for Assessing HCF/LCF Interactions in Multiaxial Loadings," Proceedings of the 9th National Turbine Engine High Cycle Fatigue Conference, North Carolina, (2004)

58. Xu Chen, Dan Jin, KwangSoo Kim, “fatigue life prediction of type 304 stainless steel under sequential biaxial loading”, International Journal of Fatigue ,vol-28,pp 289–299,(2006)

59. Itoh T, Chen X, Nakagawa T, Sakane M., " A simple model for stable cycle stress strain relationship of type 304 stainless steel under non proportional loading. Transaction of ASME",Journal of Engineering Material Technology,vol-12-2,pp 1-9 (2000)

60. Bannantine, J. A. and D. F. Socie, "A Variable Amplitude Multiaxial Fatigue Life Prediction Method, Fatigue under Biaxial and Multiaxial Loading," Mechanical Engineering Publication, ESIS,vol-10,pp 35-51,(1991)

61. Wang C.H., Brown M.W., "Life prediction techniques for variable amplitude multiaxial fatigue-part 1:theories",Journal of Engineering Materials and Technology, ASME, vol 118,pp 367-370,(1996). (Standard teminology relating to fatigue and fracture, 2000) (W, 1959) (W, 1959)

62. Langlais T.E., Vogel J.H. Chase T.R., " Multiaxial cycle counting for critical plane methods" International Journal of Fatigue, vol- 25,pp 641-647,(2003)

63. C. Ngiau and D. Kujawski, Sequence effects of small amplitude cycles on fatigue crack initiation and propagation in 2024-T351 aluminum. International Journal of Fatigue, vol-**23,** pp. 807–815, (2001)

64. Z. Wang and Z.W. Chen,Influence of small load cycle omission on fatigue damage accumulation. In: Proceedings of the 7th International Fatigue Congress, Beijing**vol. 2**, EMAS, Cradley Heath, UK, pp. 1113–1118, (1999)

65. P. Heuler and T. Seeger, A criterion for omission of variable amplitude loading histories. International Journal of Fatigue ,vol-8- 4, pp. 225–230, (1986)

66. Haibach E., "ModifiziertelineareSchadensakkumulations-HypothesezurBerücksichtigung der DauefestigkeitmitfortschreitenderSchädigung. TechnischeMitteilungen," 50/70. LaboratoriumfürBetriebsfestigkeit, LBF, Darmstadt, 1970.

67. Mayer H., Edea C. and Allison J. E., “Influence of cyclic loads below endurance limit or threshold stress intensity on fatigue damage in cast aluminum alloy 319-T7”, International Journal of Fatigue ,vol-27-2, pp 129-141(2005)

68. Hines J.A. and Lütjering G., “Propagation of microcracks at stress amplitudes below the conventional fatigue limit in Ti–6Al–4V”. Journal of Fatigue and Fracture of Engineering Materials and Structures, vol-**22,** pp. 657–665. (1999)

69. Department of Defense Handbook: Engine Structural Integrity Program (ENSIP), MIL-HDBK-1783,(1997).

70. Nicholas T, Maxwell DC. ,“Evolution and effects of damage in Ti-6Al-4V under high cycle fatigue, progress in mechanical behavior of materials”. Proceedings of the eighth International Conference on Mechanical Behavior of Materials, ICM-8, (1999)

71. Goodin, E., Kallmeyer, A., and Kurath, P. ,"Multiaxial Fatigue Evaluation of Ti-6Al-4V under Simulated Mission Histories," Proceedings of the 7th National Turbine Engine High Cycle Fatigue Conference, Florida, (2002).

72. Goodin, E., Kallmeyer, A., and Kurath, P., "Cyclic Event Identification and Fatigue Damage Assessment for Multiaxial Mission Loadings," Proceedings of the 8th National Turbine Engine High Cycle Fatigue Conference, California, (2003).

73. Nicholas T., “Step loading for very high cycle fatigue.” Journal of Fatigue and Fracture of Engineering Materials and Structures,vol-25,pp. 861–869,(2002)

74. Lanning D., Haritos G.K., Nicholas T. and Maxwell D.C., “ Low-cycle fatigue/high-cycle fatigue interactions in notched Ti-6Al-4V”, Journal of Fatigue and Fracture of Engineering Materials and Structures, vol- 24,pp. 565–578,(2001)

75. Mall S, Nicholas T, Park TW, “Effect of predamage from LCF on HCF strength of Ti-6Al-4V”, International Journal of Fatigue,vol-25,pp1109–1116,(2003)

76. Yan J.H. ,Zheng X.L. and Zhao K, “Experimental investigation on Small load omitting criterion”, International Journal of fatigue,vol-23,pp 403-41,(2001)

77. Morrow DL, “Biaxial-tension fatigue of Inconel 718”,Doctoral thesis, Department of Mechanical Industrial Engineering, University of Illinois, Urbana Champaign,(1988)

78. Kallmeyer AR, Krgo A, Kurath P, “Evaluation of Multiaxial fatigue life prediction methodologies for Ti-6Al-4V”,Journal of Engineering Materials and Technology, ASME, vol -124, pp 229-237,(2002)

79. Mourer,P.,Huron.S.,Bain R.,Montero E.,Reynolds L. and Schirra J., “Super-alloy optimized for high temperature performance in high pressure turbine disks” U.S. patent 6,521,175 (2003)

80. Krueger D.,Kissinger D., and Menzies G., “Development and introduction of a damage tolerant high temperature Nickel-based Disk alloy, Rene 88 DT” Illinois: Super alloys, pp 277-286,(1992)

81. Krueger D., “The development of Direct Age 718 for Gas turbine disk applications” ,Illinois Super -alloy 718 –Mettalurgy and Applications, pp 279-296,(1989)

82. Feierabend SP, “ A critical plane approach for modeling multiaxial fatigue damage in high strength alloys”, Master thesis, North Dakota State University,(2007)

83. Kallmeyer AR & Kurath P, " Development of Multiaxial Fatigue Damage Assessment Methods Considering HCF/LCF Interactions" Final Report submitted to AFRL (Contract No. FA8650-04-1-5211, AFRL/MLLMN), Wright Patterson Air Force Base, Dayton, Ohio (2006)

84. Gallagher, J.P. , Van Stone, R.H., deLaneuville, R.E., Gravett, P., and Bellows, R.S., " Improved High Cycle Fatigue Prediction", Report AFRL-ML-WP-TR-2001-4159, University of Dayton Research Institute.(2001)